WEAR AND FRACTURE OF TYRE TREAD RUBBER

A THESIS

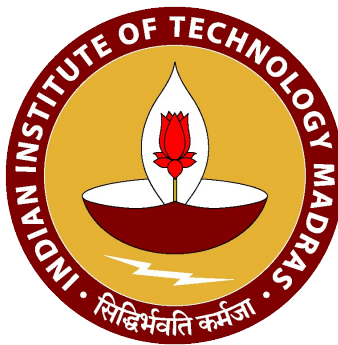*submitted by*

PRASENJIT GHOSH

for the award of the degree

of

DOCTOR OF PHILOSOPHY

DEPARTMENT OF ENGINEERING DESIGN
INDIAN INSTITUTE OF TECHNOLOGY MADRAS
CHENNAI-600 036

MAY 2015

Dedicated

to

my Parents

THESIS CERTIFICATE

This is to certify that the thesis entitled **"WEAR AND FRACTURE OF TYRE TREAD RUBBER"** submitted by **PRASENJIT GHOSH** to the Indian Institute of Technology Madras, Chennai for the award of the degree of **Doctor of Philosophy** is a bonafide record of research work carried out by him under my supervision. The contents of this thesis, in full or in parts, have not been submitted and will not be submitted to any other Institute or University for the award of any degree or diploma.

The research work has been carried out at Indian Institute of Technology Madras and Hari Shankar Singhania Elastomer & Tyre Research Institute.

Research Guide

Dr. R. Krishna Kumar
Professor
Department of Engineering Design
Indian institute of Technology Madras
Chennai- 600 036
India

Research Co-ordinator

Chennai 600 036

Date: May 2015

Dr. R. Mukhopadhyay
Director & CE
Hari Shankar Singhania Elastomer &
Tyre Research Institute
Kankroli, Rajasthan, 313342
India

ACKNOWLEDGEMENTS

ABSTRACT

KEYWORDS: *Rubber blends, Tyre, Wear, Fracture mechanics, Fatigue crack growth, Tearing energy, Hyperelastic, Viscoelastic, Stress relaxation, Glass transition, Finite Element Analysis.*

Tyre is one of the most important components in a vehicle. It performs multiple functions like carrying the load while rolling, aid in acceleration, braking, cornering and resist radial, lateral and longitudinal forces without losing its form. In this process the tyre tread wears out. Incessant loss of rubber material occurs from tyre treads due to repetitive interaction with the road asperities. The mechanism of material loss is a complex phenomenon as it depends on many factors like tread's material composition, vehicle operating condition, road surface, environmental conditions etc. There are a number of physical and chemical processes that take place at the tyre-road interface, which are responsible for the tyre wear. Thus a clear understanding of the contribution of these parameters is necessary for the development of better products. Mechanically, tyre wear occurs due to frictional energy, which is a function of contact shear stresses and micro slippage at the tyre-road interface. The loss of material from the tread surface can occur due to sudden tearing of the material by sharp asperities or fatigue failure due to repetitive interaction with the road surface. Therefore, tearing or fracture properties of rubber play an important role in the wear resistance. Major objective of this work is to study the Fatigue Crack Growth (FCG) properties of truck bus radial tyre tread materials to gain better insight about the wear process.

In the beginning of the thesis, relevant literature pertaining to rubber materials, wear mechanism and rubber fracture mechanics are reviewed. The tyre wear could be categorized into two major classes: abrasive wear and fatigue wear. Occurrence of either of these two categories or combination depends on the type of material and service conditions including the road surface texture. Factors influencing the wear characteristics are identified and taken into consideration in the present work. The fracture mechanics approach used in the rubber area is reviewed and also the influencing parameters like temperature, strain, waveform type, R-ratio etc. are identified.

Rubber blends have been widely used in tyre tread application for many years to achieve desired properties which are otherwise impossible to obtain from single rubber. However, blend system possesses many complexities as most of the general purpose rubbers are thermodynamically immiscible and also migration of different ingredients to a specific component leads to heterogeneous phase structure.

In the present work, series of rubber compounds comprising of NR, BR, SBR, NR/BR and NR/SBR blends are developed. The fundamental properties (rheometric, stress-strain, viscoelastic, glass transition temperature and crosslink densities) of rubber vulcanizates are characterized. Influence of rubber blend composition on these properties is explained. Appearance of two glass transition temperature in most of the rubber blend compounds confirms the heterogeneous phase structure at micro level.

FCG measurements of all the compounds are performed using Tear & Fatigue Analyser (TFA). In order to understand the influence of various parameters on FCG behaviour, measurement is carried out under variable strain, temperature, waveform and R-ratio. Reversal of FCG ranking is observed beyond a certain tearing energy (strain) level. Waveform has the highest influence on FCG characteristics. FCG rates of these compounds are much higher in the Pulse mode compared to the Sine mode. The influence of R-ratio is most prominent in pure NR compound. NR/BR blends scores better with respect to FCG resistance compared to NR/SBR blends.

Laboratory Abrasion Tester (LAT 100) is used to measure the wear characteristics of these compounds under variable speed, slip angle and different surfaces of varied roughness (Corundum 60 & 180). The wear rises significantly with the increase of both speed and slip angle. A considerable amount of temperature increase on rubber surface is also observed due to the speed and slip angle variation. The measured wear data is fitted into an equation published in the literature, which relates wear with speed, energy dissipation and their interactions. The coefficients are calculated and one of the coefficients indicates that the crack growth dominates the wear process. This effect is more prominent in blunt surfaces (Corundum 180). A good correlation is observed between the wear and the FCG properties, especially with Corundum 180 surface.

Finite Element (FE) simulation using Abaqus software has been carried out in order to understand the inherent mechanism of FCG with different waveforms (Sine and Pulse modes). Simulations are performed using pure hyperelastic, linear viscoelastic and non-linear viscoelastic (Parallel Rheological Framework, PRF) material models. PRF model is able to capture the phenomena more clearly. It is observed that in the Pulse loading, crack tip experiences higher stress and Strain Energy Density (SENER) in comparison with the Sine mode. This is attributing to the higher FCG rate in the Pulse mode than the Sine mode. Further, in the Sine mode, Dissipated Energy Density (CENER) is higher and hence less energy is available for the crack propagation.

This thesis provides insights on the FCG characteristics and wear process of truck bus radial tyre tread compounds. It also suggests appropriate laboratory test configuration simulating realistic service conditions and assist in compound selection process during the tyre design stage itself.

TABLE OF CONTENTS

CHAPTER 1   INTRODUCTION

CHAPTER 2   OVERVIEW OF LITERATURE

CHAPTER 3 **MATERIALS AND EXPERIMENTAL METHODS**

Table of Contents (continued)   **Page No.**

CHAPTER 6   **WEAR CHARACTERISTICS OF RUBBER BLENDS**

LIST OF TABLES

LIST OF FIGURES

List of Figures (continued)   **Page No.**

List of Figures (continued)   **Page No.**

List of Figures (continued) **Page No.**

ABBREVIATIONS

ALLCD   Dissipated Energy

ALLSE   Stored Energy

ASTM   American Society for Testing and Materials

BR   Polybutadiene Rubber

CCD   Charge Coupled Device

CENER   Dissipated Energy Density

CR   Chloroprene Rubber

C3D8R   Continuum 3 Dimensional 8 Noded Reduced Integration

CV   Conventional Vulcanization

DMA   Dynamic Mechanical Analyzer

DSC   Differential Scanning Calorimetry

EPDM   Ethylene Propylene Diene Monomer

EV   Efficient Vulcanization

FCG   Fatigue Crack Growth

FEA   Finite Element Analysis

IIR   Isobutylene Isoprene Rubber

LAT 100   Laboratory Abrasion Tester 100

MDR	Moving Die Rheometer
NBR	Nitrile Butadiene Rubber
NR	Natural Rubber
Phr	Parts by mass per hundred rubber
PRF	Parallel Rheological Framework
SBR	Styrene Butadiene Rubber
SEM	Scanning Electron Microscopy
SENER	Strain Energy Density
SEV	Semi Efficient Vulcanization
TFA	Tear & Fatigue Analyzer
T_g	Glass Transition Temperature
UCST	Upper Critical Solution Temperature
UTM	Universal Testing Machine
WAXD	Wide Angle X-ray Diffraction

NOTATION

a	Wear coefficient (energy dissipation of 1 kJ/km and 1 km/h speed)
b	Material constant of FCG equation
b1	Wear coefficient (power index of abrasion energy relation)
b2	Wear coefficient (abrasion-speed relation)
b3	Wear coefficient (speed-energy relation)
c	Crack length
C_{10}, C_{20}, C_{30}	Yeoh coefficients
da/dn	Crack growth rate
F	Force
G'	Storage modulus
G''	Loss modulus
g_R	Normalised relaxation modulus
I_1, I_2, I_3	Strain invariants
L_0	FCG Specimen height
m	Material constant of FCG equation
Mc	Molecular weight between crosslinks
n_1, n_2	Number of molecules
R_w	Rate of wear
S	Side force
t	Thickness of specimen
T	Tearing energy
$\tilde{q}^n$	Equivalent deviatoric Kirchoff stress
V	Speed

V_r	Volume fraction of rubber
W	Strain energy density
$\Delta G'$	Payne effect
ΔG_m	Change of free energy due to mixing
ΔH_m	Change of enthalpy due to mixing
ΔS_m	Change of entropy due to mixing
ΔV_m	Change of volume due to mixing
k	Boltzmann constant
α	Temperature coefficient of wear
ε	Strain
$\dot{\bar{\epsilon}}^{cr}$	Equivalent creep strain rate
λ	Extension ratio
ρ	Density
χ	Rubber-solvent interaction parameter
X	Crosslink density
σ	Stress
θ	Slip angle
τ	Relaxation time

CHAPTER 1

INTRODUCTION

1.1 BACKGROUND

For many years, rubber has been recognized as an engineering material and finds vast application in diverse areas. The properties of elasticity and resilience render it suitable for applications in load carrying structural bearings, springs, seals, shock absorbing bushes, couplings and tyres. Due to its elastic nature, a high quality natural rubber compound can store over 150 times the energy stored per unit weight of spring steel. It is this capability that makes rubber a unique candidate for engineering articles. Besides the energy storage capability, there are a number of other advantages offered by well-designed rubber products. They are light weight, tough and resistant to non-ideal, ambient environments. Rubber can be considered as incompressible material. It can be usefully distorted because of its elastic nature.

Many rubber products, due to their service requirements come in contact with various surfaces. During sliding over these surfaces, the loss of rubber material takes place on continuous basis, which is termed as Abrasion or Wear. The performance of such products is largely affected by continuous loss of material at the contact surface. For instance, a worn out rubber seal will not be able to provide adequate sealing and thereby product may fail in service. Tyre is also one such product and is the only contact between the vehicle and the road surface.

Dynamic behavior of the vehicle is greatly controlled by the tyre and hence it is associated with safety as well. Tyres in a vehicle perform multiple functions which include carrying vehicle weight, providing safety by ensuring efficient dry and wet braking, dynamic lateral and longitudinal stability, cushioning the vehicle against road shocks and many more. The tread which is a radially outermost component of the tyre is the key contributor to various properties like braking, traction (dry and wet),

rolling resistance (fuel economy), noise (comfort), wear (mileage), damping etc. Most of these performance requirements are contradictory and maximizing one result in sacrificing another. Low wear and high traction or high cushioning effect and low rolling resistance are such examples. Thus, designing a tyre almost always involves an optimization or trade-off. Further, the requirements for better products from automobile industry are ever increasing. There are two ways to meet such targets, either through design or through introduction of new materials. Many a times prioritization of these properties is done based on applications like passenger or commercial vehicle. For commercial applications, higher life of the tyres is more important as it is directly related to the economics. Tyre wear is one such attribute and got attention of researchers for many decades.

A schematic of tyre rolling process is shown in Figure 1.1. It clearly shows that in every tyre rotation, the tread rubber elements are loaded for a shorter duration (~10%) followed by a longer relaxation period (~90%). This loading pattern is of non-sinusoidal type (Pulse mode). Tyres in service, undergo millions of such fatigue cycles.
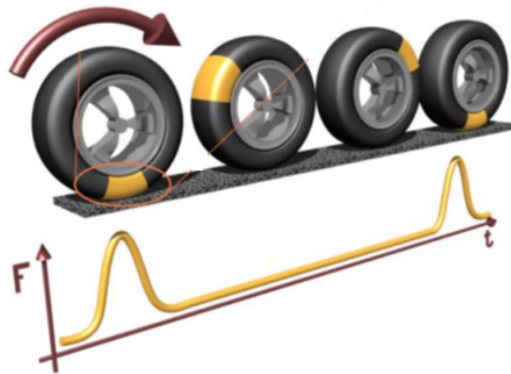
Figure 1.1 Schematic of tyre rolling process

Tyre tread material, during service directly interacts with road surfaces of varied roughness and therefore should provide adequate resistance against wear. Wear mechanism is a very complex phenomenon as it depends on tread material composition, vehicle operating condition, road surface, environmental conditions etc.

2

A number of physical and chemical processes that occur at the tyre-road interface are responsible for the wear. Mechanically, wear occurs because of the frictional energy dissipation, which is a function of contact shear stresses and micro slippage at the tyre-road interface. The loss of material from the tread surface can occur due to sudden tearing of material by sharp asperities or fatigue failure due to repetitive interaction with the road surface. The evidence from literature suggests that the fatigue failure is the major reason for wear and tearing properties of rubber (crack nucleation and propagation) may be evaluated for the purpose. In this research work, fracture mechanics based experimental methodology is adopted to study Fatigue Crack Growth (FCG) characteristics of various rubber blends using Tear & Fatigue Analyzer (TFA). The correlation establishment between FCG properties and wear would improve the predictability during the design stage of tyres.

1.2 OBJECTIVE AND SCOPE OF THE RESEARCH

Objective of this research work is to understand the wear mechanism of different radial tyre tread rubber compounds using experimental and numerical techniques.

Following tasks are undertaken to accomplish the above objective.

1. To study the FCG properties of truck bus radial tyre tread compounds based on fracture mechanics approach.

2. To study the sensitivity of different test variables viz., strain, temperature, R-ratio, waveform and cure system.

3. To develop a wear characterization method simulating real service conditions of tyres.

4. To establish a correlation between FCG properties and wear characteristics

5. To understand the influence of various waveforms on FCG properties of rubber compounds through Finite Element Analysis.

1.3 ORGANISATION OF THE THESIS

The research work is organized into a number of chapters. Chapter 1 discusses the overall introduction and objective of the research work. Chapter 2 presents relevant literature covering different rubbers and their blends, wear mechanism and application of fracture mechanics in rubber. In Chapter 3, detailed discussion on materials and experimental methods used in this work is presented. The preparation of rubber compounds comprising of NR, BR, SBR and their blends is described. The test methods of rheometric and physical properties (Hardness, Tensile, crosslink density, viscoelastic properties) are discussed. FCG and wear measurement methods are described in detail. In Chapter 4, results of fundamental properties (rheometric, physical and viscoelastic) properties are reported. The influence of material composition on these properties is studied. Chapter 5 discusses the FCG properties of all the compounds used in the present work. This clearly brings out the influence of material composition, strain, temperature, waveforms, R-ratio and cure system on FCG characteristics of these compounds. This chapter also discusses the probable mechanisms attributed to the FCG behaviour of these compounds under variable test conditions. The results of wear measurements are presented in Chapter 6. The influence of material composition and test variables (speed and slip angle), test surface (sharp and blunt) on wear characteristics is discussed. The relation between wear and FCG properties is also discussed. Chapter 7 discusses the Finite Element Analysis (FEA) of pure shear sample simulating the FCG testing under Sine and Pulse waveform. This chapter also discusses the effectiveness of non-linear viscoelastic model (PRF model) over linear viscoelastic model (Prony series) in capturing realistic material response under fatigue loading. This study clearly brings out the mechanism responsible for showing much higher FCG rate in Pulse mode compared to Sine mode. Chapter 8 summarizes the entire research work including conclusions drawn from the present research. It also includes the scope for future work.

CHAPTER 2

OVERVIEW OF LITERATURE

This chapter collates details from the literature pertaining to the present research work. This includes various forms of rubber, rubber blends, fracture mechanics approach used in rubber, rubber wear mechanisms and constitutive material modelling for Finite Element Analysis (FEA) of rubber.

2.1 NATURAL RUBBER

Natural Rubber (NR) is known to the civilized world since 1493 (Mathew, 2001). It was Christopher Columbus who found the people of Haiti were playing with balls made from latex of tree called 'cau-uchu'. The name 'rubber' was first used by Joseph Priestley in 1770 because of its ability for wiping pencil marks from paper. Chemically, Natural rubber is cis 1,4 polyisoprene and produced from the latex of Hevea Brasiliensis tree. The number average molecular weight of NR ranges from 5,00,000 to 10,00,000. The density of NR is 0.93 gm/cc. The glass transition temperature (T_g) of NR is about $- 70^0$ C. The most remarkable property of NR is high tensile strength compared to synthetic rubbers, which is due to strain induced crystallization. NR also exhibits low heat build-up characteristics. However, NR is inferior in high temperature and aging resistance compared to other synthetic rubbers.
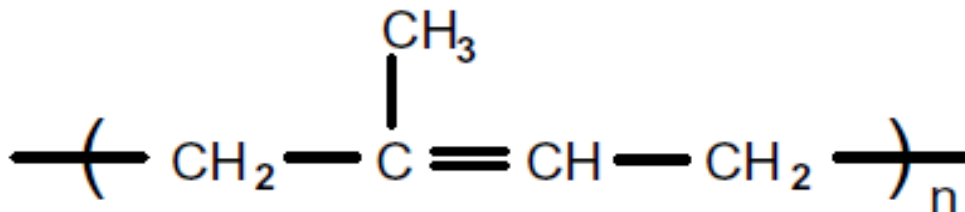
Figure 2.1 Chemical Structure of NR

2.2 STYRENE BUTADIENE RUBBER

Styrene Butadiene Rubber (SBR) was first developed in Germany as an alternative rubber due to the shortage of natural rubber supply during World War II in 1930s. It is a copolymer of styrene and butadiene, typically containing about 23% styrene. The density of SBR is 0.94 gm/cc. This rubber has T_g of approx. -55^0 C. It is the mostly used synthetic elastomer. SBR shows good traction property and resistance against high temperature aging.
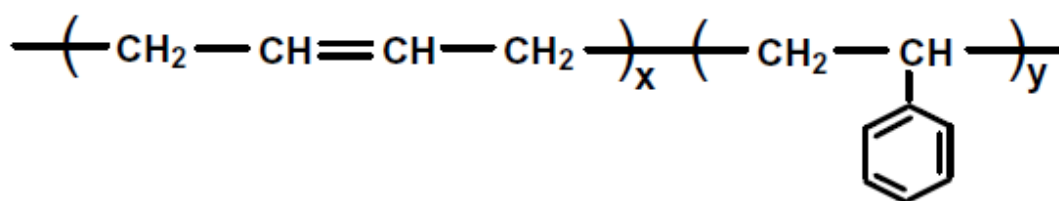
Figure 2.2 Chemical Structure of SBR

2.3 POLYBUTADIENE RUBBER

Polybutadiene Rubber (BR) is prepared by polymerization of 1,3 butadiene monomer. The high cis content (>90%) BR exhibits glass transition temperature of -90^0 C and hence exhibits very good low temperature flexibility. This rubber is known for excellent resilience and abrasion resistance.
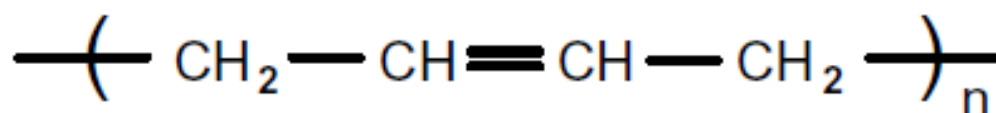
Figure 2.3 Chemical Structure of BR

2.4 RUBBER BLENDS

The blends of general purpose rubbers are widely used in various rubber products to optimize cost, processing and performance. Blending of various rubbers enable to achieve desirable properties that are not possible to be provided by a single rubber alone. The enhanced properties can be expected in terms of physical, chemical and processing properties. For example, tyre tread material should provide high traction for safety, high mileage for longer service life and cost, low rolling resistance for

6

better fuel economy and cleaner environment. It is not possible to achieve all these contradictory properties by using any single elastomer. Hence rubber blends have gained importance from both technological as well as economic point of view. Reviews on elastomer blends (Corish and Powell, 1974; Mangaraj, 2002) discussed various aspects such as rubber-rubber miscibility, cure characteristics, filler and ingredient distribution in different phases of a blend, characterization, property enhancement etc. in great detail and will also be referred here as background information.

2.4.1 Rubber – Rubber Miscibility

Generally, from a thermodynamic consideration, a spontaneous mixing of two components in a binary mixture demands the decrease of Gibbs free energy. A complete miscibility can only happen, when the change of free energy of mixing (ΔG_m) is either zero or negative. The ΔG_m due to mixing is the sum of entropy change and enthalpy change. This relation is expressed as,

$$\Delta G_m = \Delta H_m - T\Delta S_m \tag{2.1}$$

This relation clearly says that to satisfy the criteria of $\Delta G_m \leq 0$, ΔS_m should be higher than the enthalpy change (ΔH_m). There are two contributions for this entropy change. The first contribution comes from statistical thermodynamics consideration in which ΔS_m is directly proportional to the number of distinct configurations that can be assumed by an assembly of n_1 and n_2 molecules. This can be given by,

$$\Delta S_m = k \ln [(n_1+n_2) / (n_1! + n_2!)] \tag{2.2}$$

This value is very small for rubber blends due to the constraints on segmental movement of large molecules. Another contribution is due to the volume change (ΔV_m), which is also very low. On the other hand, enthalpy change (ΔH_m) arises due to various interaction energies, viz., Van der Walls, dipole-dipole, hydrogen bonding etc. For rubber-rubber blends, due to very less entropy gain, it is almost impossible to offset the positive ΔH_m except in the cases where due to presence of specific interaction leading to negative enthalpy change. It should be noted that, most of the commercial rubber blends made out of NR, BR, SBR etc. are thermodynamically

immiscible because of positive free energy change on mixing. This thermodynamic immiscibility implies that there will not be any mixing in segmental level and thereby existence of heterogeneous morphology. However, thermodynamic immiscibility does not restrict these rubbers to be used as a blend provided they are compatible and can still yield advantageous properties. The term compatible signifies that the blend does not undergo macroscopic phase separation. It is important to mention here that most of these rubber blends have Upper Critical Solution Temperature (UCST), which means that above this critical temperature, components are miscible in all proportions.

2.4.2 Filler Distribution in Blend

The fillers (carbon black, silica etc.) in rubber compounds are widely used for reinforcement purpose and reduction of cost. The reinforcement effect of filler varies among rubbers which are due to the differences in rubber-filler interactions. In rubber blends, non-uniform distribution of filler is very common due to the preferential migration towards a specific component in a blend system. Mangaraj (1992) have demonstrated that in 50/50 blends of different rubbers, the affinity of carbon black decreases in the order of BR, SBR, CR, NBR, NR, EPDM and IIR. Sircar and Lamond (1974) also showed that higher concentration of carbon black exists in BR phase of NR/BR and SBR/BR blends. According to Hess *et al.* (1967), higher carbon black concentration exists in BR phase of 50-50 NR/BR blend tyre tread compound is better to achieve superior wear resistance.

2.4.3 Crosslink Distribution in Blend

The non-uniform distribution of vulcanizing agents like sulfur, accelerator, peroxide etc. in blends is possible because of the differences in solubility, polarity, reaction sites etc. This leads to uneven distribution of crosslink densities in two phases and therefore properties are also affected. The misdistribution of crosslink density can arise from several factors such as curatives (amount, type and combination of curatives), curing time, incorporation sequence of curatives etc. Groves (1998) studied the influence of curing temperature on crosslink density distribution of 70-30 NR/BR blends. It was observed that at 130^0 C, higher crosslink density was achieved in NR phase compared to BR. However, reversal of the crosslink distribution was observed when curing temperature was increased to 140^0 C and beyond.

2.5 APPLICATION OF FRACTURE MECHANICS IN RUBBER

Fracture mechanics approach deals with the characteristics of a cracked structure under application of loads. It assumes the existence of cracks in the structure and its propagation under stresses, strain etc. The pioneering work by Rivlin and Thomas (1953) is considered to be the foundation of fracture mechanics based research to study the crack growth behaviour of elastomeric materials. They have extended the Griffith's energy balance criterion which was originally developed to study crack growth behaviour of brittle materials and applied in rubbers. In rubber, the energy required to drive the crack is termed as energy release rate or more commonly called as tearing energy and can be defined as

$$T = - (\delta W / \delta A) \tag{2.3}$$

where, T is the tearing energy, W is the elastic strain energy and A is the interfacial area of grown crack. Note that the above derivative is calculated at a constant displacement and hence no external work is added. It was also demonstrated that the static crack growth occurs after exceeding the critical value of tearing energy or stored energy release rate which is independent of test specimen geometry and hence it can be considered as a true material property (Thomas, 1994). The description about different test specimen geometries which are commonly used for measuring tearing energy is given in the subsequent section.

2.5.1 Trouser Test Specimen

Trouser specimen is the most commonly used test specimen for measuring tearing energy and is shown in Figure 2.4. The thin sample is cut to provide two legs for clamping in testing equipment. The tearing energy calculation for this type of specimen is given by,

$$T = (2F\lambda/t) - w.W \tag{2.4}$$

where, F is the applied force, λ is the extension ratio, w is the width of the specimen, t is the thickness of the specimen and W is the strain energy density.

2.5.2 Pure Shear Specimen

Pure shear specimen is shown in Figure 2.5. In this geometry, width is much higher compared to height of the sample and preferred height to width ratio should be equal or higher than 1:10. The tearing energy for pure shear specimen can be calculated by the following equation,

$$T = WL_o \qquad (2.5)$$

where W is the strain energy density and L_0 is the height of the sample. Since tearing energy is independent of crack length, multiple crack growth measurements can be performed using a single pure shear specimen. This in turn reduces chances of variation in results due to differences in specimens. Stocek *et al.* (2009, 2012) used pure shear specimens having notch on both edges for fracture studies of various rubber compounds which is advantageous with respect to the testing time. Andreini *et al.* (2013) compared FCG properties of pure shear and tensile samples using SBR, NR and BR compounds.

2.5.3 Simple Tension Specimen

In simple tension (Figure 2.6), notch is provided on one edge and the tearing energy is calculated by the following relation,

$$T = 2kWc \qquad (2.6)$$

where, *W* is the strain energy density, *c* is the crack length and k is approximately calculated by the following expression

$k = \pi/\sqrt{(1+\varepsilon)}$
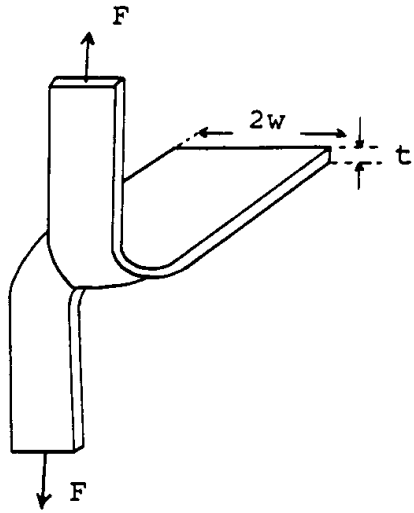
Figure 2.4 Trouser specimen geometry
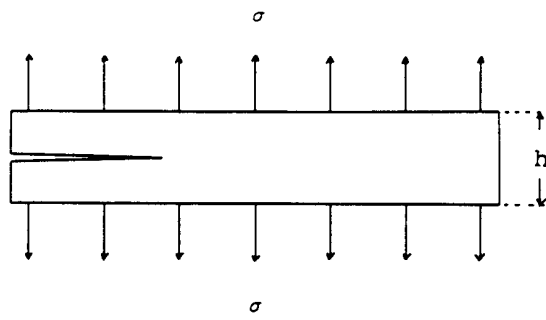
Figure 2.5 Pure shear specimen geometry
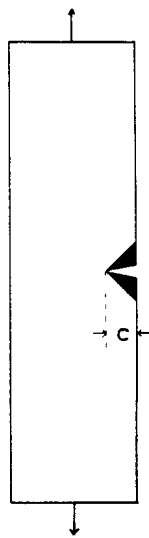
Figure 2.6 Simple tension specimen geometry

11

2.6 FATIGUE CRACK GROWTH AND INFLUENCING FACTORS

During service, rubber products like tyres, belts, bushings etc. are subjected to cyclic loading. This repetitive loading cause progressive weakening of physical properties of the rubber products and eventually fails much below their catastrophic tear strength due to cumulative accumulation of damage in the object. These types of failures are termed as fatigue failure and this behaviour can be studied using fracture mechanics. One of the basic premises of fracture mechanics is the presence of natural cracks in any structure. In rubber material such type of intrinsic defects are present in the form of micro voids, inhomogeneous distribution of additives like filler, curatives etc. These heterogeneities lead to high local stress concentrations and initiate fatigue failure. The fatigue crack growth rate of rubber is a function of tearing energy. Mars and Fatemi (2002) identified four distinct regimes of fatigue crack growth behaviour which are shown in the Figure 2.7.
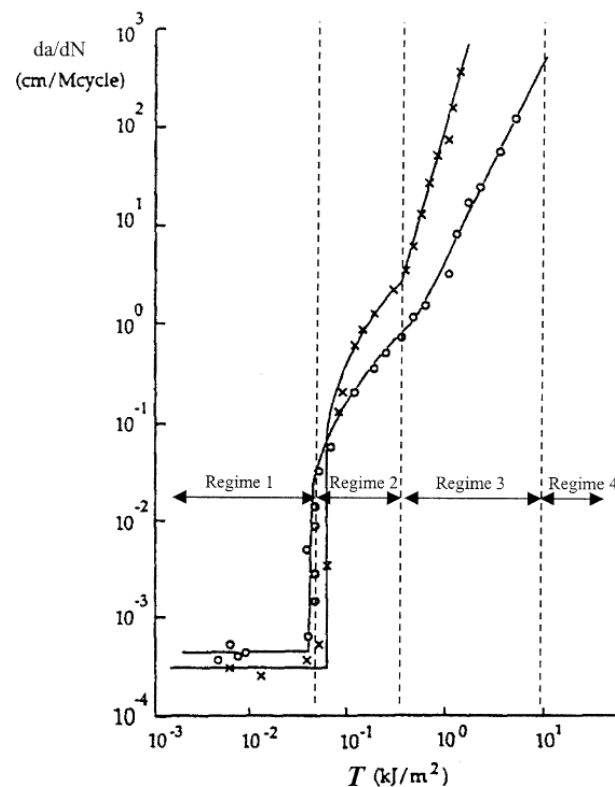
Figure 2.7 Fatigue crack growth regimes of rubber (Mars and Fatemi, 2002)

In the regime I where tearing energy T is below the threshold value T_0, crack growth proceeds at a constant rate r, solely due to environmental (ozone) attack and can be expressed as,

$$da/dn = r \quad T \leq T_0 \tag{2.7}$$

The regime II is the transition region and the mathematical relation between the crack growth rate and the tearing energy is given by,

$$da/dn = r + A (T-T_0) \quad T_0 \leq T \leq T_t \tag{2.8}$$

where A is the material property.

In regime III, crack growth rate and tearing energy obeys power law relation, in which b and m are material constants. As per Grosch (2005), the rate constant b is influenced by the temperature and the presence of oxygen. The exponent m mainly depends on type of rubber. It was also mentioned that wear mostly occurs in this region of FCG curves except for very sharp track.

$$da/dn = bT^m \quad T_t \leq T \leq T_c \tag{2.9}$$

The value of m ranges between1 to 6 for vulcanized rubbers depending upon the type of rubber, composition etc.

In regime IV, unstable crack propagation occurs and crack growth rate is infinite,

$$da/dn = \propto \quad T=T_c \tag{2.10}$$

Several researchers (Lake and Thomas, 1992; Ellul, 1992; Mars and Fatemi, 2004) have reviewed different factors which affect the fatigue life of rubber including mechanical load history, environmental conditions, rubber formulation and constitutive behaviour. The effect of some of the important parameters covering both material and testing condition is presented in the subsequent sections.

2.6.1 Rubber

The influence of various types of rubber on fatigue crack growth behaviour is due to variation in their molecular architecture. For example, some rubbers such as NR, CR etc. have the ability to strain crystalize which influence mechanical properties in comparison with non-strain crystallize rubbers. Young (1985) reported FCG power law parameters for four different rubbers and their blends. It has been observed that the crack growth exponent is low for NR and CR due to strain crystallization and also superior at higher tearing energy compared to other rubbers. It was also suggested that better FCG resistance could be achieved by blending process. Lee (1993) reported higher mechanical fatigue limit for 50-50 NR/BR blend compared to the pure NR and BR compounds. Chung and Chang (2001) presented fatigue crack growth study of NR/EPDM blends. They also found that the fatigue crack growth rate of all blends is lower compared to average properties of constituent elastomers over a wide range of tearing energy.

2.6.2 Filler

Practical rubber compounds contains various fillers like carbon black, silica, clay, magnetic fillers etc. to achieve various objectives. As reported by Mars and Fatemi (2004), the contribution of fillers on fatigue properties are attributed to various mechanisms which include enhancement of stiffness characteristics, changes in dissipation characteristics, crack tip blunting, crack path deviation and increase in effective initial flaw size due to agglomeration of filler particles. It was also reported that fatigue properties improve when the filler loading is below the optimal volume fraction. The deterioration of fatigue properties is observed above the optimal volume fraction which is due to the increase in the effective initial flaw size. The coarseness of filler also plays an important role towards fatigue life and finer grades are better than coarser grades (Dizon *et al*., 1974). Kim and Jeong (2005) studied the influence of N330, N650 and N990 carbon black on fatigue properties of NR compound. They have observed the fatigue life as follows: the ranking of N330 is greater than N990 or N650. Nie *et al.* (2010) shown that NR with N330 carbon black exhibited superior FCG characteristics due to higher viscoelastic dissipation compared to N770 carbon black. Reincke *et al.* (2009) shown that at similar filler loading, silica provide better FCG resistance compared to carbon black.

2.6.3 Curing System

Rubber compounds are vulcanized (cured) using various curing agents (Sulphur/Accelerator, Peroxide etc.) and in this process crosslinks are formed between polymer chains. In sulphur / accelerator curing system, crosslinks formed could be of mono, di and polysulphidic type. Polysulphidic linkages are better for fatigue compared to mono or disulphidic because it can break before the main polymer chain carbon-carbon bonds and there can be subsequent reformation of the linkages (South, 2001). Yanyo (1989) studied the influence of peroxide curing vs. sulphur curing in NR compound and found that the crack growth rate follows the order of Peroxide (c-c), sulphur (monosulphidic), sulphur (polysulphidic). Kim and Lee (1994) compared various curing systems, EV (Efficient Vulcanization), SEV (Semi Efficient Vulcanization) and CV (Conventional Vulcanization) for filled and unfilled compounds. They have observed that for unfilled compounds (unaged), these curing systems have no influence on fatigue properties. However for filled compounds, crack growth rate follows the order of EV, SEV and CV in the high tearing energy zone.

2.6.4 Temperature

According to Lake and Lindley (1965), influence of temperature on fatigue properties is much higher in amorphous rubbers compared to NR. It was reported in this work that in unfilled SBR compound, crack growth rate increased by 10^4 times when the temperature was increased from 0 to 100^0 C. On the other hand, NR compound reported only a four-fold increase in the FCG rate for the same temperature range. The deleterious effect of temperature on fatigue properties was also observed by Young and Danik (1994) for under-cured NR belt skim compound. Legorju-jago and Bathias (2002) also found significant increase in crack growth rate with temperature increase for NR compound. The influence of temperature on fatigue properties of single component vs. blend system was investigated by Qazvini *et al.* (2002). They have found that continuous decrease in fracture energies with the temperature increase for single component system whereas for blend compounds it passes through the minima and then increases considerably.

2.6.5 Waveform

Majority of the rubber products are subjected to dynamic loading during service such as tyres, engine mounts, belts etc. Due to experimental convenience, most of the dynamic testing is carried out under sinusoidal loading. However, considering the realistic service condition of the tyres, the loading pattern is more of non-sinusoidal type. In every cycle of rotation, components of the tyre experiences loading for a very short duration followed by a longer rest period, which closely resembles the Pulse mode rather than the sinusoidal loading. One of the earliest research works describing the role of non-sinusoidal loading in dynamic properties was presented by Harris (1987). According to him, there are two basic limitations of sinusoidal loading. Firstly, it does not accommodate non-linearity in dynamic property definition and secondly, dissimilarities with actual service conditions. Various researchers have studied the influence of waveform type on fatigue properties of rubber. Harbour *et al.* (2007) provided dwell time between fatigue cycles and found significant increase in FCG rate compared to the constant amplitude test (sinusoidal). It was also observed that the influence was higher in SBR than NR. Andreini *et al.* (2010), compared the FCG rates of NR, BR and SBR under Sine and Pulse loading with dwell period of 900 ms. Although Pulse loading showed higher FCG rate in NR and BR material, no such increase was observed in SBR. The influence of waveform frequency on fatigue life was reported by Harbour *et al*. (2008). They have observed two times decrease in the fatigue life at 1 Hz test frequency in comparison with 0.2 Hz test condition due to 25^{0} C increase of the sample surface temperature.

2.6.6 R- ratio

During service, many of the rubber products are subjected to constant pre-load condition, which certainly has an impact on the fatigue properties. The loading sequence is conveniently defined as R-ratio (ratio of minimum to maximum amplitude of applied force, strain etc.) and a schematic diagram is shown in Figure 2.8. The work of Lindley (1973) revealed that the FCG rate decreases considerably in unfilled NR compound for positive R-ratios as shown in Figure 2.9. Mars and Fatemi (2003) also studied this aspect in great details and proposed a phenomenological model. Saintier *et al.* (2011) studied the fatigue behavior of NR compound under relaxing (R=0) and non-relaxing (R > 0) condition. SEM and WAXD studies

revealed that the crack branching due to crystallization is attributed to the excellent fatigue resistance under non-relaxing condition. Abraham *et al.* (2004) studied the influence of minimum stress on the fatigue life of non-strain crystallising rubbers and found that the fatigue life increases with the increase in minimum stress at constant strain amplitude. Stadlbauer *et al.* (2013) also reported significant influence of the amplitude ratio (R-ratio) on fatigue behaviour including blends comprising of non-strain crystallising rubbers (50-50 BR/SBR). They have also reported that in the case of negative amplitude ratio, crack growth rate increased considerably which is contrary to the results obtained with the positive amplitude ratio.
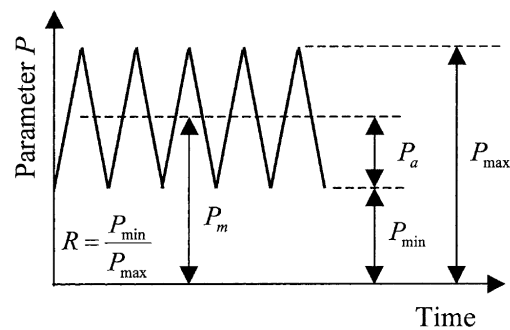
Figure 2.8 Schematic of loading history (Mars and Fatemi 2004)
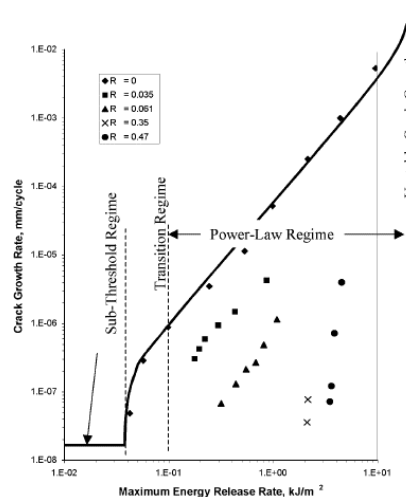
Figure 2.9 Fatigue crack growth results for unfilled NR compound under relaxing and non-relaxing condition (Lindley, 1973)

17

2.7 WEAR MECHANISM

Tyre tread material, during service, directly interacts with road surfaces of varied roughness. The repetitive interactions lead to continuous loss of material from the tread surfaces because of friction between the two mating surfaces. Therefore, the tread material should have adequate resistance against abrasion loss or wear. There are a number of physical and chemical processes, which take place at the tyre-road, interface that are responsible for the tyre wear. Mechanically, tread wear occurs because of frictional energy dissipation, which is a function of contact shear stresses and micro slippage at the tyre-road interface. As reported by Liang (2007), rubber wear process takes place in three different phases. It starts with the initiation phase where wear rate is relatively faster. In the second phase, steady state condition is achieved with a lower rate of wear. The majority of the life span of rubber components is in this phase. In the final phase, wear rate is again faster leading to catastrophic failure. So, it is important to investigate the mechanisms associated with the steady state phase considering the fact that the rubber products spent most of the life time here.

Numerous research works have been carried out to understand the wear mechanism which mostly focused on the steady state phase. Schallamach (1956) has shown that when rubber is subjected to sliding, a characteristic ridge formation takes place on the rubber surface perpendicular to the sliding direction. These ridges are termed as abrasion or Schallamach pattern. During sliding, interaction with sharp road asperities leads to stress concentration at the root of these patterns and thereby material is torn off after a number of cycles. Fukahori and Yamazaki (1994a) proposed the stick-slip mechanism for rubber wear which also considers formation of abrasion pattern (ridges) perpendicular to the sliding direction. When a hard slider slides over the rubber surface, it sticks on the surface for a while followed by rapid slip (Figure 2.10). The initiation of the crack occurs during the slip phase due to the existence of violent micro-vibration (500-1000 Hz). The subsequent propagation of the cracks takes place mostly in the stick phase because of higher contact compared to the slip phase. Fukahori and Yamazaki (1994b) also studied the micro-vibration behaviour of carbon black filled and unfilled rubbers. It was observed that the micro-vibration attenuates more rapidly in the filled rubbers compared to the unfilled rubbers (Figure 2.11).

Further spreading of the vibration is near to its origin only in the filled rubbers. These effects have great influence towards the wear resistance characteristics of filled rubbers. Fukahori *et al.* (2008) also studied the crack initiation and its growth using both experimental and FEA simulation approach. They have shown from the FEA prediction that the crack nucleates at the location where the tensile stress is maximum.
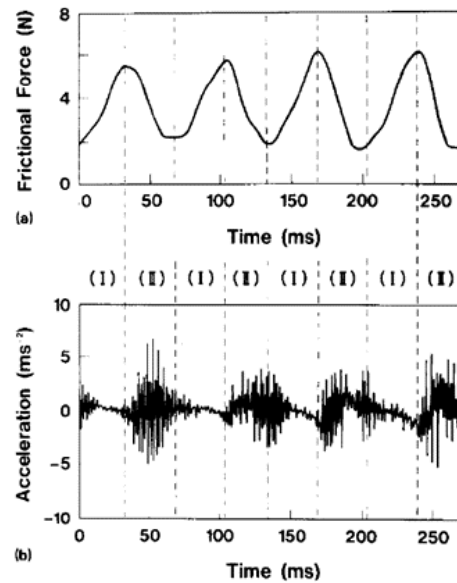
Figure 2.10 Spectrum of (a) frictional force vs sliding time, (b) acceleration vs sliding time. I – Stick phase, II – Slip phase (Fukahori and Yamazaki 1994a)
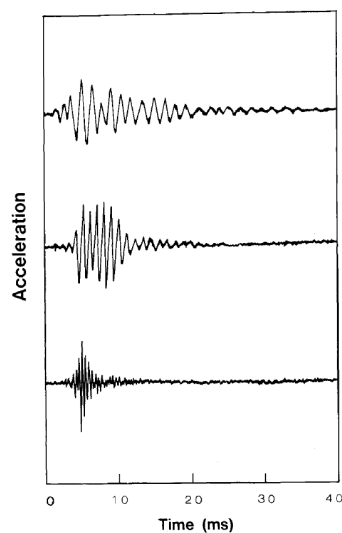
Figure 2.11 Attenuation of the micro-vibration; NR1 (Upper-Unfilled), NR2 (Middle - 20 parts carbon black), NR3 (Lower – 50 parts carbon black). (Fukahori and Yamazaki 1994b)

19

Petitet *et al.* (2005) investigated the tread wear pattern generated during straight highway driving at constant speed. In this mild condition, the wear pattern appears like small holes on the surface which are of 100 μm in diameter and 10 μm deep. This is termed as crater wear pattern. These craters are created because of the detachment of filler agglomerates from the rubber compounds. The stiffness of agglomerates is much higher than rubber materials and its plastic yield is around 10% strain. Scratch and roll type wear patterns have also been reported. Scratch type wear patterns are more likely formed when sliding length is long and the speeds are high. Roll formation takes place when the surface is very smooth because of very high adhesion friction. The images of various wear patterns are provided in Figure 2.12 (Petitet *et al.*, 2005).

a) Ridges. They are perpendicular to the sliding direction.

b) Scratches. They are parallel to the sliding direction.

c) Rolls. They are dust particles stuck onto the rubber surface.

d) Craters. They are holes on the rubber surface.
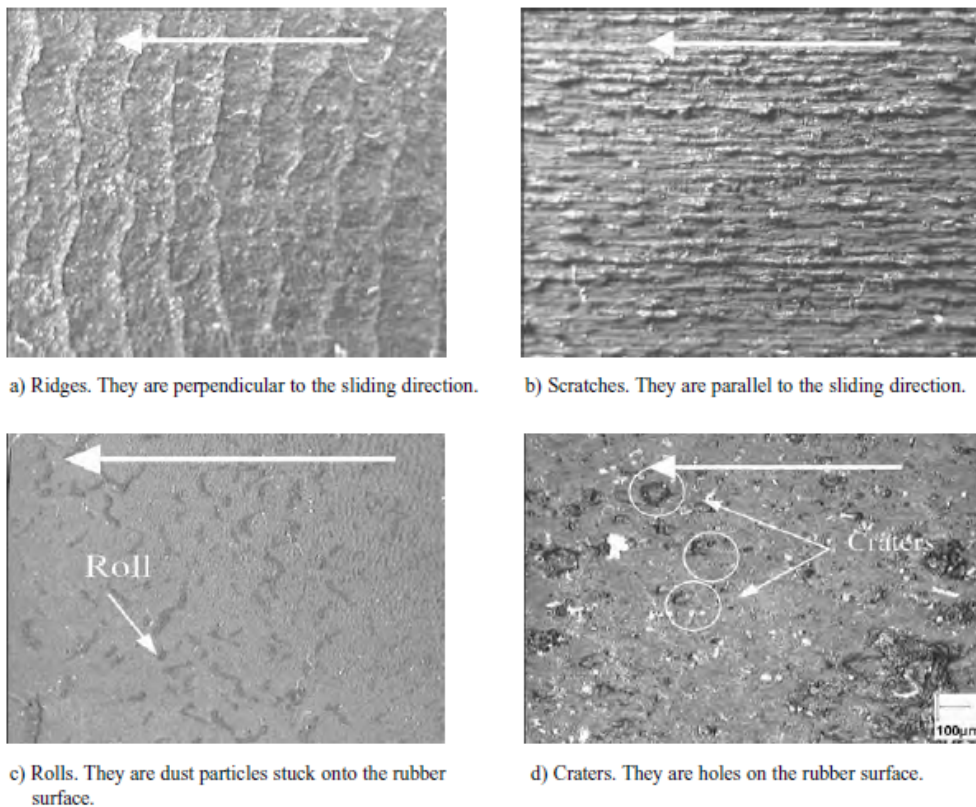
Figure 2.12 Four different types of wear patterns (Petitet *et al.*, 2005)

According to Southern and Thomas (1979), cut growth characteristics of rubber and the angle of the crack at the base of the wear pattern decides the wear rate. Further, they have also concluded that the viscoelastic effects are also important for rubber wear. Gent and Pulford (1983) studied the abrasion mechanism of various gum and

carbon black filled rubbers and concluded that the rate of wear is partly due to the mechanical fatigue and partly because of the direct fracture process. According to Cho and Lee (2000), fatigue induced wear occurs below a critical tearing energy and above which it is due to tearing of the rubber material.

The work of Moore (1980) emphasized the role of friction on tyre wear. The two major components of rubber friction i.e. adhesion and hysteresis friction are responsible for abrasion and fatigue wear respectively depending upon the surface condition. Fukahori and Yamazaki (1995) also proposed a model on abrasive wear mechanism and shown the relation between friction and wear. A comprehensive review on important factors affecting tread wear can be found in the work published by Veith (1994). All the major aspects like material, tyre construction, road texture etc. were taken into consideration. One of the important observations from this work is that the influence of various factors on abrasion and fatigue wear does not reinforce each other. Parameters such as tread material tread material glass transition temperature (Tg), road macro and micro texture etc. may compensate one another. Kern and Futamura (1988) discussed the effect of macro and micro structure of rubber on tyre wear performance. It was reported that higher molecular weight is preferred to achieve superior wear resistance.

According to Persson *et al.* (2005), the wear process involves nucleation of crack like defects and subsequent propagation of these cracks leads to detachment of rubber particles. They have also concluded that the majority of tyre wear takes place due to the fatigue failure of the interface rubber material. In recent years, several researchers have tried to correlate the laboratory abrasion data with the road wear test. Krishnan *et al.* (1995) obtained a good correlation between the road wear test and the laboratory abrasion data measured using silicon carbide surface. Grosch (2004) used LAT 100 equipment to generate abrasion data under various loads, speeds, slip angle combination and able to predict tyre tread life (mileage) using a computer program. The predicted mileage was in good agreement with the actual road tests.

This literature survey revealed that the tyre wear could be categorized into two major classes: abrasion and fatigue wear. The occurrence of either of these two categories or their combinations depends on the type of material and service conditions including

21

road surface texture. It is also evident from the survey that the cut growth properties of rubber plays important role in the wear process and hence fracture mechanics of rubber needs to be understood.

2.8 CONSTITUTIVE MATERIAL MODELLING

The rubber materials are composed of macromolecules and can undergo large non-linear elastic deformation. The theory of rubber elasticity presented by Treloar (1975) is extensively used for describing large strain deformation characteristics of rubber materials. For many decades, FEA became an integral part of the design process while designing rubber components such as engine mounts, rubber bushing, tyres etc. Hence constitutive material modelling of rubber plays very important role in the FEA of rubber products. The material description of rubber consists of Hyperelastic (time independent) and Viscoelastic (time dependent) properties that are discussed in the subsequent sections.

2.8.1 Hyperelastic Material Modelling

Hyperelastic material models are used to describe the materials which undergo large deformation, non-linear elastic and nearly incompressible behaviour. These materials are defined by strain energy density function, as given in Appendix A (Holzapfel, 2000; Treloar, 1975). There are many hyperelastic models that have been developed to describe mechanical behaviour of rubber and rubber like materials. These are also implemented in commercial FEA codes (Abaqus, Ansys, Marc etc.). Boyce and Arruda (2000) presented a comprehensive review on constitutive models of rubber elasticity. Broadly, these models have been classified into two major categories: statistical and phenomenological models. The statistical models are also known as physically motivated models which considers statistical distributions of length, orientations and structure of rubber molecular networks. Neo-Hookean, Arruda-Boyce, Gent, Extended Tube models are developed based on the statistical approach.

Phenomenological models are based on the continuum mechanics approach which mathematically describes the stress-strain behaviour of the material without reference to the microscopic structure. Examples of such models include Mooney-Rivlin, Ogden, Yeoh, Valins-Landel, Peng etc. Seibert and Schoche (2000) compares

different constitutive models with respect to predictability of multi-axial deformation states on the basis of uniaxial test data. Arruda-Boyce, van der Walls and Yeoh models predicted biaxial states quite well from the uniaxial input data. Yeoh model (1990, 1993) is a special form of polynomial model in which the second invariant is omitted and is also known as reduced polynomial model. This is a simple model and capable to describe large strain behaviour quite efficiently. The mathematical expression of Yeoh model is given below.

$$W = C_{10}(I_1 - 3) + C_{20}(I_1 - 3)^2 + C_{30}(I_1 - 3)^3 \tag{2.11}$$

where W is strain energy density, I_1 is the first strain invariant, C_{10}, C_{20} and C_{30} are material constants. These material constants are the key inputs for FEA of rubber materials. Several researchers (Chow and Cundiff, 1987; Charlton *et al.*, 1994) have highlighted the importance of material characterisation of rubbers for use in FEA. Seibert and Schoche (2000) also emphasized on the selection of material models for FEA. It clearly brings out that the predictability of FEA largely depends on the quality of the material parameters and the selection of the constitutive model.

2.8.2 Viscoelastic Material Modelling

Maxwell and Kelvin-Voigt models are the most commonly used material model to represent the linear viscoelastic behaviour such as stress relaxation, creep etc. for rubber materials using spring and dashpot combinations. In Maxwell model, spring and dashpot are arranged in series. The Kelvin-Voigt model consist spring and dashpot in parallel. In Abaqus, linear viscoelasticity is represented by Generalised Maxwell model in which multiple springs and dashpots are used in series. The viscoelastic response (stress relaxation or creep) can be defined using Prony series representation which takes the following form.

$$g_R(t) = 1 - \sum_{i=1}^{N} \bar{g}_i^P \left(1 - e^{-t/\tau_i^G} \right) \tag{2.12}$$

where, $g_R(t)$ is normalised relaxation modulus, N = no. of Prony terms, $\bar{g}_i^P$ and τ_i^G are the material constants.

Hurtado *et al.* (2013) proposed a model, called Parallel Rheological Framework (PRF) model which can model non-linear viscoelasticity, permanent set and Mullins effect of rubber. The schematic of this model is shown in Figure 2.13 where multiple elastic and viscoelastic networks are connected in parallel.
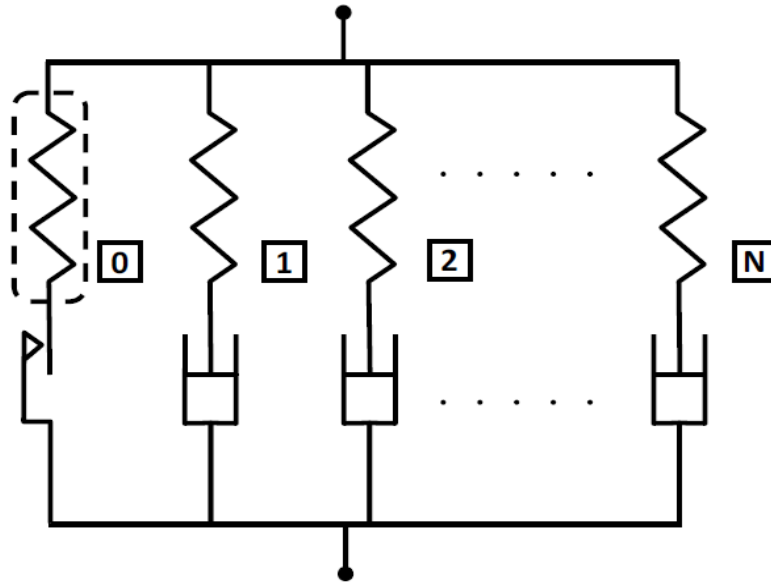
Figure 2.13 Schematic representation of PRF model (Hurtado *et al.*, 2013)

The overall stress response is additive for this model. This model also has one equilibrium network whose response could be completely elastic or elasto-plastic. This model is implemented in Abaqus and also a tyre rolling simulation using this model is presented by Nandi *et al.* (2014). The elastic response of each network is represented by hyperelastic material behaviour (Neo-Hookean, Yeoh etc.). The viscous response can be defined using creep laws (Strain Hardening Power Law, Hyperbolic Sine Law etc.).

The Strain Hardening Power Law takes the following form:

$$\dot{\bar{\epsilon}}^{cr} = \left(A \ \tilde{q}^n \ \left[(m+1)\overline{\epsilon}^{cr} \right]^m \right)^{\frac{1}{m+1}} \tag{2.13}$$

Where $\dot{\bar{\epsilon}}^{cr}$ is the equivalent creep strain rate, $\overline{\epsilon}^{cr}$ is the equivalent creep strain, $\tilde{q}^n$ is the equivalent deviatoric Kirchhoff stress and *A, m & n* are material parameters.

24

2.9 SUMMARY

This chapter reviews the state-of-the art literature on various aspects of rubbers and mechanisms of various properties relevant to the present work from the published literature. This review discussed the characteristics of different general purpose rubbers and their blends. The complexities associated with the blend system are discussed in detail. Different mechanisms and influencing factors pertaining to FCG and wear behaviour are presented. A brief discussion on hyperelastic and viscoelastic constitutive models is also presented.

CHAPTER 3

MATERIALS AND EXPERIMENTAL METHODS

This chapter describes the materials and experimental details including test equipment and test methodologies used in this work.

3.1 MATERIALS

This section provides details on all the raw materials used, material compositions and preparation of rubber compounds.

3.1.1 Details of Raw Materials

Details of different raw materials used in the present study are provided in Table 3.1. This includes information about sources, grades and technical specifications of all the materials.

Table 3.1 Raw material details

Material	Source	Technical Specification
Natural Rubber (NR) RMA - IV	IRITTY SPICES, Tripura, India	Mooney Viscosity – 80 Dirt Content – 0.50 % max.
Polybutadiene Rubber (BR)	Reliance Industries Ltd., India	Specific Gravity – 0.910 Mooney Viscosity – 45 Cis Content – 97%
Styrene Butadiene Rubber (SBR) SBR 1502	KKPC	Specific Gravity – 0.940 Mooney Viscosity – 52 Bound Styrene – 23.5%
Carbon Black, N339	PCBL, India	Iodine No. - 90.0 N2 Surface Area – 90 m^2 /gm

Table 3.1 Raw material details (contd.)

Material	Source	Technical Specification
Aromatic Oil	Indian Oil Corporation Ltd., India	Specific Gravity – 0.990 Aniline Point – 40^0 C
Zinc Oxide	Upper, India	Specific Gravity – 5.570 N2 Surface Area – 1.5 m^2/gm
Process Aid (A 60)	Sri Pukhraj Additives, India	Specific Gravity – 1.10 Ash Content – 20%
Stearic Acid	Godrej Soaps	Specific Gravity – 0.930 Saponification No. – 201.5 mg KOH /gm
6PPD [N-(1,3-dimethylbutyl),N'-phenyl-p-phenylenediamine]	NOCIL, India	Specific Gravity – 1.015 Melting Point – 49^0 C
Micro Crystalline Wax	Rhein Chemie, Germany	Specific Gravity – 0.920
Paraffin Wax	Gujarat Paraffins, India	Specific Gravity – 0.915 Drop Melting Point – 65^0 C
Soluble Sulphur	Jaisheel Chemicals, India	Specific Gravity – 2.050 Solubility in CS_2 – 100
NOBS (N-Oxydiethylene, 2-benzothiazole sulfonamide)	NOCIL, India	Specific Gravity – 1.370 Melting Point – 84^0 C
N cyclo hexyl thio thalimide	NOCIL, India	Specific Gravity – 1.3 Melting Point – 91.5^0 C
Pentacholoro thiophenol	AcmeChem Ltd., India	Specific Gravity – 2.200

3.1.2 Composition of Rubber Compounds

In the present work, compounds made of NR, BR, SBR, and blends of NR/BR and NR/SBR were used. Detailed compositions of these compounds are provided in Table 3.2 and 3.3.

3.1.3 Preparation of Rubber Compounds

The rubber compounds were prepared using a laboratory Banbury mixture (Make: Stewart Boling, UK) of 1.5 litre capacity in three stages. In the first stage, rubbers and all chemicals except curatives were mixed at 60 rotations per minute (rpm) for 4 min time at about 140^0 C temperature. Then the mixed compound is re-milled at 30 rpm for 3 min time at about 120^0 C. The final batch containing curatives is mixed at 30 rpm for 3 min at 100^0 C.

Table 3.2 Composition details of NR, BR and NR/BR blends

Ingredients	A1	A2	A3	A4	A1-Modcure	A4-Modcure	A5
NR	100	80	70	60	100	60	-
BR	-	20	30	40	-	40	100
Peptizer	0.15	0.12	0.10	0.10	0.15	0.10	0
Carbon Black	50	50	50	50	50	50	50
Aromatic Oil	14	12	8	6	14	12	5
Process Aid	2	2	2	2	2	2	2
Zinc Oxide	2.50	2.50	2.50	2.50	2.50	2.50	2.50
Stearic Acid	2.50	2.50	2.50	2.50	2.50	2.50	2.50
Antioxidant	2.25	2.25	2.25	2.25	2.25	2.25	2.25
Microcrystalline Wax	1	1	1	1	1	1	1
Paraffin Wax	1	1	1	1	1	1	1
Soluble Sulphur	2	1.7	1.6	1.5	1.5	2	1.30
Accelerator	0.50	0.55	0.60	0.80	0.80	0.50	1.15
Pre-Vulcanization Inhibitor	0.20	0.04	0.04	0.02	0.20	0.02	0.02

Table 3.3 Composition details of SBR and NR/SBR blends

Ingredients	B2	B3	B4	B5
NR	80	70	60	-
SBR	20	30	40	100
Peptizer	0.12	0.10	0.10	0
Carbon Black	50	50	50	50
Aromatic Oil	14	16	17	16
Process Aid	2	2	2	2
Zinc Oxide	2.50	2.50	2.50	2.50
Stearic Acid	2.50	2.50	2.50	2.50
Antioxidant	2.25	2.25	2.25	2.25
Microcrystalline Wax	1	1	1	1
Paraffin Wax	1	1	1	1
Soluble Sulphur	2	1.90	1.80	1.60
Accelerator	0.70	0.85	1	1.80
Pre-Vulcanization Inhibitor	0.04	0.04	0.04	0.02

3.2 EXPERIMENTS

This section provides details on different equipment used for the present work and test methods followed for characterisation of various properties.

3.2.1 Rheometric Properties

Rheometric properties of all the mixed compounds were measured using a Moving Die Rheometer (Dynesco MDR 2000E, Figure 3.1) under 0.5 arc and 100 CPM frequency. The measurement temperature and duration was 141^0 C and 1 hour respectively.

3.2.2 Sample Preparation for Mechanical Property Measurement

Tensile slabs of 150 mm x 150 mm were prepared by curing rubber compounds for 60 min at 141^0 C temperature in a compression mould (Make: Santosh Industries Ltd., India) and the pressure is maintained at 14.7 MPa.
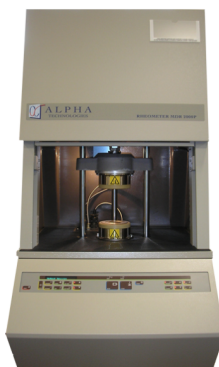
Figure 3.1 Moving Die Rheometer (MDR 2000)

3.2.3 Mechanical Properties

Tensile stress-strain properties of all the compounds were measured as per ASTM D412 standard using Zwick Z010 Universal Testing Machine (Figure 3.2). The dumbbell specimens are tested at the speed of 500 mm/min crosshead displacement. The hardness of these compounds is measured using Hardness Meter of Shore A type.

Figure 3.2 Universal Testing Machine (Zwick Z010)

3.2.4 Crosslink Density

Crosslink density of all the compounds was determined as per the method described in literature (Ellis and Welding, 1964; De and Gent, 1996). Sample (weight ~ 0.2 gm) is taken from vulcanized rubber sheet and the initial weight (T) is recorded. Then the

sample is immersed in toluene and kept for 48 hrs. After this time period, the sample is removed and it is blotted with filter paper to remove the loose solvent from the sample. Then the swollen weight of the sample is recorded. The sample is then dried in an air oven at 70^0 C and the weight of the de-swollen sample (D) is taken. The insoluble fraction (F) is also calculated by dividing the weight of carbon black and zinc oxide by the total weight of the stock. The volume fraction of the rubber (v_r) is calculated by the following equation.

$$v_r = (D - FT)\, \rho^{-1} / (D - FT)\, \rho^{-1} + A_0\, \rho_s^{-1} \qquad\qquad (3.1)$$

where A_0 is the weight of the absorbed solvent, ρ and ρ_s are the densities of rubber and solvent respectively.

Then crosslink density (X) is calculated using Flory – Rehner relation,

$$ln\, (1\text{-}v_r) + v_r + \chi v_r^{\,2} = -\, (2\rho VX) v_r^{\,1/3} \qquad\qquad (3.2)$$

where χ is rubber – solvent interaction parameter, V is the molar volume of the solvent which is 106.36 mole / cc.

Molecular weight between crosslinks (M_c) is calculated by the following equation

$$Mc = 1/2X \qquad\qquad (3.3)$$

where X is the crosslink density in gm mole / gm.

3.2.5 Hyperelastic Properties

The hyperelastic properties of all the compounds were measured in uni-axial extension mode in Zwick Z010 machine. The dumbbell sample of ASTM D 412 Type 1 was used for these measurements. The mechanical conditioning of samples were done by providing 8 cycles of pre-stretching up to 150% strain to eliminate Mullins effect (stress-softening). During the mechanical preconditioning, 2 min relaxation time was provided between the unloading and the reloading cycles. At the end of this

31

step, samples were removed from the grip and allowed to relax for a period of 30 min before performing the final test. Samples were then tested and the stress values were recorded at different strain intervals. All these measurements were done at room temperature only.

3.2.6 Stress Relaxation

Stress relaxation behaviour of these compounds was measured in uni-axial tension mode using Zwick Z010 UTM. Stress relaxation tests were carried out at multiple strain levels (25%, 50%, 75% and 100% strain) using ASTM D412 Type 1 Dumbbell samples. The preconditioning of the test samples were carried out as described in Section 3.2.5 for hyperelastic property measurement. After the preconditioning cycles, samples were allowed to rest for 30 min time. Then the samples were stretched to the specified strain level and hold it for 15 min time. This step is repeated for other strain levels. The stress decay with time was recorded for all the strain levels.

3.2.7 Dynamic Mechanical Properties

Dynamic mechanical properties of these compounds were evaluated using a Dynamic Mechanical Analyser (VA 4000, Metravib, France, Figure 3.3) under strain sweep condition. For DMA measurements, circular specimen of 10 mm diameter and thickness of 2 mm was used. The rubber samples were bonded to the test stubs, using a cyanoacrylate adhesive. Each disc was sandwiched between two stubs. A pair of discs was mounted in a jig in a double shear arrangement. Then, the jig is mounted in the DMA and the temperature set to 30°C. The sample was held at this temperature for 20 min prior to starting the test. Strain sweep tests were conducted for the strain range of 0.1% to 100% shear strain at 10 Hz frequency. For measuring glass transition temperature by DMA, tests were conducted at 0.1% strain at 10 Hz frequency. The temperature was varied in the range of -110^0 C to -20^0 C except for A5 compound (100 BR) where temperature sweep was done in the range of -110^0 C to -70^0 C.

3.2.8 Glass Transition Temperature

The glass transition temperature (T_g) of compounds were measured using Diamond Differential Scanning Calorimetry (Perkin Elmer, USA, Figure 3.4). The instrument was calibrated at 20^0 C/min, with 50 mL/min N_2 purge flow rate using Indium metal. Measurements were carried out using sample weight of approx. 5 mg. The samples were cooled down to -120^0 C and then heated up to 10^0 C at the scanning rate of 10^0 C/min.

Figure 3.3 Dynamic Mechanical Analyzer (Metravib VA 4000)

Figure 3.4 Differential Scanning Calorimeter (DSC)

3.2.9 Fatigue Crack Growth

Fatigue crack growth properties of all the compounds were measured using Tear & Fatigue Analyzer (TFA, Coesfeld, Germany). The schematic diagram of the TFA equipment is given in Figure 3.5. The detailed description of the equipment can be found in Eisele *et al.* (1992). The test specimens are fixed in TFA using bottom and top clamps. The bottom clamps are connected to the traverse. The hydropulser supplies power to the traverse through a piston. A frequency sweep generator drives the hydropulser under various loading modes (Sine, Pulse etc.) in the frequency range of 0.1 to 20 Hz. The upper clamps are fixed to the load cell. To ensure constant pre-load during the entire test, a computer controlled stepping motor is also attached with the instrument. A high speed CCD monochrome camera is mounted on the linear motion axis system to monitor the crack growth of rubber specimens. Image processing software was used for calculation of crack contour lengths of rubber specimens.
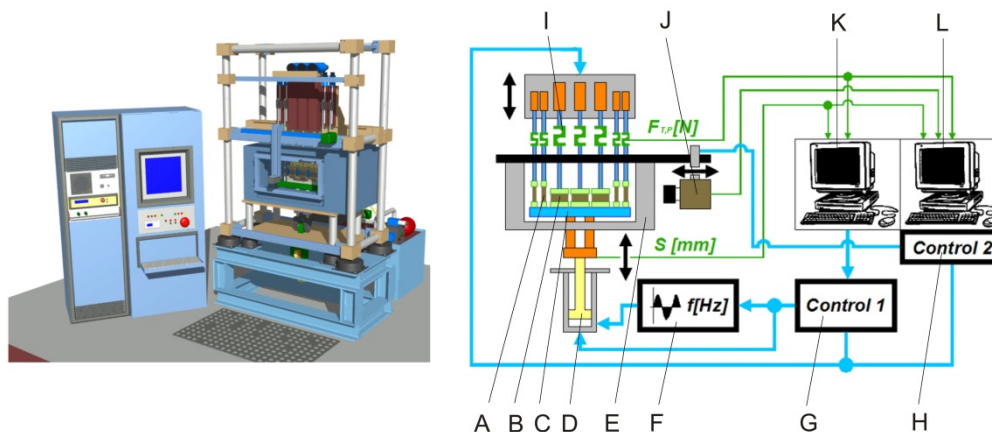
Figure 3.5: Schematic and functional diagram of TFA machine: A-tensile test specimen; B-pure-shear test specimen; C-traverse; D-hydropulser; E-isolated chamber; F-frequency generator; G-control unit 1; H-control unit 2; I-load cells; J-CCD monochrome camera;K-PC1;L-PC2.

The geometry of standard pure-shear test specimen is shown in Figure 3.6, where the length L_0 =15 mm, width Wp = 120 mm and thickness B =1.5 mm. The notch of 21 mm was provided on both edges of the specimen. FCG experiments were carried out at various temperatures, R-ratios and waveforms to study the influence of these parameters. FCG measurement conditions are provided in Tables 3.4. One parameter is varied at a time. As a default test condition Sine loading with zero R-ratio, 30^0 C

temperature and strain range of 10%-50% is used. In the case of Pulse loading, the width of the Pulse was calculated for a tyre of 538 mm outer radius running at a speed of 60 kmph, with the loaded tyre footprint comprising of a 35^0 segment of the whole tyre. Under this condition, the tread (rubber) element experiences loading of 20 millisecond duration for every tyre rotation. The schematics of Sine and Pulse loadings are shown in Figure 3.7 and the relevant test parameters for both the waveforms are given in Table 3.5. As a general test procedure, the fatigue loading cycle was applied as per the condition mentioned against each test tabulated in Table 3.4 and 3.5 and the crack length was monitored continuously for calculating the crack growth rate (*da/dn*). Un-notched test specimens were loaded up to the desired strain level to obtain elastic strain energy density, W and the tearing energy *T,* is then calculated using the following equation,

$$T = W L_0 \qquad\qquad (3.4)$$

where L_0 is the height of the sample.
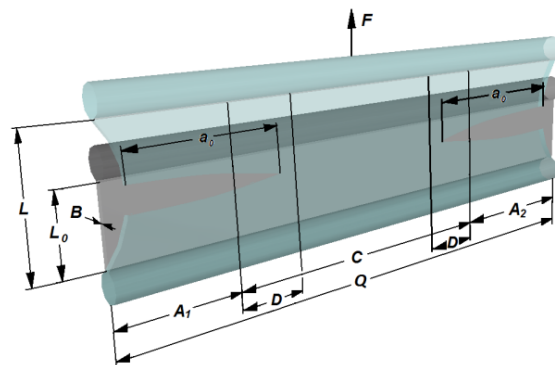
Figure 3.6 Pure shear sample

Table: 3.4 FCG Test condition details

Parameters	Temperature effect	R-ratio effect	Waveform effect	
			Sine	Pulse
Temperature	30 and 70^0 C	30^0 C	30^0 C	30^0 C
R-ratio	0	0 and 0.14	0	0
Waveform type and frequency	Sine & 10 Hz	Sine & 10 Hz	Sine & 10 Hz	Pulse

Table 3.5 Details of Sine and Pulse waveforms

Waveforms	Width of Sine / Pulse (ms) wave	Dwell Time (ms)
Sine	100	0
Pulse I	20	80
Pulse II	20	980
Pulse IV	20	180
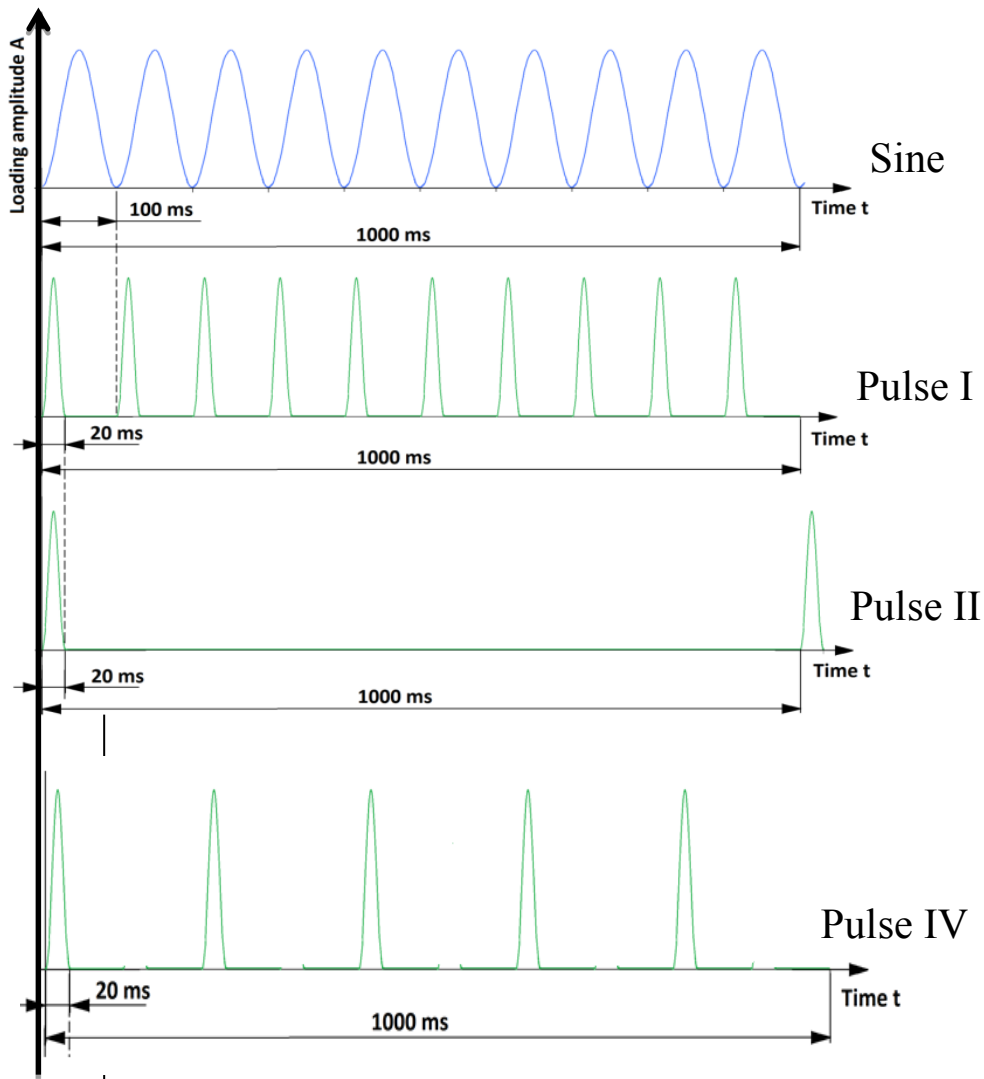
Figure 3.7 Schematics of Sine and Pulse loading

3.2.10 Wear

Laboratory Abrasion Tester (LAT 100, VMI, The Netherlands, Figure 3.8) was used for measuring the wear characteristics of the compounds. This equipment is capable of applying load range between 10 N to 150 N, speed between 2 kmph -100 kmph and slip angle range of $\pm 40^0$. The abrasive disk of different grain size and sharpness can be used. The wear measurement at elevated temperature up to 70^0 C is possible. The circular disk sample as shown in Figure 3.9 was used having dimensions: 80 mm outer diameter, 35 mm inner diameter and 18 mm width.

Figure 3.8 LAT 100 Equipment

Figure 3.9 LAT 100 sample

For the present work, wear measurements were carried out at one load, variable speeds and slip angles combination as per ISO 23233. Corundum 60 and 180 surfaces were used for wear measurements. The detailed test conditions are provided in Table 3.6. Before actual measurement, a run-in condition was provided for sample conditioning purpose. In run-in tests, 75 N load, 25 kmph speed and 16^0 slip angle was applied. In each test programme, measurements were conducted for five specimens of different compounds (two control and three experimental compounds). Control compound was tested twice to check the measurement repeatability in the following sequence: Control→Ex1→Ex2→Ex3→Control. Each specimen was tested for eighteen abrasion runs as per the standard. Since these tests continues for many days (approx.70 hrs), run-in was given at the beginning of the test every day. During testing, a mixture containing aluminum oxide and magnesium oxide was sprayed between the abrasive disk and the rubber sample to overcome smearing problem of rubbers due to thermo-oxidative degradation.

Table 3.6 Wear measurement test conditions

Parameters	Test conditions								
	1	2	3	4	5	6	7	8	9
Load (N)	75	75	75	75	75	75	75	75	75
Speed (kmph)	25	12	2.5	2.5	12	25	25	12	2.5
Slip Angle (^{0})	16	16	16	9	9	9	5.5	5.5	5.5
Distance (m)	250	140	200	600	600	600	2500	1500	1400

3.3 SUMMARY

In this chapter, details including sources and properties of different raw materials used for compound preparation are reported. The tests methods including relevant standards and test equipment pertaining to various property characterizations is discussed. The detailed discussion on Fatigue Crack Growth (FCG) and Wear measurements is presented.

CHAPTER 4

CHARACTERIZATION OF RHEOMETRIC, MECHANICAL AND VISCOELASTIC PROPERTIES

This chapter describes the results of rheometric, mechanical and viscoelastic properties of the rubber compounds used in this work. The detailed test methodology has been described in sections 3.2.1 to 3.2.8 of Chapter 3. The influence of material compositions on various fundamental properties is discussed here.

4.1 RHEOMETRIC PROPERTIES

Rheometric properties of rubber compounds are very important because they provide information about the processing and curing characteristics of the compound. For rubber processing, viscosity of the compound plays a vital role and obtained as lowest and highest torque (M_L and M_H) values from the rheometer curve. The information about premature curing also known as scorch safety is obtained from t_s2 parameter. Time required for achieving the optimum cure is represented by t_c90 parameter.

Table 4.1 summarizes the rheometric properties of NR, BR and NR/BR blend compounds. Both M_L and M_H values marginally increase from A1 to A5 which can be attributed to reduction in aromatic oil dosage in the NR/BR blends and 100 BR compounds (A2-A5) compared to 100 NR compound. The lowest t_c90 of 25.03 min is obtained in A4 compound which is due to usage of higher dosage (0.80 phr) of accelerator. This in turn increases the cure rate in A4 compound.

Table 4.2 summarizes the rheometric properties of SBR and NR/SBR blend compounds. Results revealed that the properties for B5 compound are different than rest of the compounds as it is a pure SBR compound.

Table 4.1 Rheometric properties of NR, BR and NR/BR blends

Parameters	A1	A2	A3	A4	A1-Modcure	A4-Modcure	A5
Lowest Torque, M_L (Nm)	0.246	0.266	0.294	0.299	0.285	0.267	0.279
Highest Torque, M_H (Nm)	1.394	1.406	1.554	1.570	1.394	1.63	1.743
ΔM (M_H- M_L) (Nm)	1.148	1.14	1.260	1.271	1.109	1.372	1.464
t_s2 (min)	13.88	12.7	14.92	12.5	15.35	13.2	16.42
$t_c 50$ (min)	18.32	16.93	19.41	15.6	18.17	18.29	20.68
$t_c 90$ (min)	30.01	28.74	31.47	25.03	25.5	30.2	31.45

Table 4.2 Rheometric properties of SBR and NR/SBR blends

Parameters	B2	B3	B4	B5
Lowest Torque, M_L (Nm)	0.224	0.216	0.201	0.159
Highest Torque, M_H (Nm)	2.875	2.90	2.765	1.457
ΔM (M_H- M_L) (Nm)	2.65	2.683	2.564	1.298
t_s2 (min)	12.46	13.75	13.46	17.83
$t_c 50$ (min)	16.83	17.79	17.1	21.96
$t_c 90$ (min)	29.68	30.05	29.03	36.12

4.2 MECHANICAL PROPERTIES

Table 4.3 summarizes the mechanical properties of NR, BR and NR/BR blend compounds. There is a marginal variation in M_{100} values. The compound A5 (100 BR) exhibited lowest value of M_{300}. Tensile strength and elongation at break are also lower for A5 compound when compared to others. However, hardness values are almost constant for these compounds.

Mechanical properties of SBR and NR/SBR blend compounds are provided in Table 4.4. Negligible variation is observed except for lower tensile strength of B5 compound which is attributed to 100 parts SBR.

Table 4.3 Mechanical properties of NR, BR and NR/BR blends

Parameters	A1	A2	A3	A4	A1-Modcure	A4-Modcure	A5
100% Modulus (MPa)	2.0	1.9	2.0	1.9	1.7	1.9	1.7
300% Modulus (MPa)	9.6	9.2	9.5	9.4	9.4	9.4	7.6
Tensile Strength (MPa)	25.3	24.2	23.7	25	26.2	23.9	15.1
Elongation at break (%)	595	600	555	632	623	608	477
Hardness (Shore A)	60	60	58	62	57	59	57

Table 4.4 Mechanical properties of SBR and NR/SBR blends

Parameters	B2	B3	B4	B5
100% Modulus (MPa)	1.9	1.9	1.9	1.9
300% Modulus (MPa)	10.1	9.5	9.7	9
Tensile Strength (MPa)	26.4	26	23.3	19.4
Elongation at break (%)	596	602	571	520
Hardness (Shore A)	59	59	61	58

4.3 CROSSLINK DENSITY

Crosslink density values for NR, BR and NR/BR blend compounds are provided in Table 4.5. It can be observed that the crosslink density increases with increasing BR content in the blends which is in agreement with the literature (Mathew and De, 1983). The modification of cure package also leads to increase in crosslink density for both A1-Modcure and A4-Modcure compounds. Molecular weight between crosslinks (M_c) is also reported here.

Table 4.5 Crosslink density of NR, BR and NR/BR blends

Compound	Crosslink density (mole /cc)	Molecular weight between crosslinks, M_c (gm /mole)
A1	6.03 E-05	7627
A2	7.52 E-05	6100
A3	7.81 E-05	5874
A4	8.36 E-05	5480
A1-Modcure	6.79 E-05	6772
A4-Modcure	8.71 E-05	5255
A5	8.96 E-05	5078

Table 4.6 summarizes the crosslink density values of SBR and NR/SBR blend compounds. Here also increasing trend of crosslink density is observed with higher SBR content in the compound which is in agreement with the literature (Sabbabagh-EL and Yehia, 2007). It is also observed that the higher crosslink density is exhibited by NR/SBR blend compounds when compared to NR/BR blends.

Table 4.6 Crosslink density of SBR and NR/SBR blends

Compound	Crosslink density (mole /cc)	Molecular wt. between crosslinks, M_c (gm / mole)
B2	8.18 E-05	5647
B3	8.56 E-05	5406
B4	8.47 E-05	5477
B5	1.03 E-04	4580

4.4 HYPERELASTIC PROPERTIES

The coefficients of hyperelastic material model proposed by Yeoh (1990) are determined by least square curve fitting method using Abaqus software. The least square method works on the principle of error minimization technique for given stets of stress-strain data. The relative error,

$$E = \sum (1 - T_i^{th} / T_i^{test})^2 \qquad (4.1)$$

where T_i^{test} is a stress value from the test data and T_i^{th} comes from the nominal stress expression obtained from the polynomial strain energy function. Drucker stability criterions for all the materials have also been checked. Hyperelastic property evaluation curve (test data vs. Yeoh model fitted data) of A1 compound is presented in Figure 4.1. Coefficients (C_{10}, C_{20} and C_{30}) of NR, BR and NR/BR blend compounds are provided in Table 4.7. The C_{10} represents the initial stiffness of the stress-strain curve. The C_{20} coefficient represents the flat portion of the stress-strain curve followed by upturn due to positive C_{30} coefficient. C_{10} values of these compounds are shown in Figure 4.2. It can be observed that C_{10} increases with increase in BR content in the compounds.
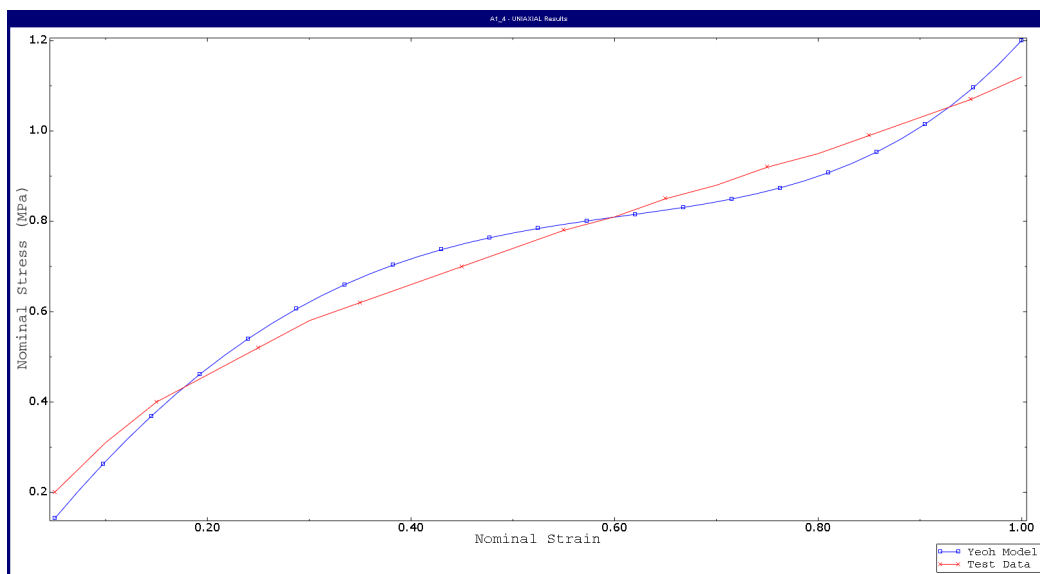
Figure 4.1 Hyperelastic property evaluation of A1 compound

Table 4.7 Hyperelastic properties of NR, BR and NR/BR blends

Compound	C_{10} (MPa)	C_{20} (MPa)	C_{30} (MPa)
A1	0.4988	-0.1438	0.0350
A2	0.5497	-0.1601	0.0385
A3	0.5688	-0.1642	0.0395
A4	0.5986	-0.1684	0.0402
A1-Modcure	0.5026	-0.1463	0.0364
A4-Modcure	0.6257	-0.1770	0.0424
A5	0.6690	-0.2410	0.0590
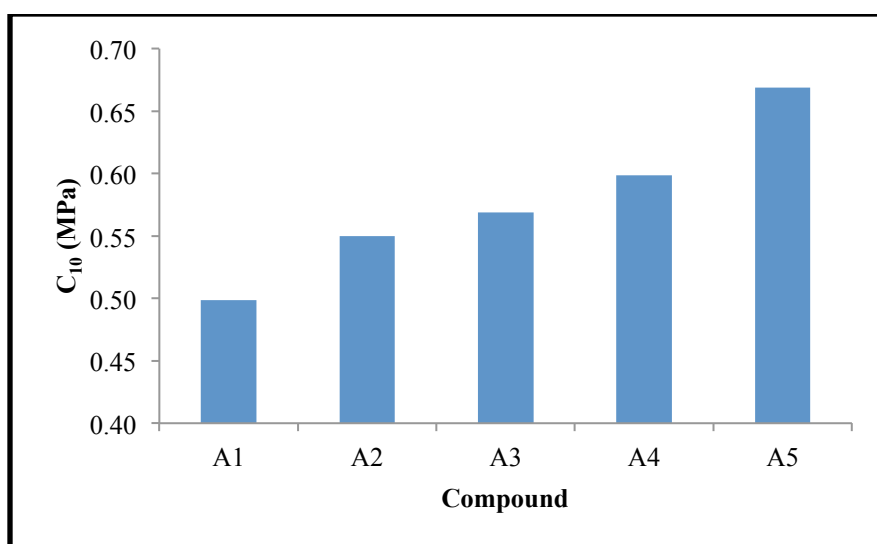
Figure 4.2 C_{10} plot of NR, BR and NR/BR blend compounds

The hyperelastic property evaluation curve of B2 (NR/SBR blend) is shown in Figure 4.3. Yeoh coefficients of NR/SBR blend compounds are provided in Table 4.8. The decrease in C_{10} with increase in SBR content in the blend is observed which is contrary to the observation made for NR/BR blends.
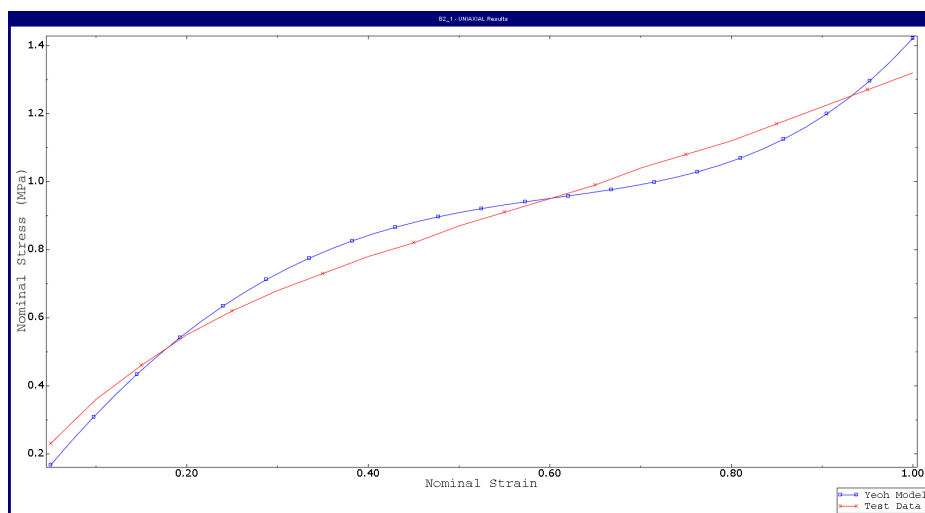
Figure 4.3 Hyperelastic property evaluation of B2 compound

Table 4.8 Hyperelastic properties of NR/SBR blends

Compound	C_{10} (MPa)	C_{20} (MPa)	C_{30} (MPa)
B2	0.5861	-0.1697	0.0416
B3	0.5797	-0.1686	0.0421
B4	0.5562	-0.1567	0.0394

4.5 GLASS TRANSITION BEHAVIOUR

The DSC thermograms of NR, BR and NR/BR blend compounds are shown in Figure 4.4. Single glass transition temperature is observed in compounds of 100 NR (A1 and A1-Modcure) and 100 BR compound (A5). However, all NR/BR blend compounds (A2-A4 and A4-Modcure) show two glass transition temperatures (T_g) and these values are very close to the response of individual blend components. This observation is in satisfactory agreement with the literature (Marsh *et al.*, 1968; Callan *et al.*, 1971) in which NR/BR and SBR/BR blends also shown double peaks in DTA thermograms of gum and filled compounds. This indicates the presence of two discrete zones in the blends as expected because high polymers are thermodynamically immiscible. This ia also discussed in section 2.4.1 of Chapter 2.

The existence of two phases in NR/BR blend at molecular level can be attributed to the difference in solubility parameter of NR (16.7 MPa$^{1/2}$) and BR (17.2 MPa½). In contrast to this observation, only single Tg is reported for all the compounds including blends from DMA measurements. Further, Tg values from DMA measurements are found to be on the higher side when compared to the DSC results. This could be attributed to the dynamic movement of the polymer molecule in the former case.

Figure 4.5 shows the DSC curves for NR/SBR and SBR compounds. All the compounds showing only one distinct peak except B4 compound which has two peaks. In NR/SBR blends, up to 30 parts of SBR, compounds shows Tg corresponding to the dominant NR phase only. Mansilla *et al.*, (2012) also reported similar glass transition behaviour for NR/SBR blends. As reported by them, almost all NR/SBR blends exhibited two glass transition temperature except in NR10/SBR90 and NR20/SBR80 where only one T$_g$ was observed.
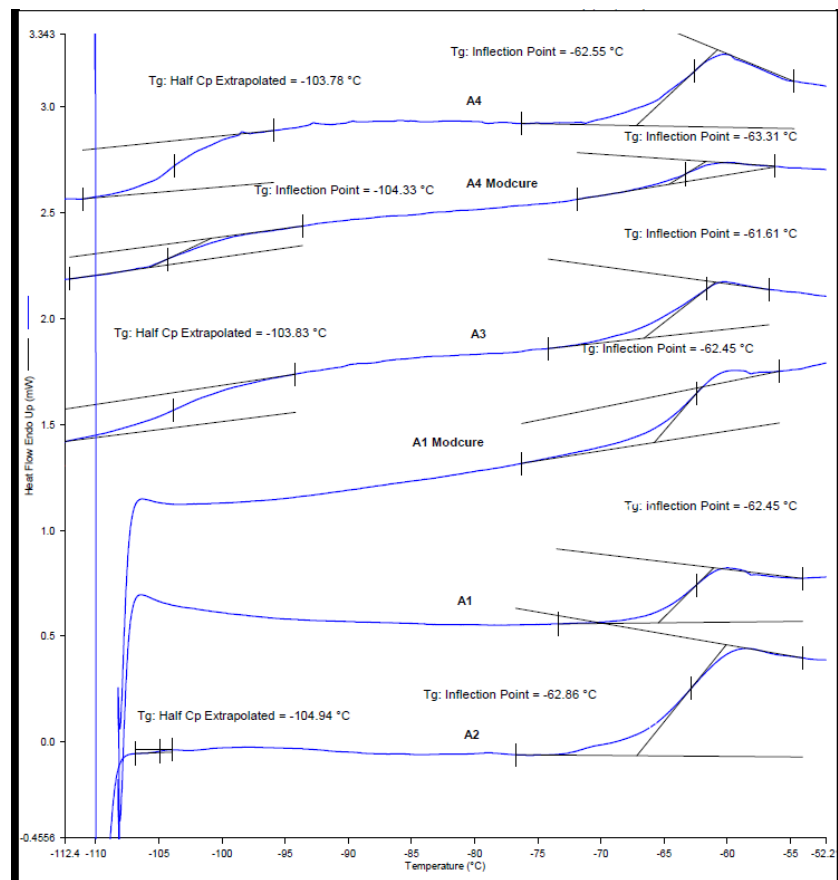
Figure 4.4 DSC thermograms of NR, BR and NR/BR blends

46

Table 4.9 Glass transition temperature of NR, BR and NR/BR blends

Compound	T_g by DSC		T_g by DMA
	T_g^1	T_g^2	
A1	-62.4	-	-41.2
A2	-62.9	-104.7	-47.8
A3	-61.6	-102.9	-49.6
A4	-62.6	-103.4	-52.8
A1-Modcure	-61.6	-	-49.7
A4-Modcure	-63.3	-104.3	-51.5
A5	-	-103.7	-93.4
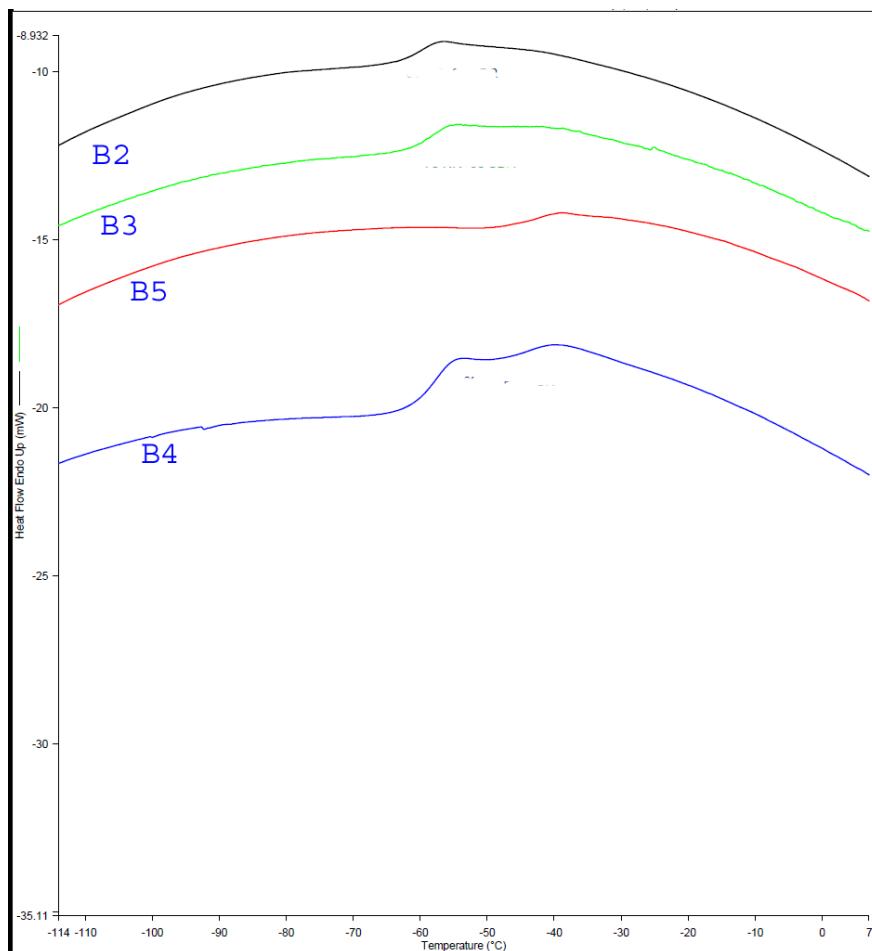
Figure 4.5 DSC thermograms of NR/SBR blend compounds

Table 4.10 Glass transition temperature of NR/SBR blends

Compound	T_g by DSC		T_g by DMA
	T_g^1	T_g^2	
B2	-59.9	-	-48.6
B3	-59.6	-	-32.2
B4	-57.6	-43.85	-32.8
B5	-	-44.19	-32.9

4.6 VISCOELASTIC PROPERTIES

In this section stress relaxation and dynamic mechanical properties are discussed. Prony series and PRF model parameters are estimated using the stress relaxation properties.

4.6.1 Stress relaxation and estimation of Prony / PRF model parameters

Stress relaxation behaviour of NR and NR/BR blend compounds at four different strain levels are shown in Figures 4.6 to 4.9. In all the compounds and strain levels, rate of stress relaxation is very fast at the beginning, followed by a slow relaxation behaviour. According to Bartenev and Lyalina (1972), stress relaxation mechanism of filled rubber vulcanizates involves multi-stage process. The first three stages are associated with the physical relaxation in bulk of the rubber material, fourth one is linked to the filler and the fifth stage is related to the chemical relaxation of vulcanizates. As evident from this literature, the initial rapid decrease of stress is due to the physical phenomena of orientation and shifting of free segments of the macromolecular chain. Since all these compounds under study contain 50 parts of carbon black (filler), the fourth stage mechanism will also be present which gives rise to non-linearity in the viscoelastic behaviour. Figure 4.10 represents time vs. normalized stress (σ_t / σ_0) for A1 compound in four different deformation levels and it can be clearly seen that these curves are not superimposing over one another which indicates significant non-linearity in the viscoelastic property. A comparison of normalized stress relaxation behaviour of all NR and NR/BR blend compounds at

48

100% strain is shown in Figure 4.11. It has been observed that the stress relaxation behaviour of 100 NR compound (A1) slightly differs from the blend compounds (A2-A4) which could be attributed to the difference in inherent stress relaxation characteristics of NR and BR.
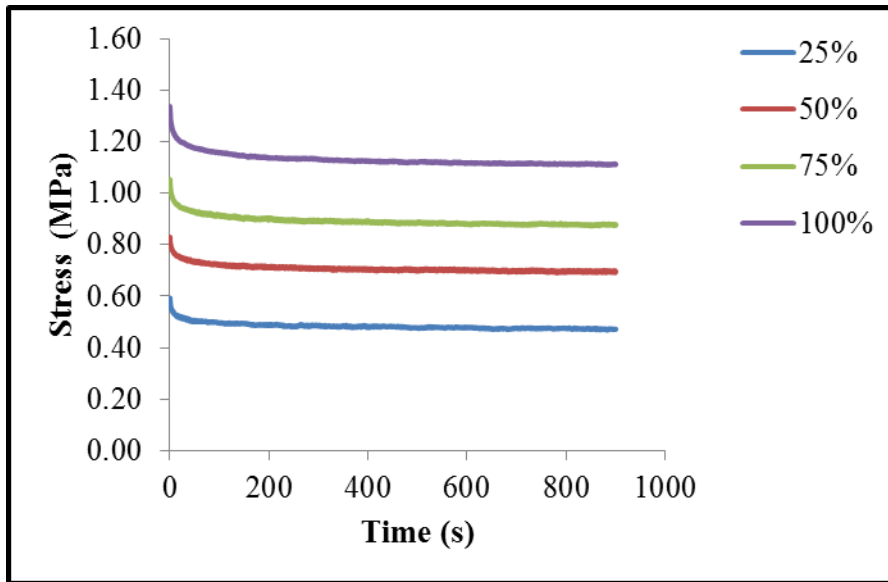
Figure 4.6 Stress relaxation property of A1 compound at multiple strains
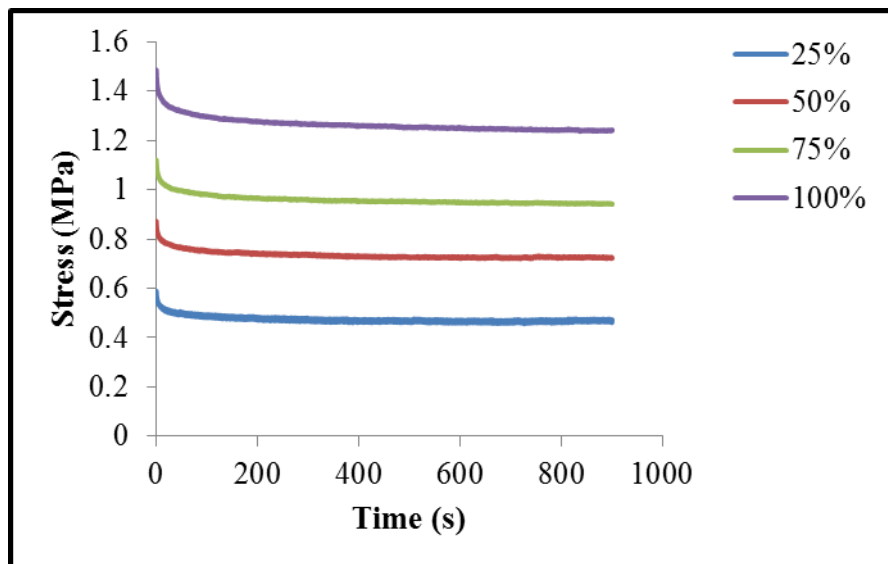
Figure 4.7 Stress relaxation property of A2 compound at multiple strains
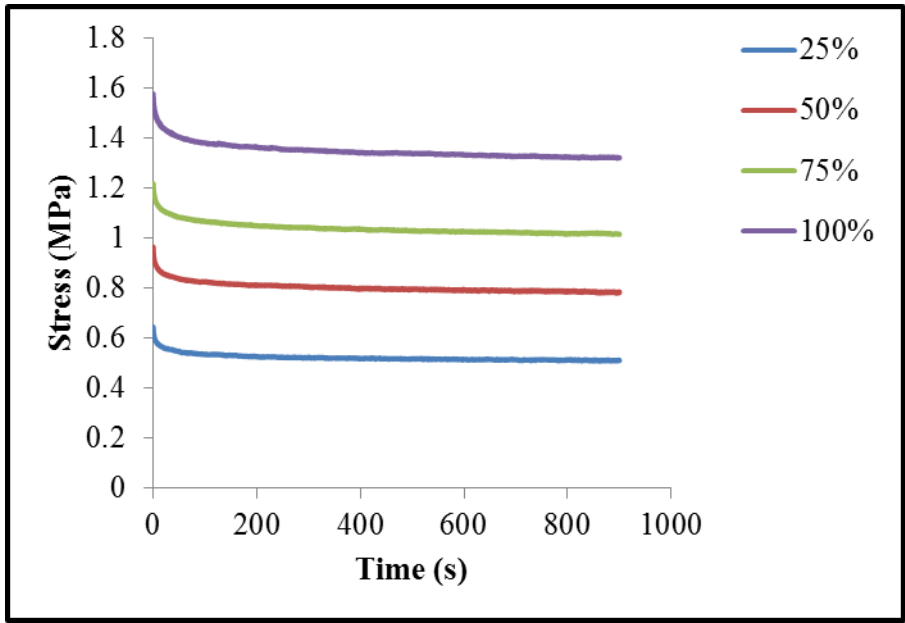
Figure 4.8 Stress relaxation property of A3 compound at multiple strains
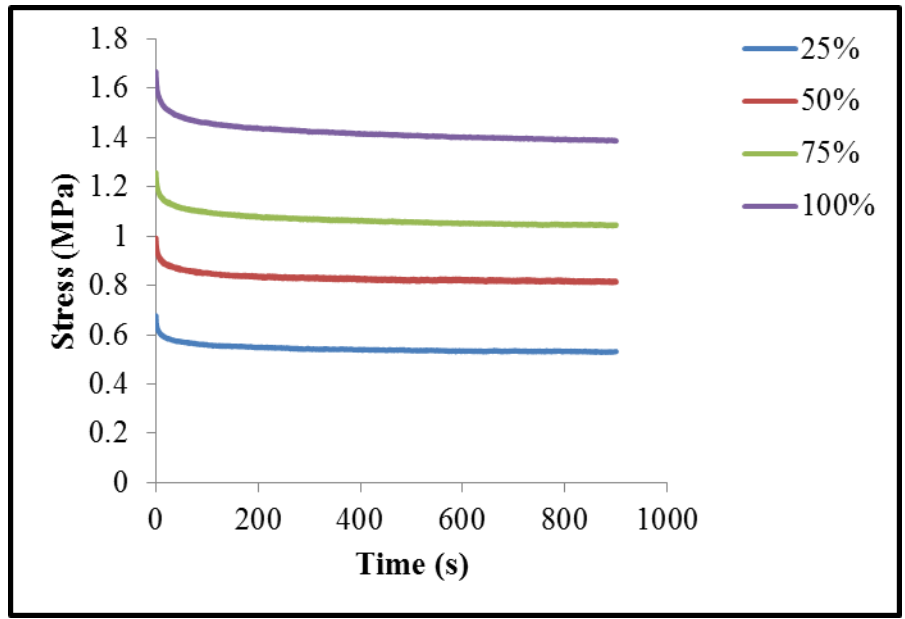
Figure 4.9 Stress relaxation property of A4 compound at multiple strains
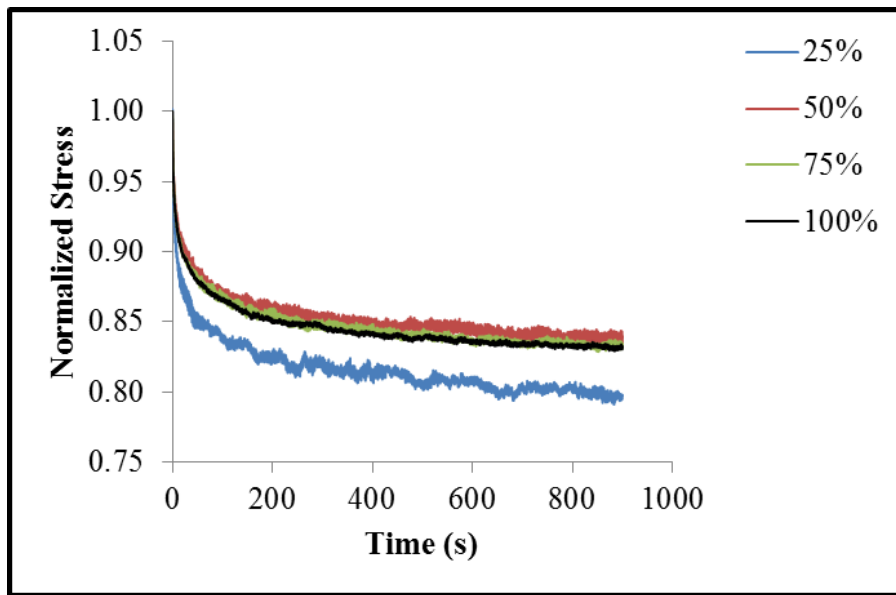
Figure 4.10 Normalized stress relaxation plot of A1 compound at multiple strains
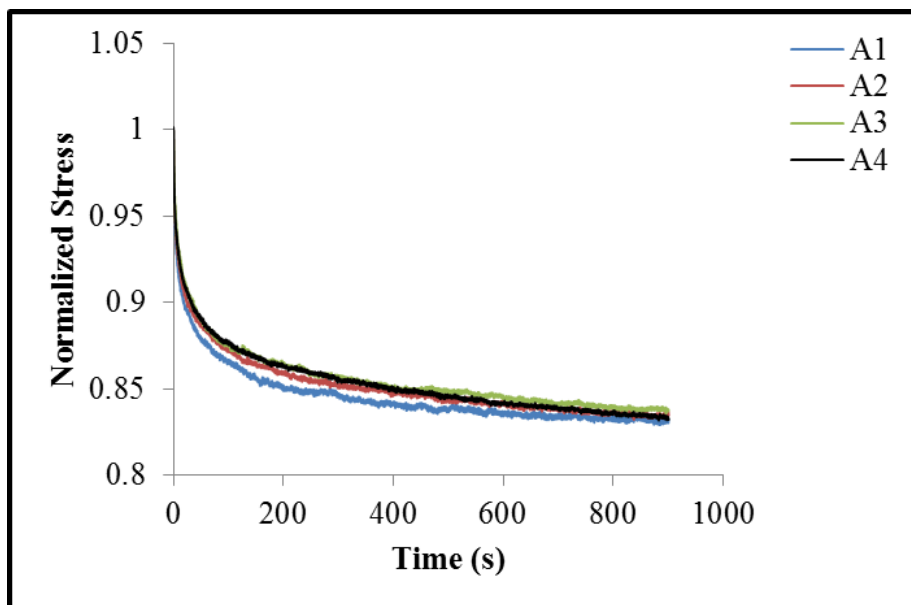
Figure 4.11 Normalized stress relaxation plot of NR and NR/BR blends at 100% strain

The stress relaxation behaviour of NR/SBR blend compounds (B2-B4) at various strain levels are shown in Figures 4.12 to 4.14. As observed in NR and NR/BR blend compounds, NR/SBR blend compounds also show similar stress relaxation behaviour.

51

Non-linear viscoelastic behaviour is also observed in these compounds as shown in Figure 4.15. A comparative normalized stress relaxation characteristics of all the NR/SBR blends is shown in Figure 4.16. It can be observed that up to 400 sec, normalized stress relaxation properties are almost same and slight differences could be observed thereafter.
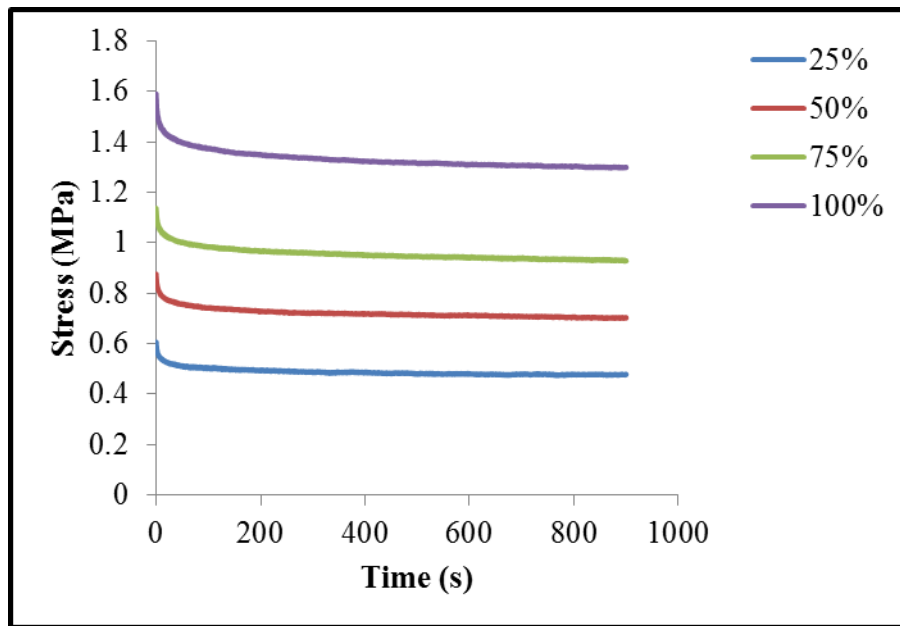
Figure 4.12 Stress relaxation property of B2 compound at multiple strains
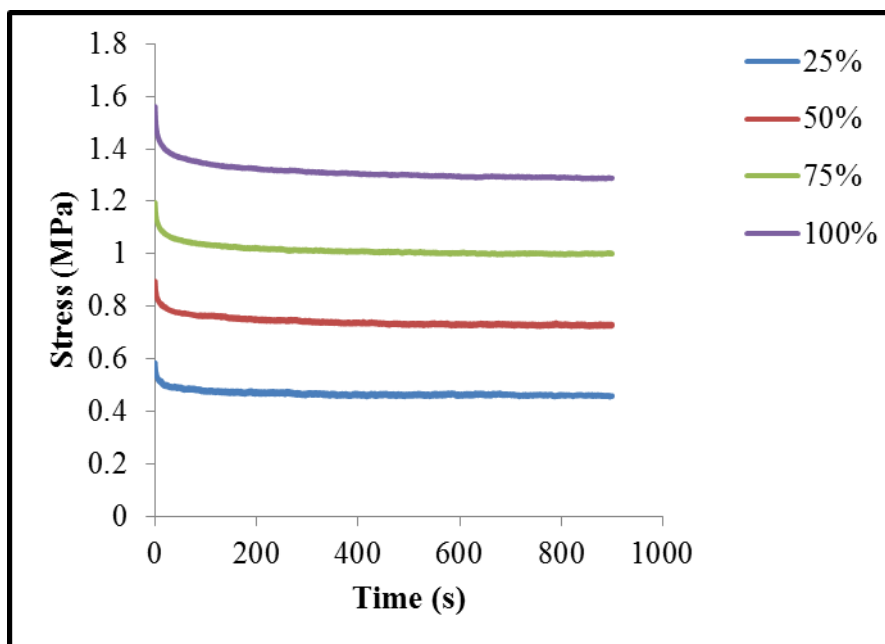
Figure 4.13 Stress relaxation property of B3 compound at multiple strains
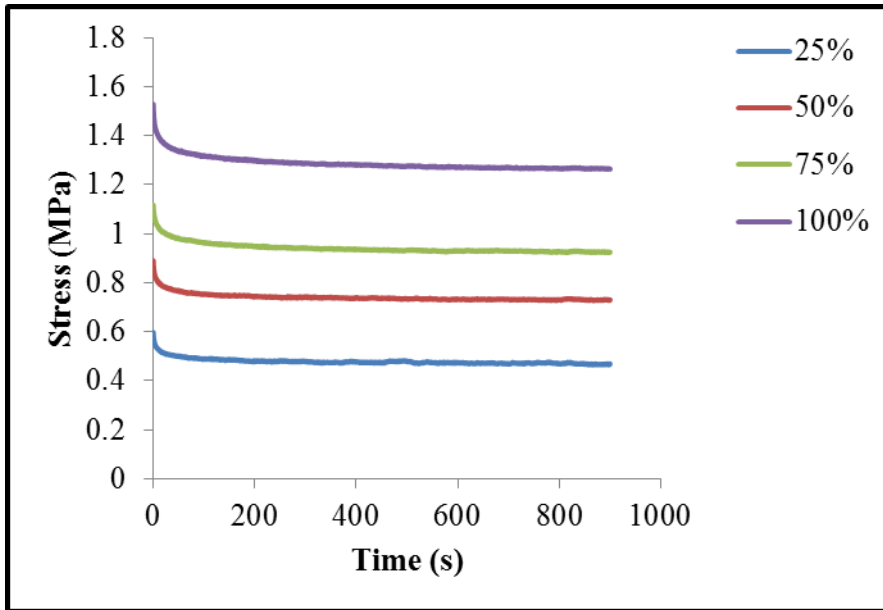
Figure 4.14 Stress relaxation property of B4 compound at multiple strains
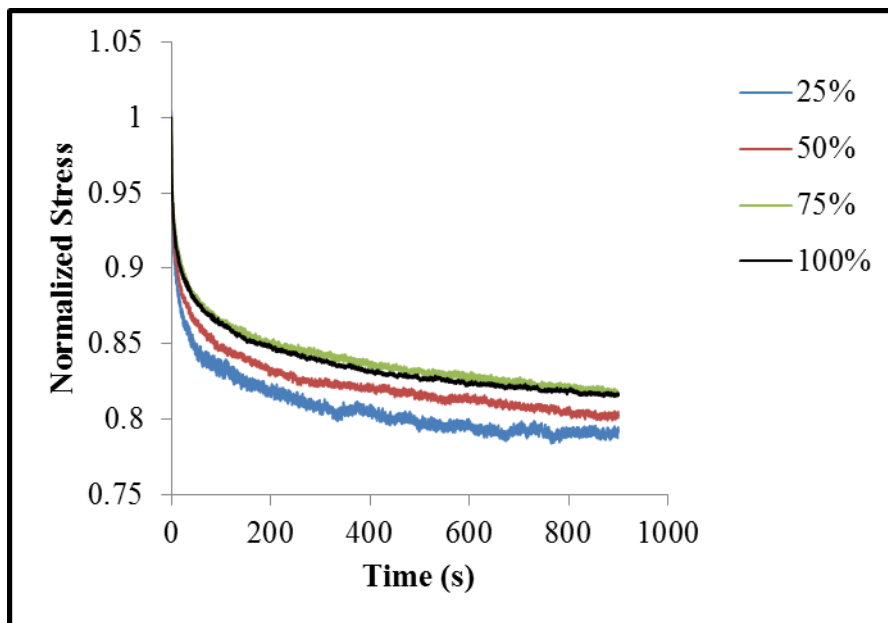
Figure 4.15 Normalized stress relaxation plot of B2 compound at multiple strains.
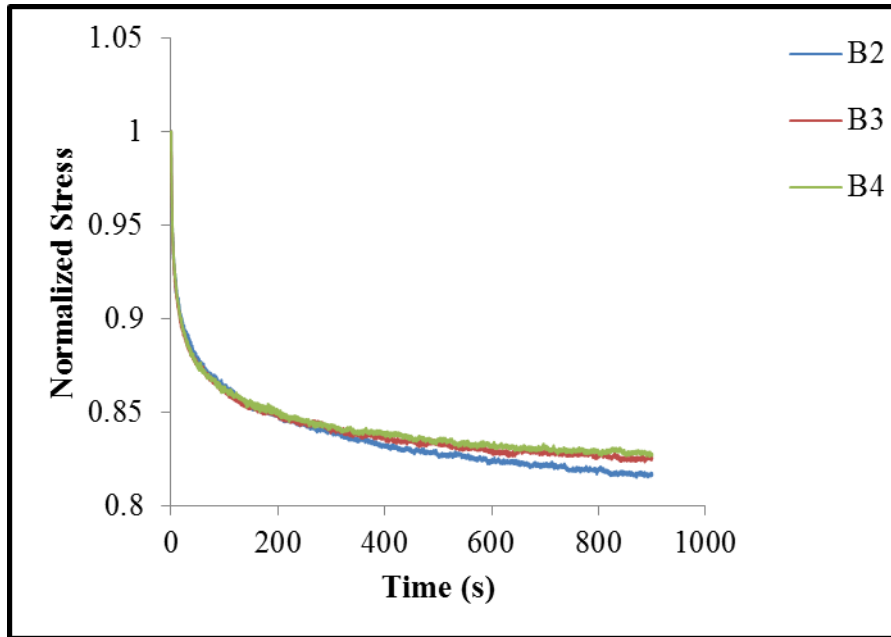
Figure 4.16 Normalized stress relaxation plot of NR/SBR blends at 100% strain.

Prony series parameters were estimated with the stress relaxation data in Abaqus FE code. Viscoelastic property evaluation curves (test data vs. Prony model) for A1 and B2 compounds are shown in Figures 4.17 and 4.18 respectively. Coefficients of NR, NR/BR and NR/SBR blend compounds are reported in Table 4.11. It has been observed that all these materials exhibited two relaxation modulus and times which are in agreement with Yang (2011).
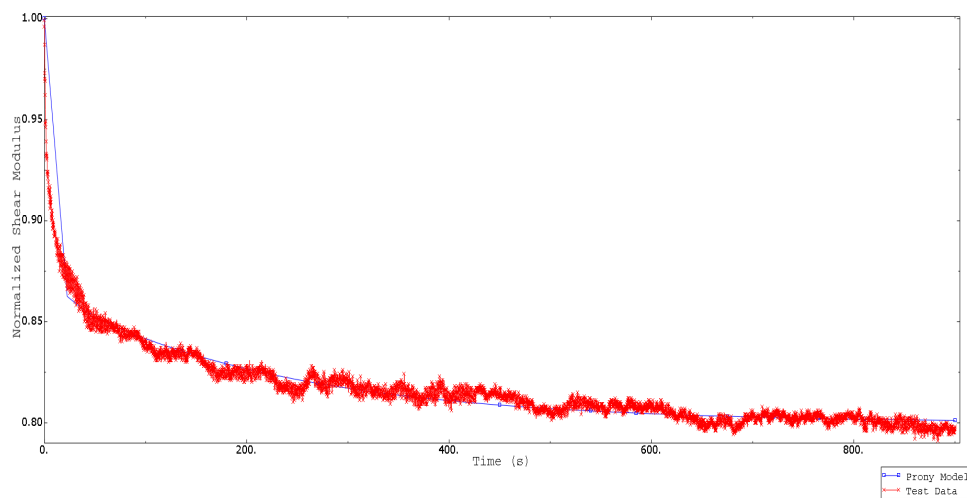
Figure 4.17 Viscoelastic property evaluation of A1 compound
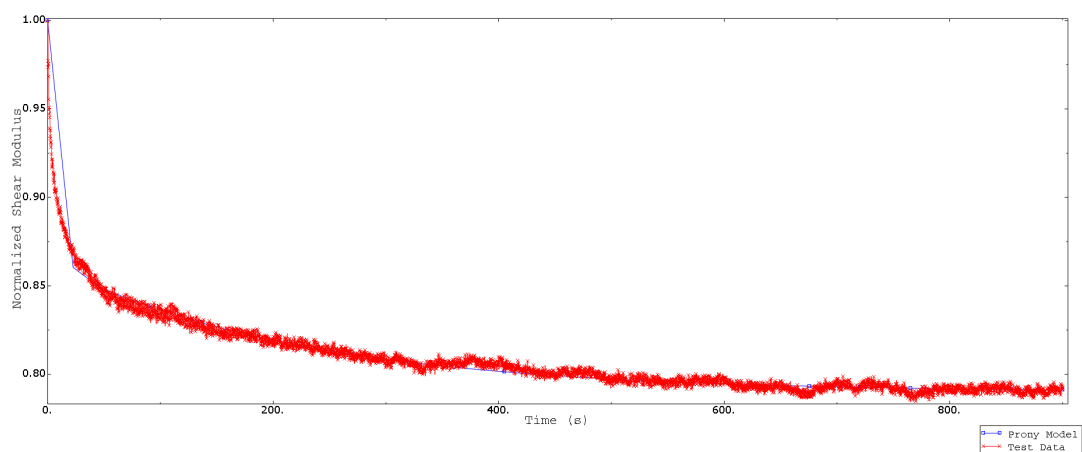
Figure 4.18 Viscoelastic property evaluation of B2 compound

Table 4.11 Prony series paramaters of NR, NR/BR and NR/SBR blends

Compound	N	Normalised Relaxation Modulus (g)	Relaxation Time(τ), (s)
A1	1	0.135010	6.2855
	2	0.065005	224.66
A2	1	0.125	4.6808
	2	0.079063	130.23
A3	1	0.13654	6.0346
	2	0.069105	180.14
A4	1	0.12759	6.5456
	2	0.075126	187.01
B2	1	0.13684	6.5784
	2	0.073146	218.05
B3	1	0.14133	4.2928
	2	0.069605	125.86
B4	1	0.14335	5.474
	2	0.067359	137.33

PRF model parameters were estimated using stress relaxation data of A1 compound using Abaqus and Isight software (Internal report from Simulia, 67). PRF model evaluation curve is presented in Figure 4.19. PRF model parameters are reported in Table 4.12.
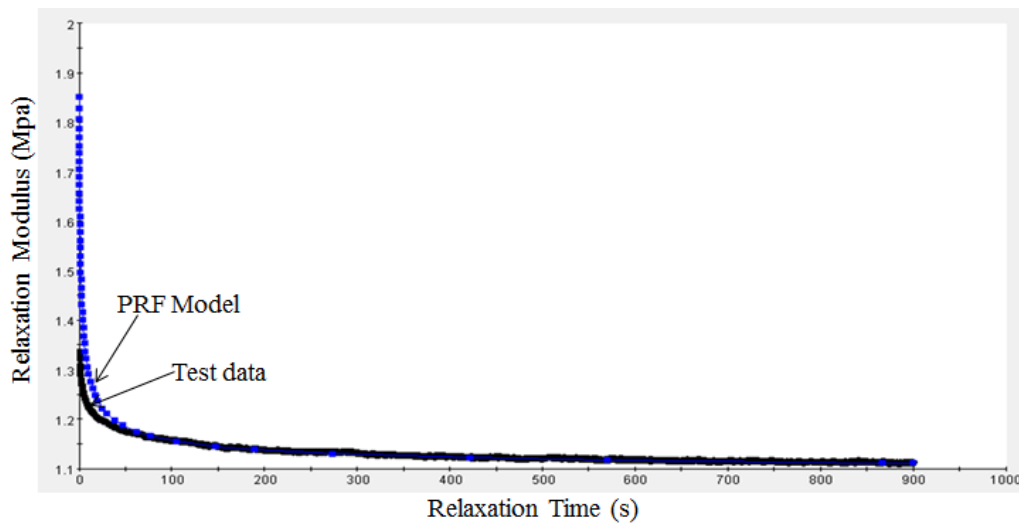
Figure 4.19 PRF model evaluation of A1 compound

Table 4.12 Material parameters of PRF model

Network ID	Stiffness Ratio	*A*	*n*	*m*
1	0.356913	4	3	-0.05252
2	0.225722	5.180188	6	-0.001
3	0.3	2	4	-0.03063

4.6.2 Dynamic mechanical properties

Variation of storage modulus with strain is shown in Figure 4.20. Due to Payne effect, the sharp decrease of storage modulus at low strain level (<5% strain) is observed in all the compounds. As explained by Wang (2007), this effect is primarily related to filler networking or agglomeration in rubber matrix. Due to the presence of filler network, rubber gets trapped into it and behaves like filler and thereby it increases the effective filler volume fraction in the system. This is reflected in the increasing stiffness (stress-strain) characteristics of the rubber compound. Upon application of increasing strain amplitude, these networks are broken and release the

trapped rubber and hence effective filler volume fraction decreases. Hence, the storage modulus also monotonically decreases with increasing strain amplitude up to a certain strain level. The Payne effect is predominant in all the compounds and corresponding $\Delta G'$ values are listed in Table 4.13. The $\Delta G'$ values gradually decreases with increasing BR content. This implies that the polymer-filler interaction increases with the BR content and also chances of formation of filler network (filler-filler interaction) reduce.
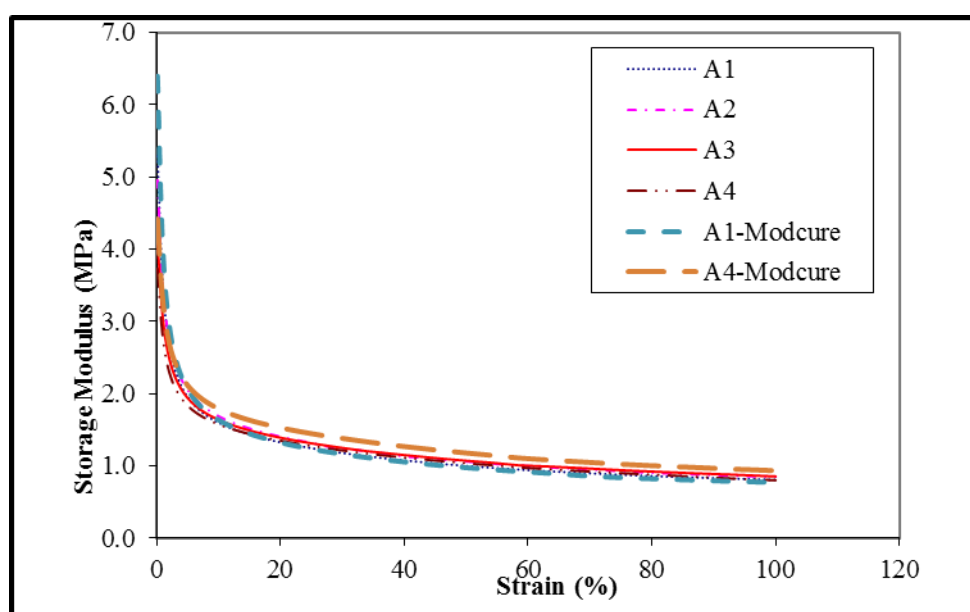
Figure 4.20 Variation of storage modulus with strain of NR and NR/BR blends

Table 4.13 Payne effect values for NR/BR blends

Compound	$\Delta G'$, MPa
A1	4.48
A2	4.10
A3	3.26
A4	2.92
A1-Modcure	5.63
A4-Modcure	3.48

Figure 4.21 shows the variation of loss modulus with strain. In contrast to the monotonic decrease of storage modulus with strain, loss modulus increases initially with strain amplitude and peaks at about 1% strain, followed by rapid decrease with increasing strain. It is a well-accepted fact that the loss modulus variation is controlled by disruption and reformation of the filler network. With this argument it can be said that at lower strain reformation process is stronger than the disruption process and hence it increases till a certain strain level. However, after reaching the peak value, the network disruption process takes place at much faster rate and therefore reformation of the network could not keep pace with that. Because of this, loss modulus sharply decreases with increasing strain after this point (Wang, 2007). It has also been observed that the loss modulus peak value decreases with increasing BR content and overall values are also lower throughout the strain range while spread has been narrowed down at higher strains (above 60%).
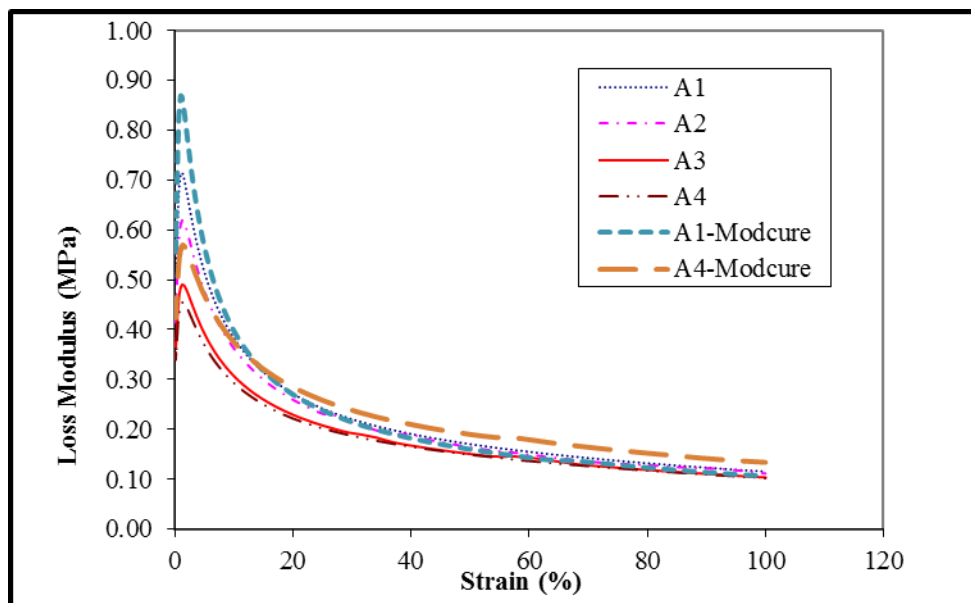
Figure 4.21 Variation of loss modulus with strain of NR and NR/BR blends

Figure 4.22 represents a cole-cole like <G> plot for all the compounds under investigation. Gerspacher *et al.* (1999) used this type of plot with an argument that as both G′ and *G″* has shown significant strain dependence and therefore these parameters can be represented as a function of strain (γ). As a more generalized form this can be expressed as *G″=f (G′).* In their study, the low frequency viscoelastic behaviour of rubber compounds filled with various carbon black grades were

described using this concept. It has been found from their study that at low strains below 10%, the mechanism responsible for variation of G′ and G″ with strain is unique and similar in nature for all the carbon black grades. At higher strains (when network is broken), variation of G″ with G′ is linear and is carbon black dependent. Similar behaviour is also observed in all the compounds studied in this work. At lower strains (0.1% to 10%), G′ vs. G″ plots of these materials have an inverse U shape. However the behaviour above 10% strain is quite different and linear dependence between G′ and G″ exists. Further, it was observed that with increasing BR content (A1 to A4), the <G> plots shifted towards lower G′ and G″. This phenomenon can also be explained with the same reasoning cited for the reduction of ΔG′. Similar observation was also made by Scurati and Lin (2006) in their work concerning the effect of coupling agent on viscoelastic property of silica filled rubber compounds. It has also been observed that the slope of the linear zone (above 10% strain) decreases with increasing BR content.
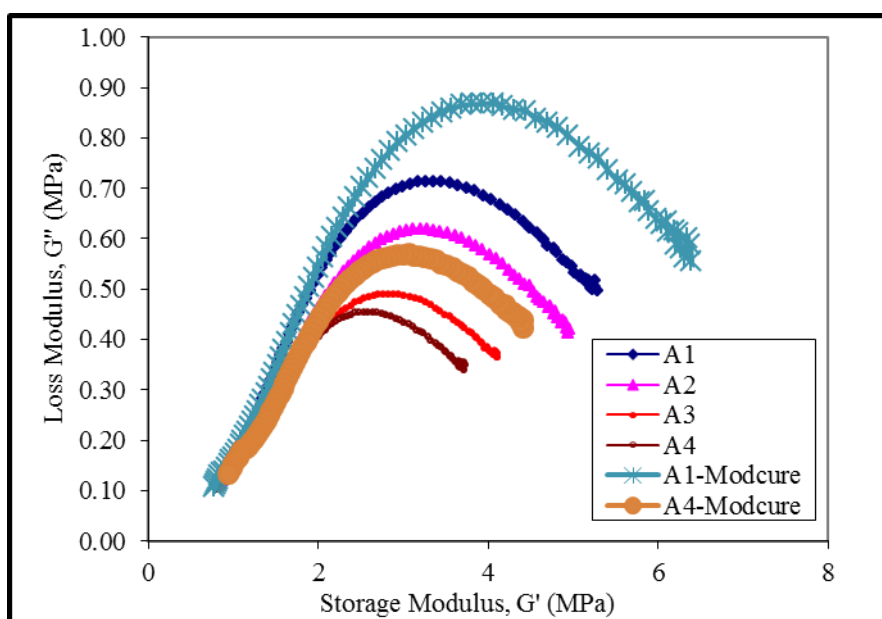
Figure 4.22 Cole-Cole plots of NR and NR/BR blends

NR/SBR blend compounds also displayed similar variations of storage and loss modulus with strain as observed in NR/BR blends and are presented in Figures 4.23 and 4.24. Cole-Cole plots are shown in Figure 4.25. The Payne effect is found to be decreased with increase in SBR content in the blend which are reported in Table 4.14.
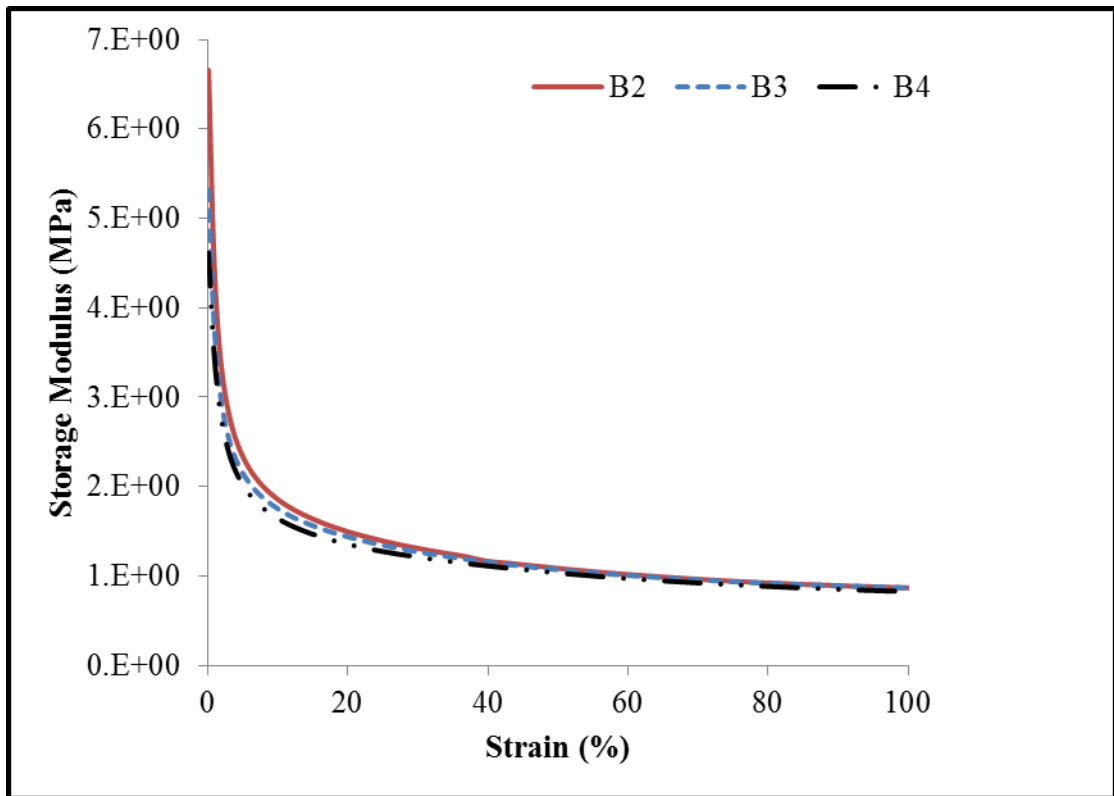
Figure 4.23 Variation of storage modulus with strain of NR/SBR blends
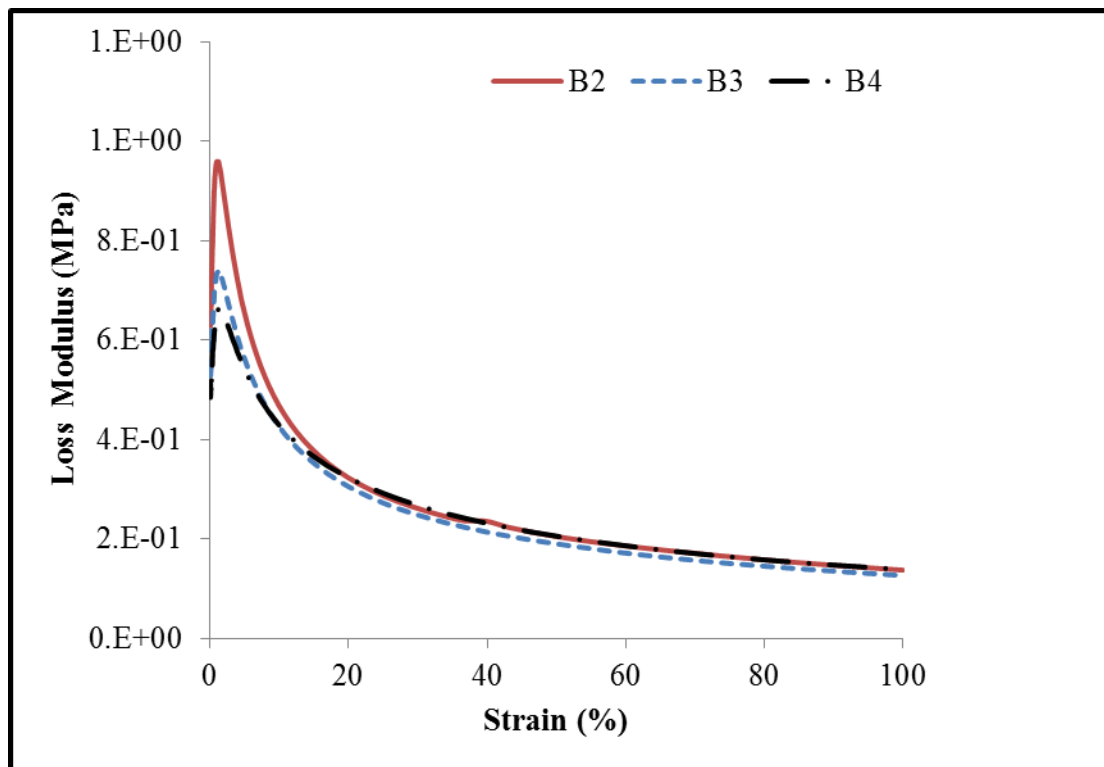
Figure 4.24 Variation of loss modulus with strain of NR/SBR blends
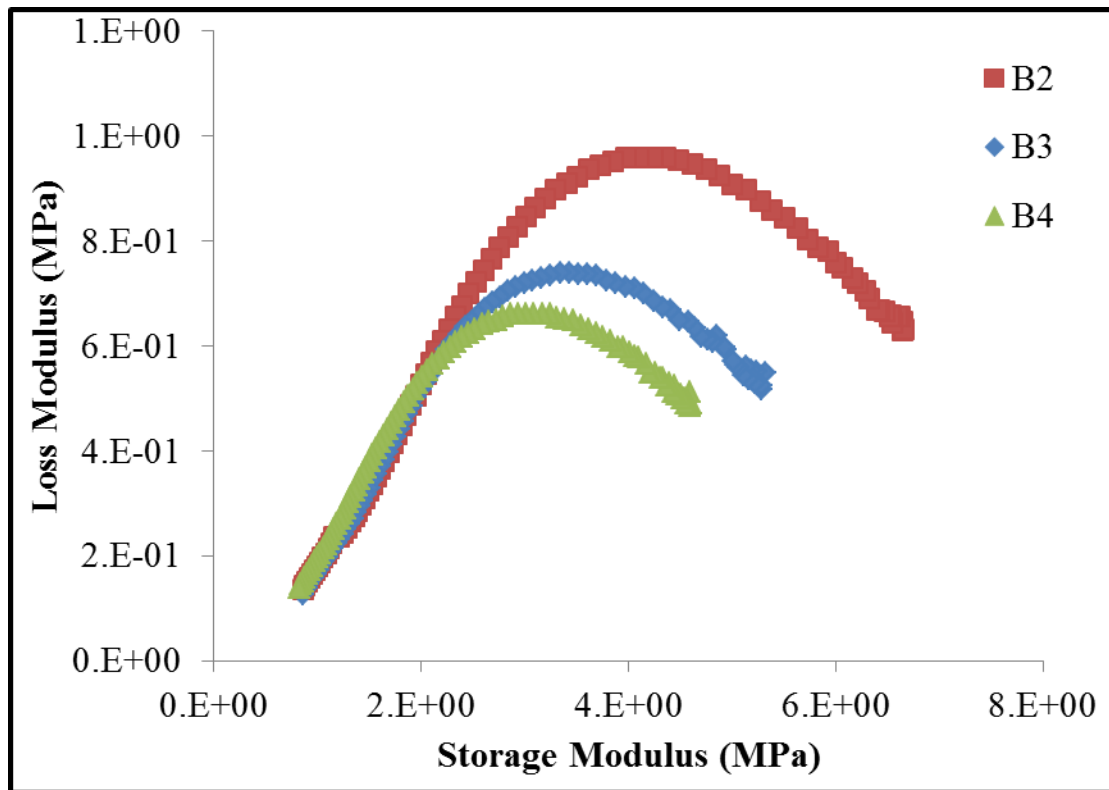
Figure 4.25 Cole-Cole plots of NR/SBR blends

Table 4.14 Payne effect values for NR/SBR blends

Compound	$\Delta G'$, MPa
B2	5.78
B3	4.44
B4	3.78

4.7 SUMMARY

In this chapter, various fundamental properties like rheometric, mechanical, crosslink density, hyperelastic, glass transition temperature and viscoelastic behaviour of rubber compounds are reported. The influence of material composition on these properties is discussed in detail. Crosslink density results revealed that it increases with increase in BR and SBR content in NR/BR and NR/SBR blends. Hyperelastic properties of NR/BR blends follow the same order as that of crosslink density whereas NR/SBR

61

blend shows reverse trend. All NR/BR blend compounds exhibited two glass transition temperatures. In the case of NR/SBR blends, all the compounds having single T_g except 60-40 NR/SBR blend.   The significant non-linear viscoelastic behaviour is displayed by all the compounds.

CHAPTER 5

FATIGUE CRACK GROWTH CHARACTERISTICS OF RUBBER BLENDS

This chapter describes the influence of material composition and test variables on Fatigue Crack Growth (FCG) characteristics of NR, BR, SBR, NR/BR and NR/SBR blend compounds. The detailed test methodology has been described in section 3.2.9 of Chapter 3. In the FCG results discussed, either the multiple points of each test condition (repeat tests) or the average value with the standard deviation are shown.

5.1 FCG CHARACTERISTICS OF NR/BR BLENDS

In this section, influence of BR content, Temperature, R-ratio, Waveforms and Cure system on FCG characteristics is described.

5.1.1 BR content

The influence of BR content in NR/BR blends on FCG properties were measured using A1, A2, A3 and A4 compounds. The compositions of these compounds are provided in Table 3.2 of Chapter 2. Figure 5.1 shows the crack growth rate, da/dn as a function of strain. It can be observed that a critical strain exists, above which crack growth rate increases rapidly. The critical strain ranges between 20%-35% for these compounds and it was also found that it decreases with increasing BR content. The compound A4, containing the highest BR content of 40 parts exhibits the lowest threshold strain value among all the studied compounds. On the other hand, A1, which is a NR based compound, gives the highest threshold strain values. This observation is in accordance with the study of Young (1985), in which FCG curves of BR and NR crosses at 15% strain. Figure 5.2 represents the double logarithmic plot of tearing energy, T vs. crack growth rate (da/dn) of these compounds. As can be seen from the plot, the curves have a bilinear form. After a certain crack growth rate, the slope of the curve increased significantly for all the compounds and can be considered as a transition point. This plot clearly shows that crack growth rate depends on the

tearing energy and a power law dependency is observed (Gent *et al.*, 1965), which can be mathematically represented as,

$$da/dn = bT^m \qquad (5.1)$$

where T is tearing energy, b and m are material constants.
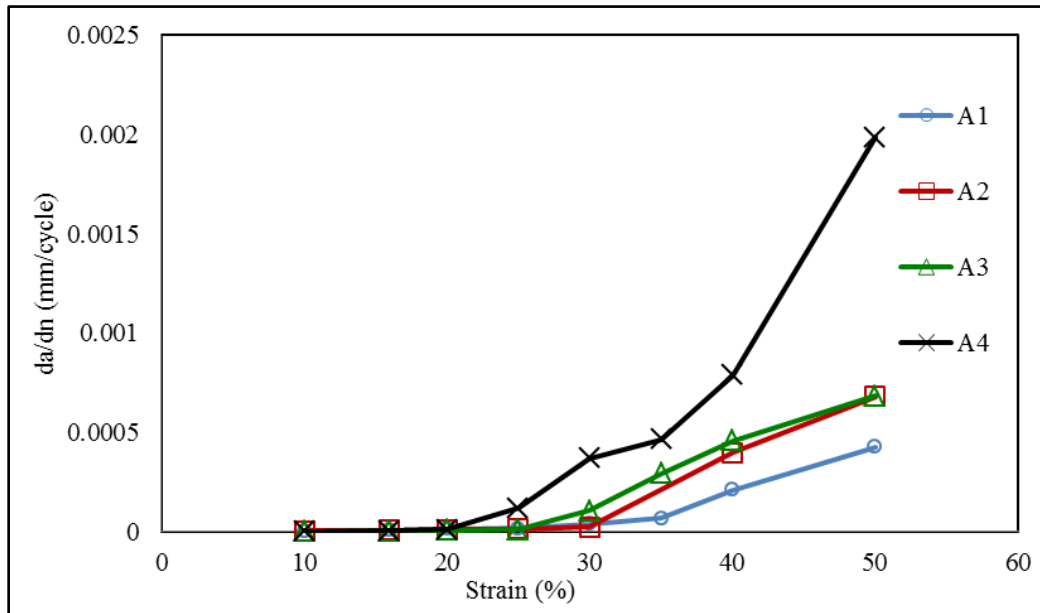
Figure 5.1 Variation of crack growth rate with strain
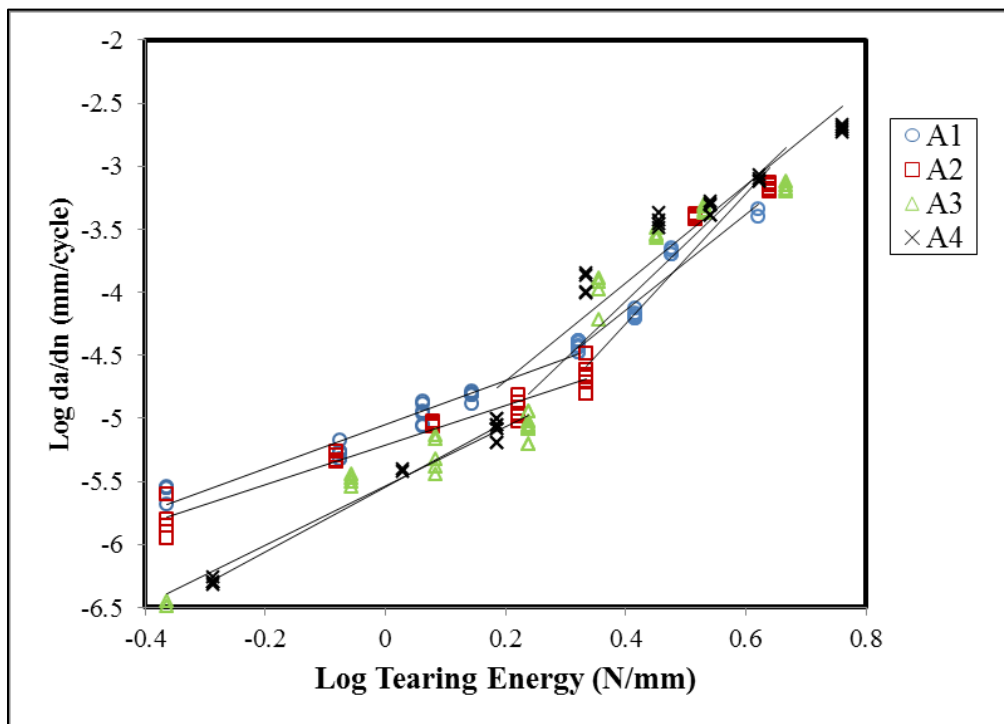
Figure 5.2 Variation of crack growth rate with tearing energy (log-log plot)

From Figure 5.2, it can also be observed that these compounds behave differently in the regions below and above the transition point. In the region, below transition point, compound A1 exhibited highest crack growth rate followed by A2, A3 and A4. Here, crack growth resistance of the material increases with increasing BR content. However, reversal of crack growth ranking of these compounds was observed above the transition point. In this region, the highest crack growth resistance was observed in the compound A1, which is attributed to strain induced crystallization in NR material at moderate to large strains. This is a very effective process to dissipate strain energy (Hamed, 1994) because further crack propagation requires disruption of crystallites at the crack tip. The energy spent for this process will not be available for crack propagation and hence the fracture resistance increases. The formation of crystalline zone in front of the crack tip also leads to a deviation of the crack path from orthogonal direction of principal strain. To understand this aspect, the profiles of the fractured surface of samples tested at 30% stain are presented in Figure 5.3.
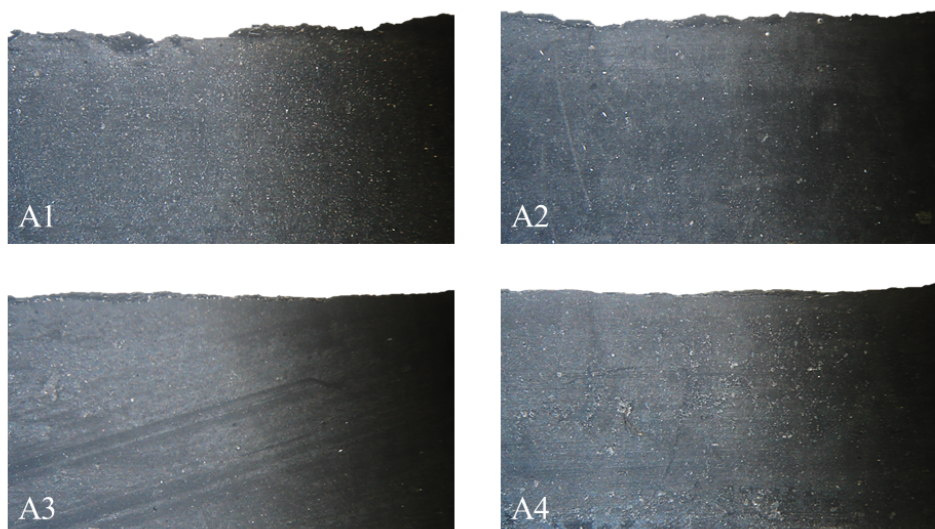
Figure 5.3 Profile of fractured surface of samples tested at 30% strain

Surface analysis of the fractured pure shear specimens was done using an optical microscope (Leica Q 500 IW, Cambridge, UK) at 20x magnification. These profiles reveal that the degree of surface roughness varies in these compounds. Compound A1 shows the highest surface roughness compared to others, which indicates crack path deviation due to crack tip blunting. It is also observed that the surface roughness decreases with increasing BR content. A similar observation was also made by

Hamed *et al.* (1996) where they have shown the presence of secondary cracking in NR and NR/BR blends and complete absence of it in 100% BR compound. Therefore, it can be inferred that the formation of secondary cracking is due to inherent characteristics of strain induced crystallization in NR based compounds. This may lead to different degrees of roughness on fractured surface. Further to the inherent ability of strain induced crystallization in NR, study of Stacer *et al.* (1985) suggested that the presence of carbon black expands the crack tip crystallization zone and increases the crystallinity.

The FCG parameters (b and m) as obtained from below as well as above the transition point tearing energy plots are provided in Table 5.1 and 5.2 respectively. To compare all the compounds at equal tearing energy, crack growth rates were calculated at two tearing energies, 1.5 N/mm and 3 N/mm using these values. The variations of crack growth rate at these two tearing energies are shown in Figures 5.4 and 5.5. On the basis of these observations it is extremely important to mention here that, while designing the compound based on fatigue crack growth behaviour, prior knowledge about the end application, with regard to strain, stress etc. is required.

Table 5.1 FCG parameters below the transition point

Compound	b	m
A1	8.43E-06	1.5311
A2	5.93E-06	1.4893
A3	2.90E-06	2.3551
A4	2.84E-06	2.5737

Table 5.2 FCG parameters above the transition point

Compound	b	m
A1	2.16E-06	3.8139
A2	0.589E-06	5.015
A3	15.6E-06	2.5864
A4	15.5E-06	2.7686
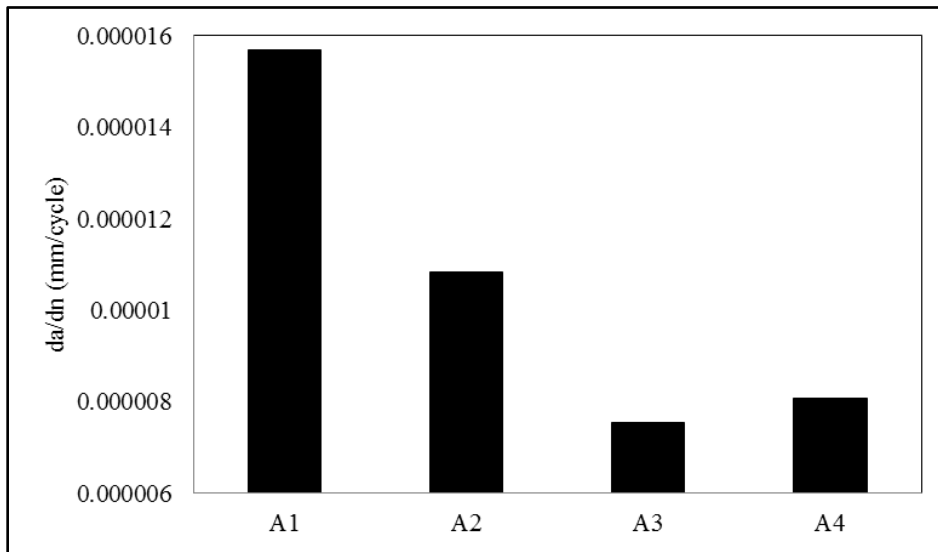
Figure 5.4 Crack growth rate at 1.5 N/mm tearing energy
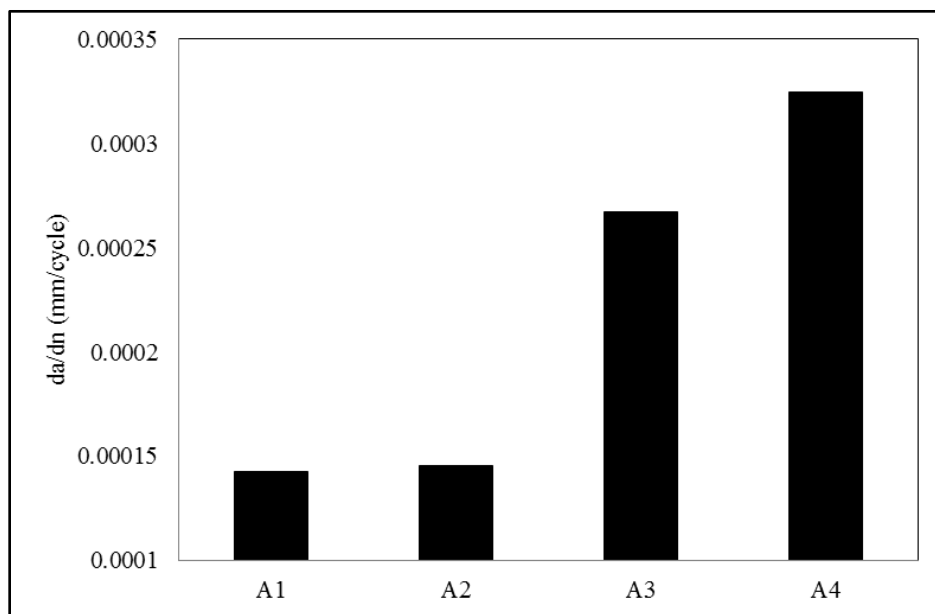
Figure 5.5 Crack growth rate at 3 N/mm tearing energy

67

5.1.2 Temperature

The influence of temperature on FCG properties were studied using A1 and A4 compounds. The temperature dependence on FCG rate of compounds A1 and A4 are shown in Figures 5.6 and 5.7 respectively.
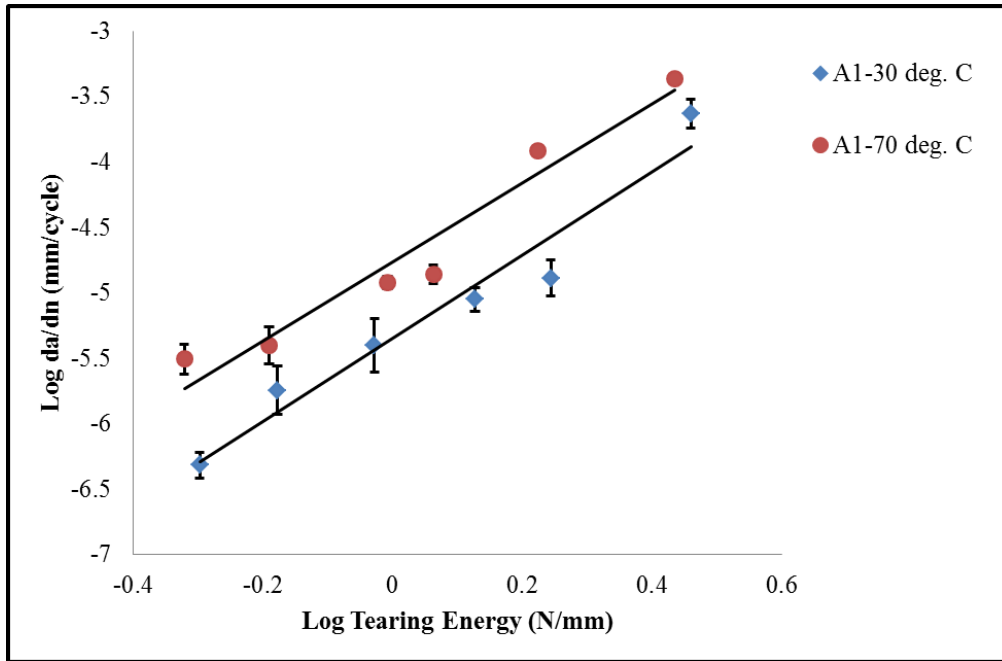
Figure 5.6 FCG curves for A1 at 30 and 70^0 C
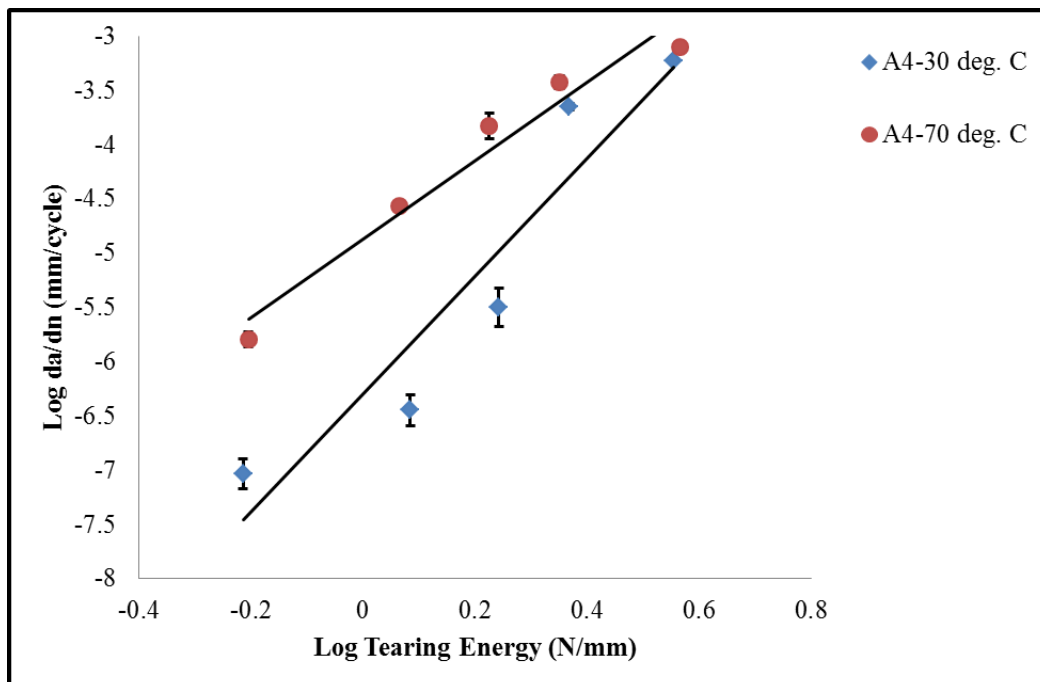
Figure 5.7 FCG curves for A4 at 30 and 70^0 C

Both the compounds exhibit significant increase of crack growth rate with temperature increase and can be explained by energy dissipation process. The viscoelastic dissipation at the crack tip is one of the most important mechanisms in fracture resistance of polymers (Persson *et al.*, 2005). This dissipation process has two contributions which are shown in Figure 5.8. The first one is related to the highly non-linear process involving cavity formation, bond breaking, chain pull out etc. at the innermost region of the crack tip (dark area). The other contribution comes from the bulk viscoelastic dissipation in the linear viscoelastic region in front of the crack tip (annular shaded area). As the temperature increases, molecular movements become easier and this leads to a decrease in viscous dissipation. This results in decrease in the fracture resistance of rubber vulcanizates as more energy is available for crack propagation and is clearly evident from the loss modulus variation with temperature as shown in Figure 5.9. There was a considerable drop (~ 35%) in loss modulus value at 70^0 C from that of 30^0 C. Kluppel (2009) also shown the relation between crack propagation rate and viscoelastic property (scaling exponent of the relaxation time spectra) of elastomers.
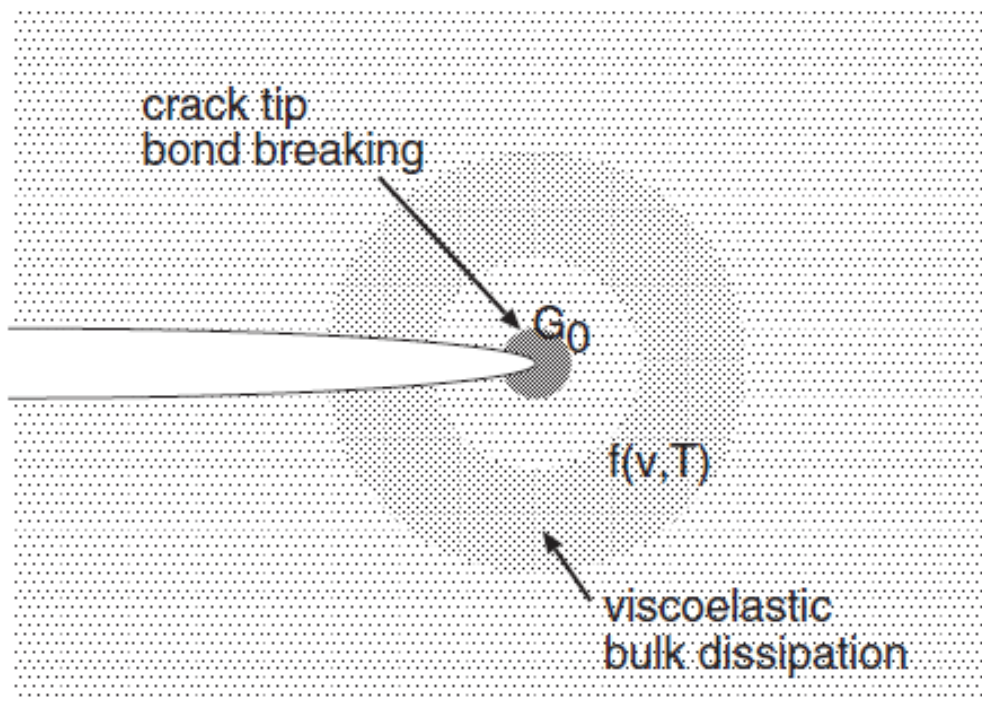
Figure 5.8 The crack propagation energy G is a product of a term G0 derived from the bond breaking at the crack tip, and a term f (v, T) derived from the bulk viscoelastic energy dissipation in front of the tip (Persson *et al.*, 2005).

It was also observed that A4 shows higher sensitivity with respect to the temperature compared to A1, which may be due to the presence of 40 parts of BR in the former compound, which is non-strain crystallizable. It is consistent with the observation made by Lake and Lindley (1965), where non-strain-crystalizing SBR showed the greatest effect towards temperature as compared to NR.

Further, the findings by Qazvini *et al*. (2002) can also be referred to here in order to understand the higher temperature sensitivity in A4, which is a 60-40 NR/BR blend. As per their observation, the fracture energies of blends initially decrease with an increase of temperature, passing through a minimum and increasing again. It was hypothesized that blend system at room temperature, tends to exist as heterogeneous phase structure. But the complete phase separation is prevented by the networks (crosslinks) between the two components which are formed during vulcanization at higher temperature. As a result, these networks bear some residual stresses which relax on increase of temperature due to improved interpenetration of polymer chains. The existence of two phases at molecular level was further confirmed by the presence of two glass transition temperatures (T_g) in all the blends and values are reported in Table 4.9 of Chapter 4. Therefore, it may be inferred that in A4, apart from reduction of viscoelastic loss with temperature, network residual stress part is also contributing for higher FCG rate.
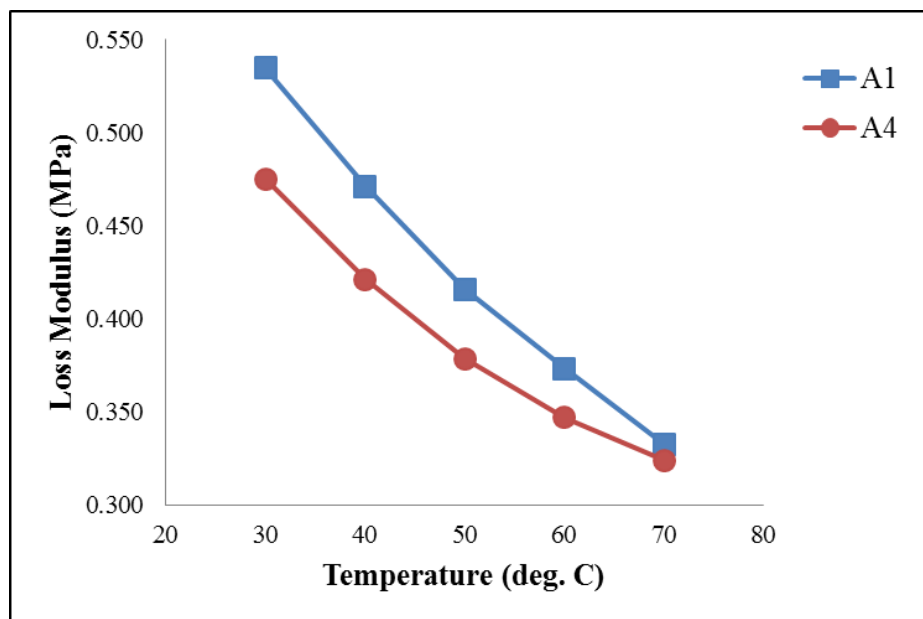
Figure 5.9 Variation of loss modulus with temperature

5.1.3 R-ratio

The influence of R-ratio on FCG characteristics was investigated using A1 and A4 compounds. Figures 5.10 and 5.11 represent the effect of R-ratio on FCG for compounds A1 and A4. It is evident from Figure 5.10 that the compound A1 under positive R-ratio, exhibits significant decrease in crack growth rate at lower tearing energy and it tends to converge with the zero R-ratio while moving towards a higher tearing energy. The linear extrapolation yields a single point convergence at tearing energy of 4.79 N/mm and crack growth rate of 6.30E-04 mm/cycle. This is similar to the observation made by Lindley (1973). The difference in absolute values may be due to the use of different compound formulation in the present work. The decrease of FCG rate at higher R-ratio is also associated with the strain induced crystallization phenomena as explained by many researchers (Lindley, 1973; Sainter et al., 2011; Bruning et al., 2013).
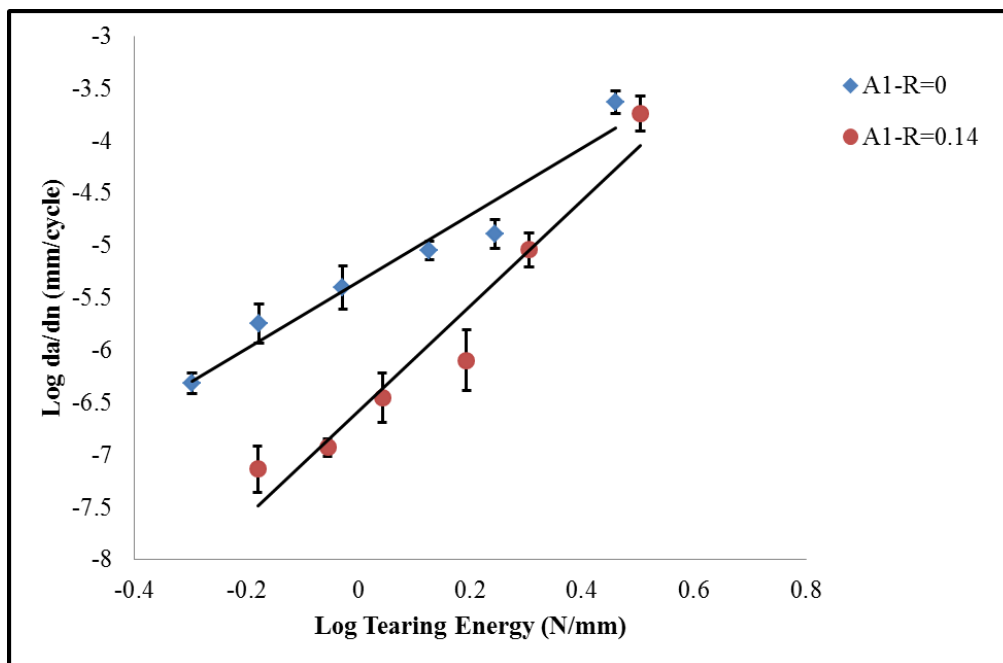
Figure 5.10 FCG curves for A1 at different R-ratios

A recent work by Saintier et al. (2011) explained the influence of strain induced crystallization of NR material under cyclic loading conditions for a positive R-ratio. It was argued that at R=0, strain induced crystallization also exists but it melts at each cycle. But in the case of R > 0, there exists a constant pre-load, which helps to prevent complete melting of crystalized zone. The complete process is shown in Figure 5.12.

Bruning *et al*. (2013) captured the crystallization behaviour around the crack tip using WAXD under quasistatic and dynamic condition. They have also described the crack branching mechanism.
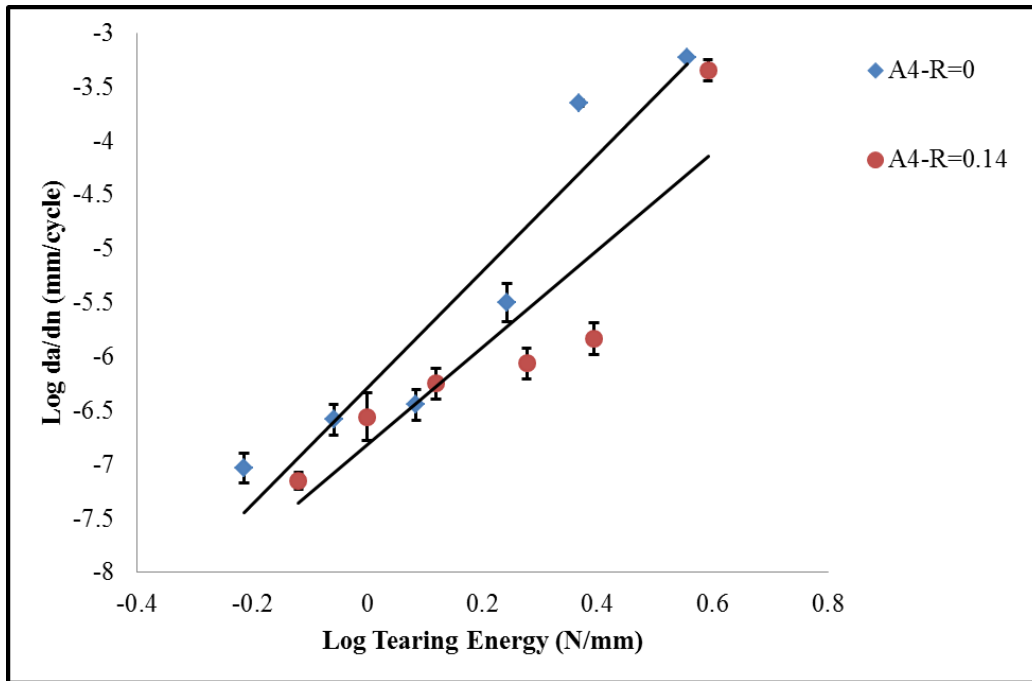
Figure 5.11 FCG curves for A4 at different R-ratios
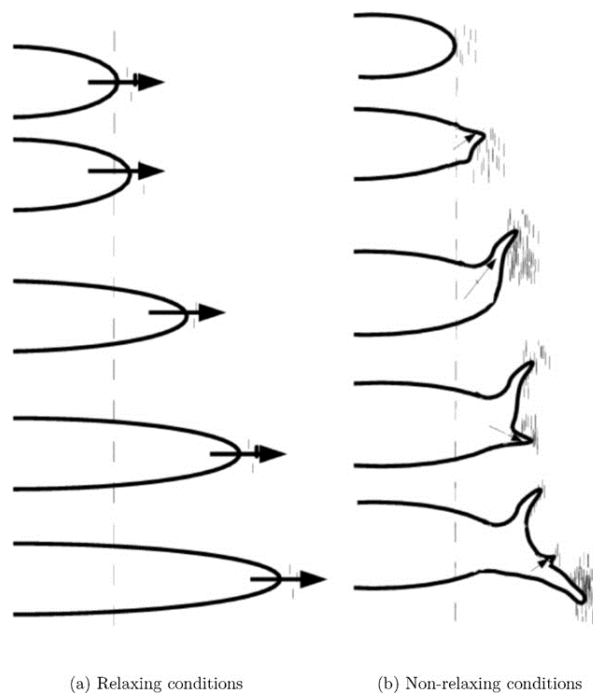
Figure 5.12 Crack propagation process for relaxing and non-relaxing condition (Saintier *et al*., 2011)

As the compound A1 is 100% NR, it achieved five to fifteen times decrease in crack growth rate. However, compound A4 which is 60-40 NR/BR blend did not show much dependence on R-ratio. As observed from Figure 5.3, an increase in BR content results in a smoother surface. This indicates that crack propagates mostly in BR phase and therefore chances of crack tip crystallization are minimized.

5.1.4 Waveforms

The effect of waveform on FCG characteristics is shown in Figures 5.13 and 5.14. The important observation is that the compounds show higher FCG rate in Pulse modes as compared to Sine mode. This is in accordance with the findings of the previous researchers (Harbour *et al*., 2007; Andreini *et al.*, 2010). Harbour *et al*. (2007) ruled out the role of strain induced crystallization as the effect of Pulse loading on crack growth rate is more in filled SBR than NR. It was hypothesized that in Pulse mode testing there will be some dwell period which may assist in time dependent recovery of rubbery microstructure at crack tip which leads to a localized and temporary elevated stress state. The reformation of broken polymer chain or reorganization of the polymer chain network or redistribution of filler at crack tip produces stiffer material at the crack tip. This leads to a localized and temporary elevated stress state, which can account for the higher crack growth rate.

In contrast to the above findings, no appreciable difference in crack growth rate was observed in SBR for Pulse loading compared to Sine waveform in the work presented by Andreini *et al.* (2010). They have argued that the higher crack growth rate in Pulse loading is linked to material's ability to rearrange the molecular chain. The molecular chains get oriented during the relaxation period in Pulse testing which inhibits the strain induced crystallization phenomena, while in the Sine waveform, a constant dynamic deformation is maintained. Both NR and BR are significantly affected by the Pulse mode. From this hypothesis, more strain crystallizable NR should have shown higher degree of influence compared to BR. Interestingly, no such effect was observed.
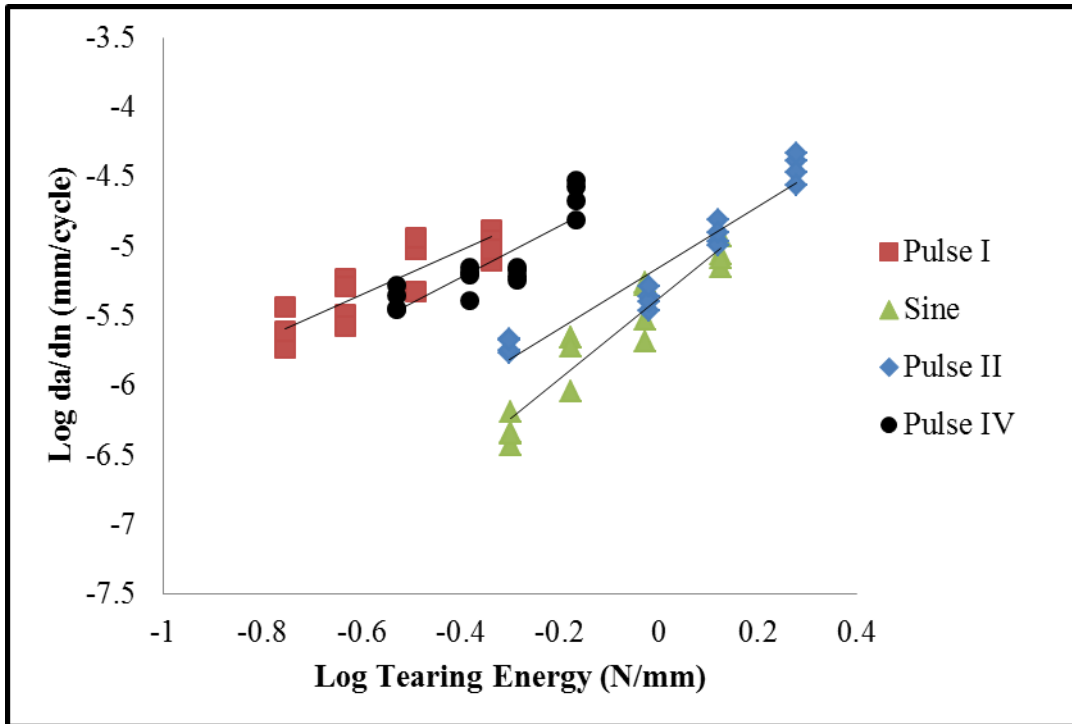
Figure 5.13 FCG curves for A1 for Sine and Pulse waveforms
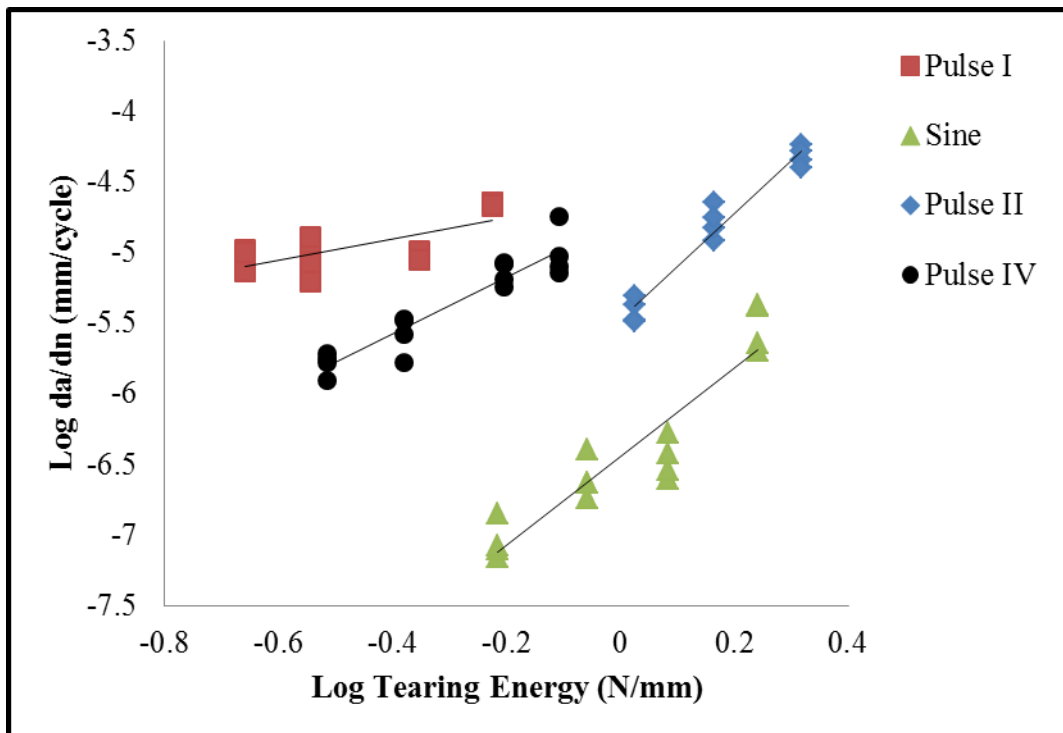
Figure 5.14 FCG curves for A4 for Sine and Pulse waveforms

From this discussion it can be inferred that no unified explanations are available which can take into account the higher FCG rate in Pulse mode. A similar observation of higher FCG rate in Pulse mode was also made from the present study. Further, FCG rate of Pulse I loading is higher than that of Pulse II and IV. The test condition details reveal that the Pulse mode deformation differs from Sine mode in two respects, strain rate and dwell time which are provided in Table 5.3.

Table 5.3 Strain rate and relaxation time of Sine and Pulse waveform

Waveform type	Strain Rate (S^{-1}) at various strains						Dwell Time (ms)
	10	13	16	20	25	30	
Sine	-	2.6	3.2	4	5	6	0
Pulse I	-	13	16	20	25	30	80
Pulse II	10	13	16	20	25	30	980
Pulse IV	10	13	16	20	25	30	180

Therefore, one of the reasons for higher FCG rate in Pulse loading could be attributed to higher impact loading due to five times higher strain rate than the Sine waveform. This may also lead to instantaneous increase of temperature at the crack tip. However this argument is valid as long as the comparison is between Sine and Pulse loading. It can be observed that Pulse I show the highest FCG rate among all the Pulse modes despite having the same strain rate. But this mode has lowest dwell time when compared to the Pulse II and IV. So it can be suggested that the higher dwell time may lead to a reduction in temperature at the crack tip and thereby lowering of the crack growth rate in Pulse II and IV. It was also observed that higher sensitivity towards Pulse loading was observed in A4 when compared to A1. However, the probable reason for exhibiting such characteristics by A4 is not clearly understood and requires further investigation.

5.1.4 Cure System

The influence of cure system on FCG characteristics was studied using A1-Modcure and A4-Modcure compounds. Crack growth results of different cure systems are provided in Figures 5.15 and 5.16.
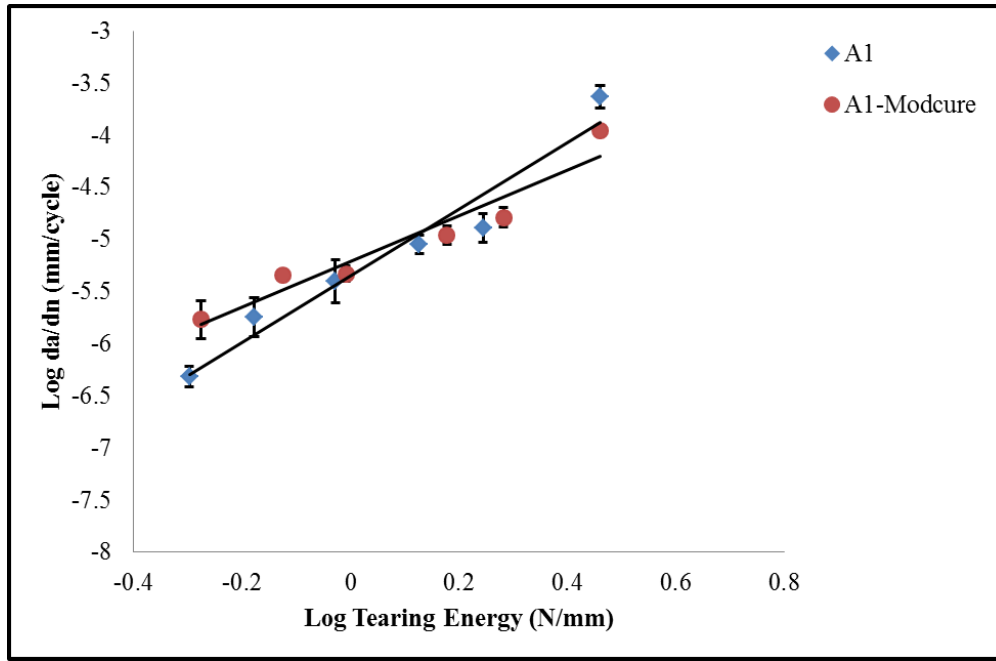
Figure 5.15 FCG curves for A1 and A1-Modcure
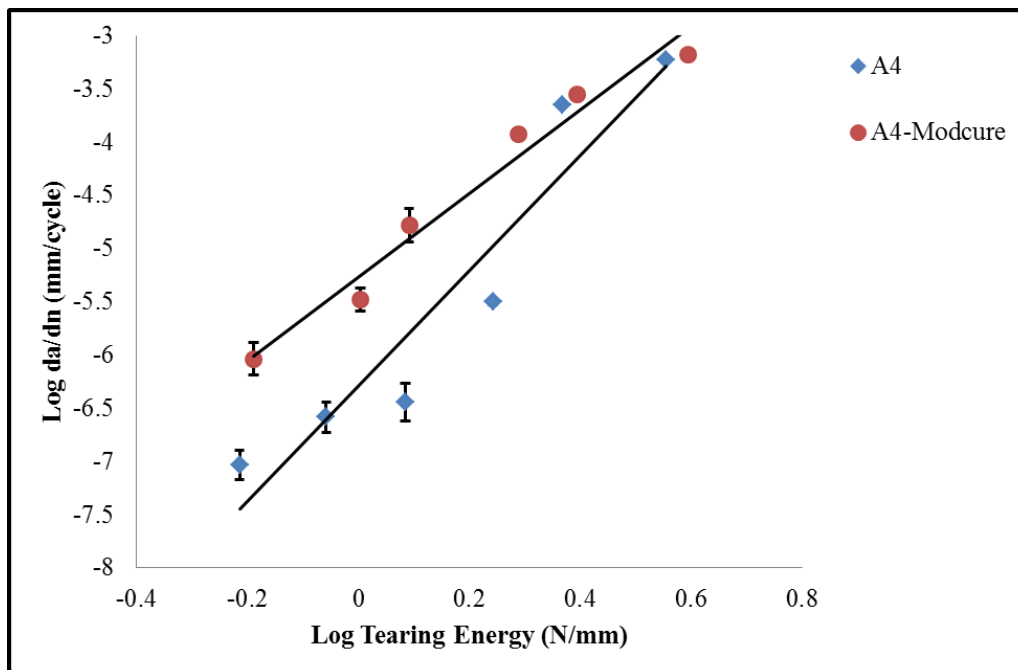
Figure 5.16 FCG curves for A4 and A4-Modcure

FCG rate of A1-Modcure is marginally higher than A1 at low tearing energy zone but at a higher tearing energy the difference is negligible. The major difference between these two compounds is in the Sulphur/Accelerator (S/Ac) ratio. The higher S/Ac (2 phr sulphur and 0.5 phr accelerator) ratio was used in A1 whereas A1-Modcure contained lower S/Ac ratio (1.5 phr sulphur and 0.8 phr accelerator). Due to the usage of higher S/Ac ratio in A1, considerable amount of polysulphide linkages in crosslink structure are produced. It is also known that polysulphide linkages are very effective in providing better fatigue resistance than mono or disulphide or carbon-carbon (c-c) linkages as it is able to break before c-c back bone and reform subsequently. This could be the reason for A1 to have a better FCG resistance compared to A1-Modcure. The study made by Kim and Lee (1994) also reported similar observation. The un-aged compound with CV system which favors polysulphide link formation, showed better FCG resistance compared to EV and SEV system.

However, the FCG rating of A4 vs A4-Modcure was not in line with the observation made for A1 vs. A1-Modcure. Here A4 contained low S/Ac ratio (1.5 phr sulphur and 0.8 phr accelerator), whereas A4-Modcure compound contained high S/Ac ratio. The A4-Modcure compound exhibited much higher crack growth rate at low tearing region compared to A4, but the difference narrowed down at a higher tearing energy level. So it is clear that the difference in FCG behaviour may be attributed to the presence of BR in A4 and A4-Modcure compound.

5.2 FCG CHARACTERISTICS OF NR/SBR BLENDS

In this section, influence of SBR content, Temperature, R-ratio, Waveforms on FCG characteristics is described.

5.2.1 SBR content

Figure 5.17 represents the double logarithmic plot of tearing energy vs. crack growth rate of NR/SBR blend compounds. It can be observed that at lower tearing energy, the crack growth rate of higher SBR content blend is much low when compared to the B2 and B3 compound. However, reversal of this trend is observed at higher tearing energy. Similar behaviour was also observed in the case of NR/BR blend compounds.
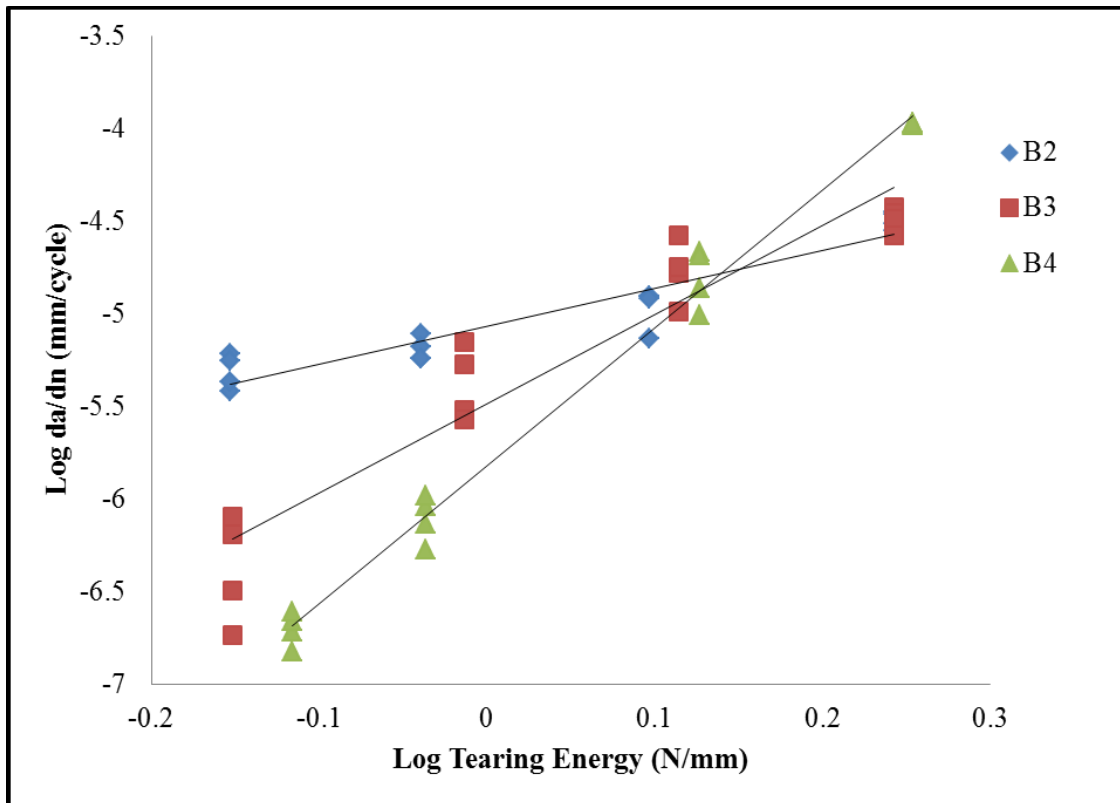
Figure 5.17 Variation of crack growth rate with tearing energy (log-log plot)

The FCG parameters (b and m) of NR/SBR blends are calculated and provided in Table 5.4. It can be observed that the exponent, m increases with increasing SBR content in the NR/SBR blends.

Table 5.4 FCG parameters of NR/SBR blend compounds

Compound	b	m
B2	8.56E-06	2.0521
B3	3.28E-06	4.817
B4	1.51E-06	7.4545

5.2.3 Temperature

The influence of temperature on FCG properties of B4 compound is shown in Figure 5.18.
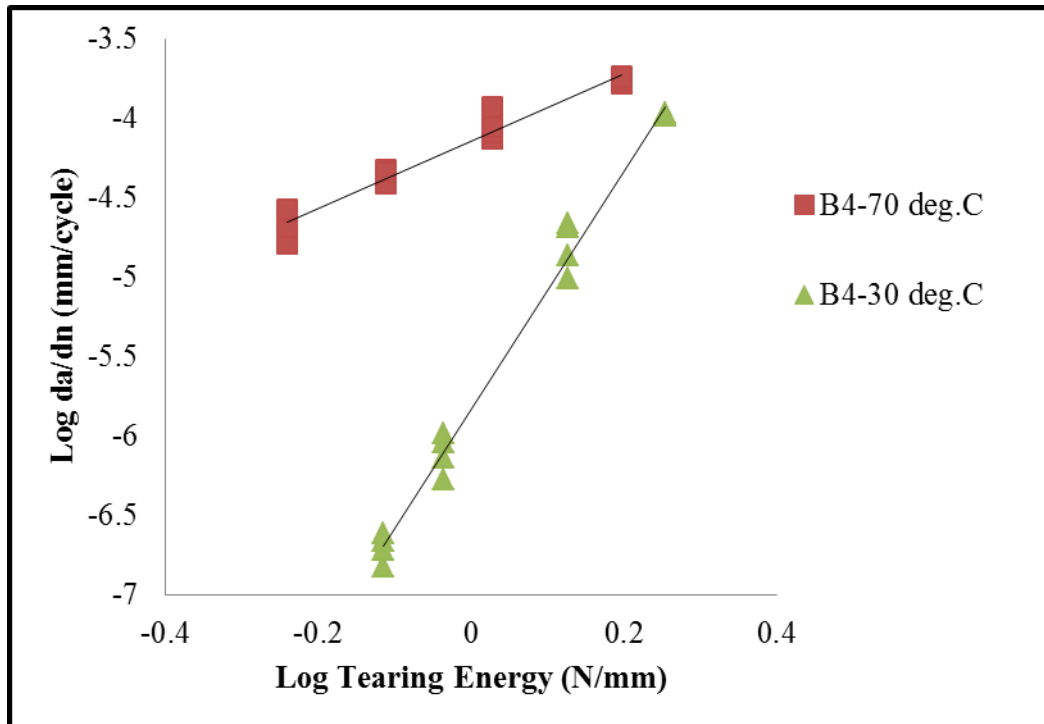
Figure 5.18 FCG curves for B4 at 30 and 70 deg. C

It can be observed that the FCG rate is much higher at 70^0 C compared to the 30^0 C. This observation is also in accordance with the NR/BR blend results. The study made by Lake and Lindley (1965), also reported that for unfilled SBR, 10^4 times reduction in fatigue life is observed for unfilled SBR due to temperature increase from 0 to 100^0 C, whereas this factor is only 4 times for unfilled NR. As the B4 compound also contains 40 parts of SBR, the drastic reduction of FCG resistance can be expected.

5.2.3 R-ratio

The influence of R-ratio on FCG characteristics is provided in Figure 5.19 for B4 compound. The significant increase in FCG resistance under 0.14 R-ratio is observed in comparison with zero R-ratio for NR/SBR blend. It is important to mention here that the influence of R-ratio is more here when compared to the corresponding NR/BR blend.
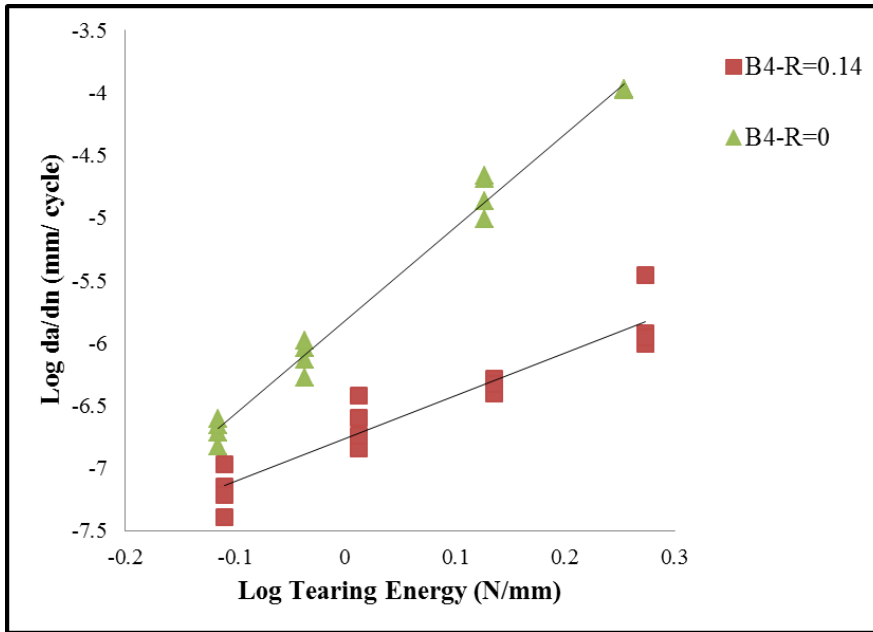
Figure 5.19 FCG curves for B4 at different R-ratios

5.2.4 Waveforms

The influence of various waveforms on FCG characteristics is shown in Figure 5.20.
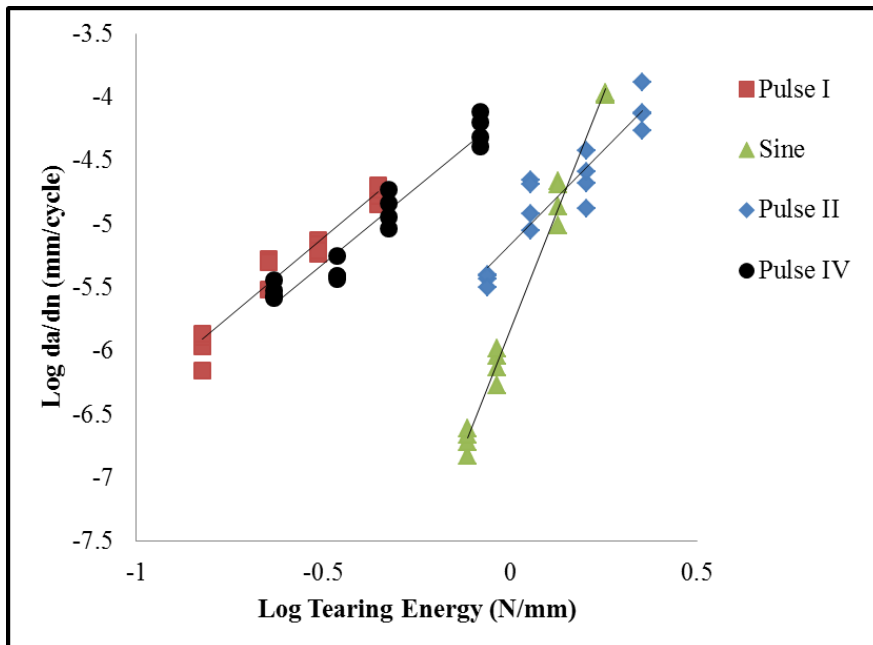
Figure 5.20 FCG curves for B4 at different Waveforms

It has been observed that the FCG rate is much higher in the Pulse mode compared to the Sine mode. Similar behaviour was also observed in the case of NR/BR blend compounds. The highest crack growth rate was observed in the case of Pulse I mode followed by Pulse IV mode. Sine mode, exhibited lower FCG rate initially when compared to the Pulse II and became higher at higher tearing energy.

5.3 FCG OF 100 NR, BR AND SBR COMPOUNDS

In this section, FCG properties of 100 NR (A1), BR (A5) and SBR (B5) compounds are discussed. The FCG properties were measured at 30^0 C under Sine, Pulse I and Pulse II mode. Tearing energy vs. crack growth rate plots of these compounds are provided in Figures 5.21 to 5.23. It has been observed that under all these conditions, B5 compound showed the highest FCG rate in low to moderate tearing energy level compared to the other two compounds. Between A1 and A5, it can be seen that A5 shows lower FCG rate in lower tearing energy level and a higher rate at higher tearing energy. This observation is in agreement with Young (1985) where crossover point between BR and NR curves is reported at 15% strain. The A1 compound shows highest FCG resistance at higher tearing energy level due to strain induced crystallization.
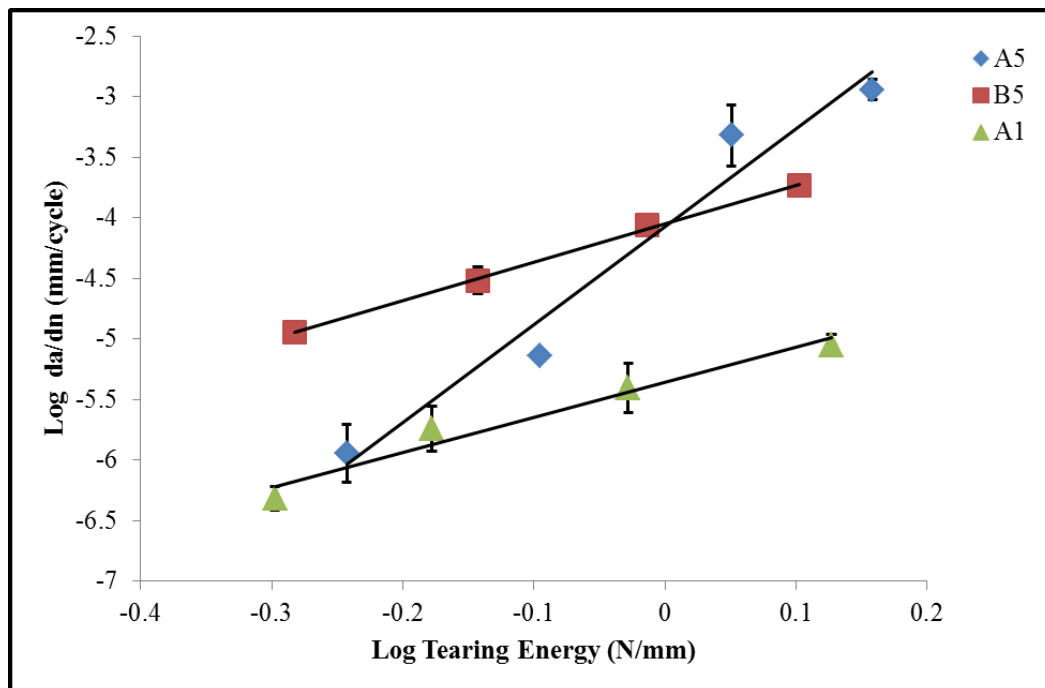
Figure 5.21 FCG curves of A1, A5 and B5 compound at 30^0 C and Sine mode
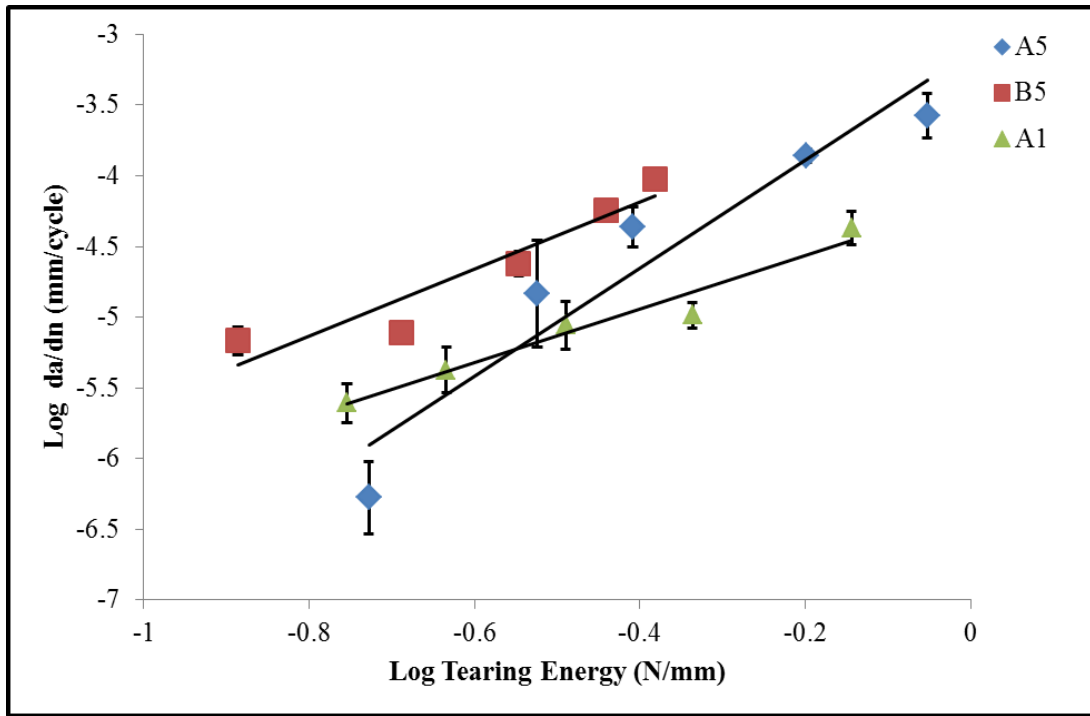
Figure 5.22 FCG curves of A1, A5 and B5 compound at 30^0 C and Pulse I mode
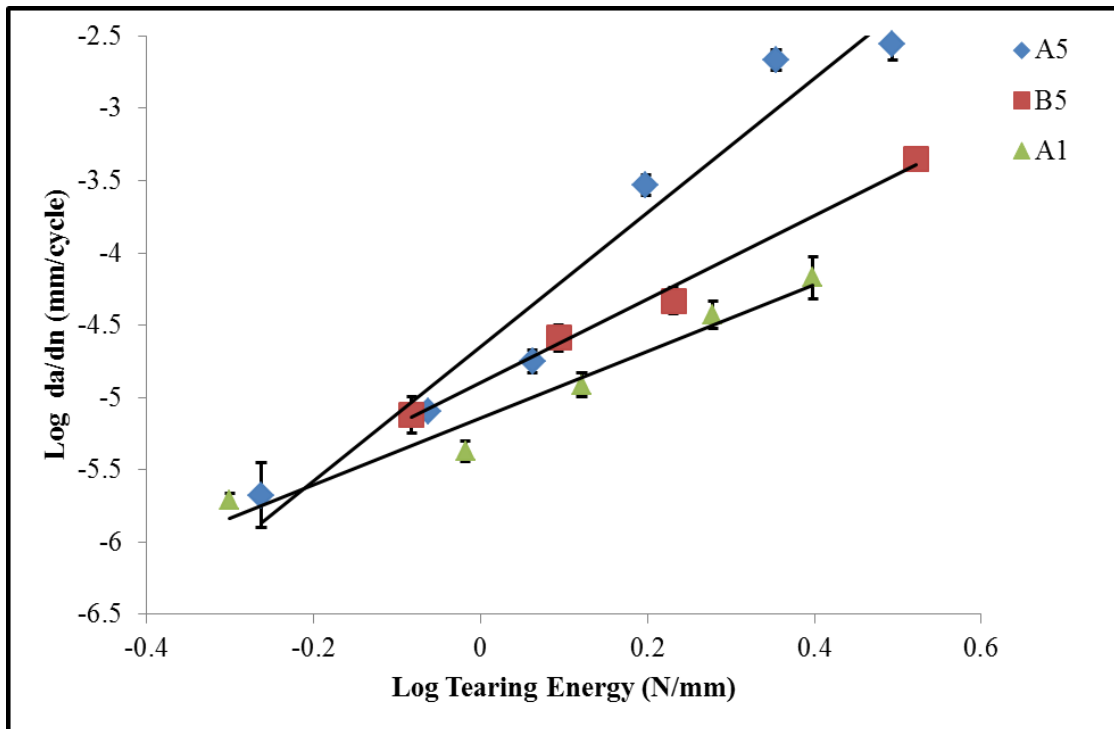
Figure 5.23 FCG curves of A1, A5 and B5 compound at 30^0 C and Pulse II mode

5.4 COMPARISON OF FCG PROPERTIES BETWEEN NR/BR AND NR/SBR BLENDS

In this section relative comparison of FCG characteristics between NR/BR and NR/SBR blends are presented for temperature, R-ratio and waveform variation.

5.4.1 Temperature

Tearing energy vs crack growth rate plots of NR/BR (A2, A3 and A4) and NR/SBR (B2, B3 and B4) blends at 30^0 C are shown in Figures 5.24 to 5.26. These plots revealed that FCG resistance of all the NR/BR blends are better than the corresponding NR/SBR blends. It has been observed that the superiority of NR/BR blends with respect to FCG resistance increases with increasing BR content.
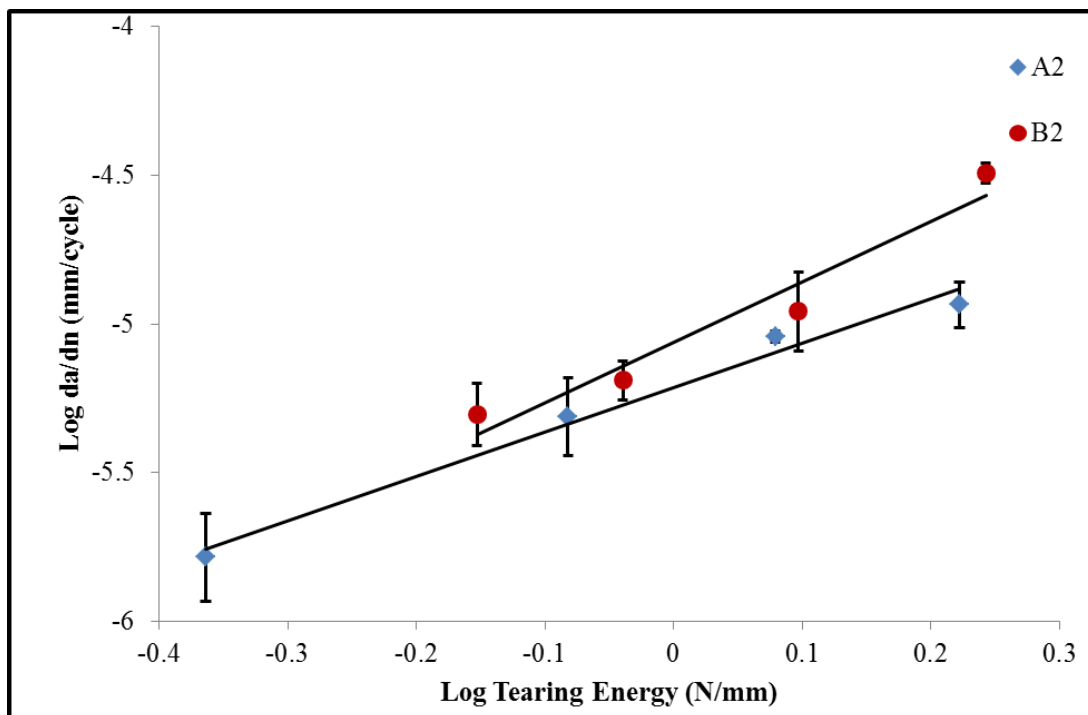
Figure 5.24 FCG curves for A2 and B2 at 30^0 C
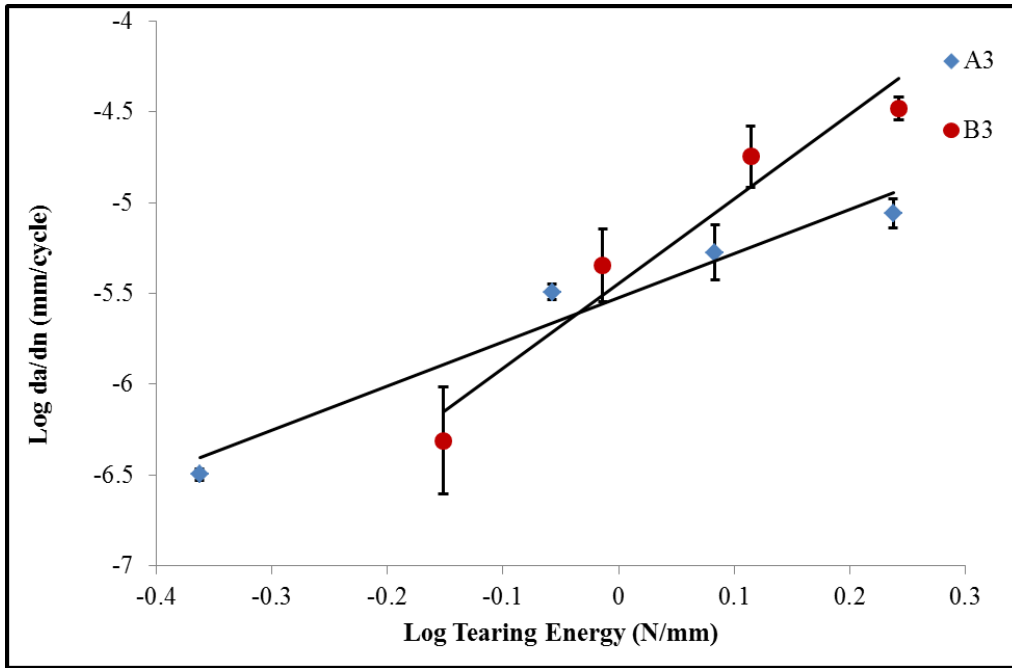
Figure 5.25 FCG curves for A3 and B3 at 30^0 C
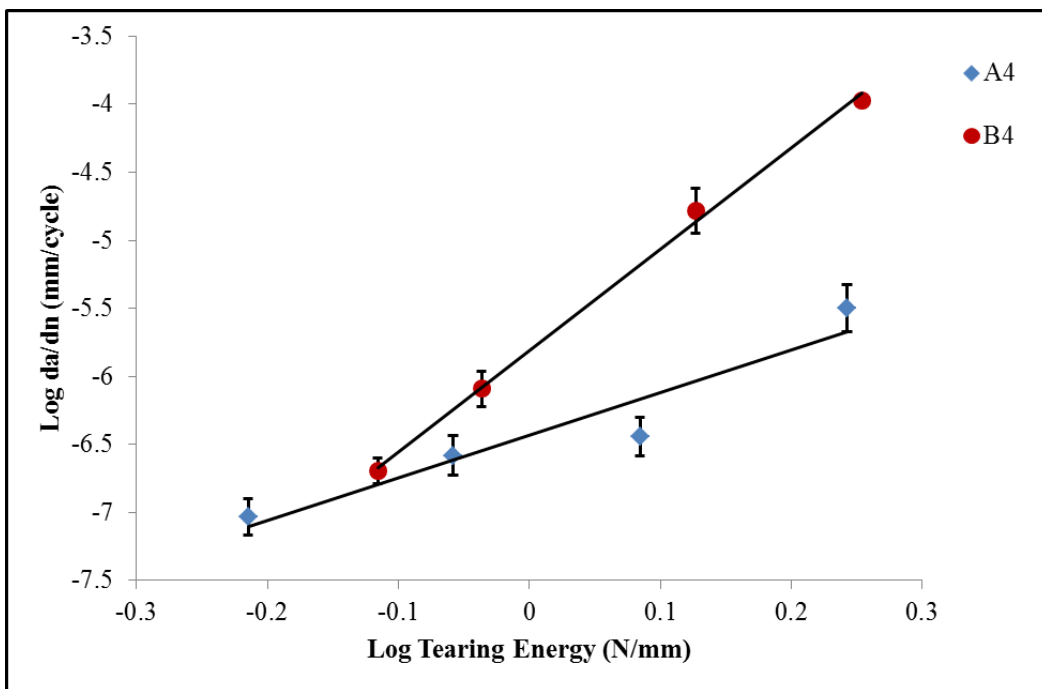
Figure 5.26 FCG curves for A4 and B4 at 30^0 C

Figure 5.27 shows the comparison of FCG properties between A4 and B4 compounds at 70^0 C and it can be seen that FCG rate for B4 compound is much higher than A4 compound.
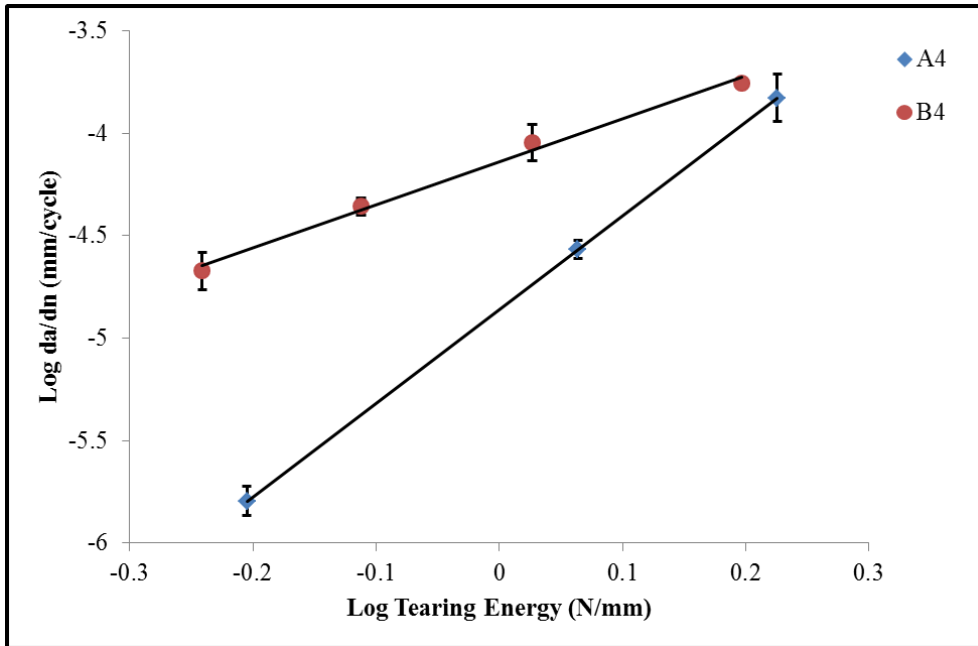
Figure 5.27 FCG Curves for A4 and B4 at 70^0 C

5.4.2 R-ratio

Figure 5.28 represents the tearing energy vs crack growth rate at 0.14 R-ratio for A4 and B4 compound. There is a very small difference in FCG characteristics between A4 and B4 compounds.
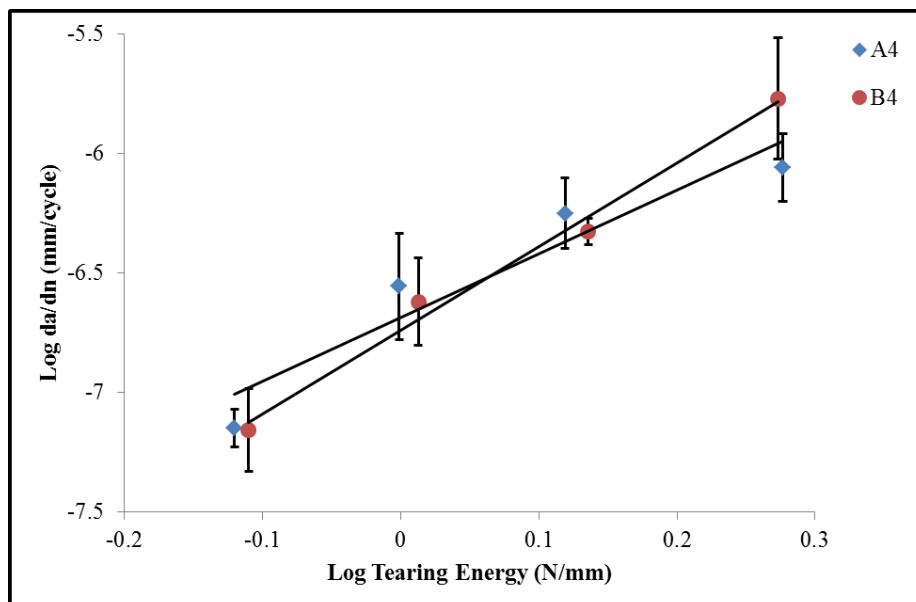
Figure 5.28 FCG Curves for A4 and B4 at 0.14 R-ratio

5.4.3 Pulse mode

Figure 5.29 shows the comparison of FCG properties of A4 and B4 compounds in Pulse mode and as can be seen that the FCG resistance of B4 is much lower in comparison with A4 compound. Overall, in almost all conditions except at 0.14 R-ratio, FCG rates are much higher in NR/SBR blends. This is in conformity with the earlier findings made by Bhowmick and De (1980) where NR/SBR blend showed much inferior crack growth resistance compared to NR/BR blend. The FCG parameters, b and m were calculated and reported in Table 5.5.
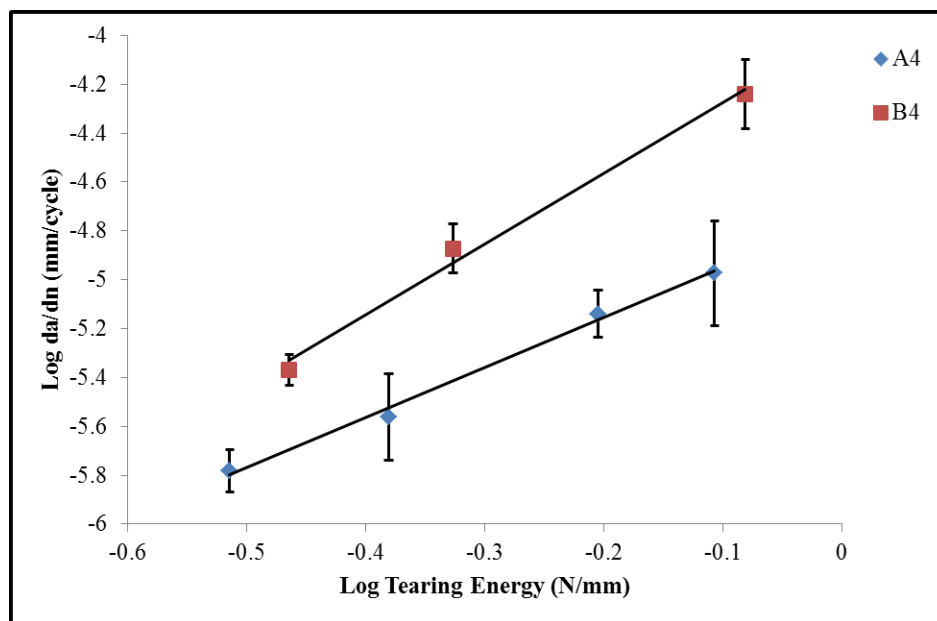
Figure 5.29 FCG Curves for A4 and B4 at Pulse mode

Table 5.5 FCG parameters of A4 and B4 compounds

FCG Test condition	A4 (60-40 NR/BR Blend)		B4 (60-40 NR/SBR Blend)	
	b	**m**	**b**	**m**
30^0 C	3.14	3.70E-07	7.44	1.54E-06
70^0 C	4.33	1.33E-05	2.09	7.25E-05
0.14 R-ratio	2.67	2.06E-07	3.49	1.82E-07
Pulse Waveform	2.04	1.79E-05	2.89	1.04E-04

For comparison purpose, crack growth rates of these two blends (A4 and B4) at equal tearing energy of 1.5 N/mm is calculated and presented in Figure 5.30. It clearly shows that NR/BR blend exhibited superior FCG resistance.

	30 deg. C	70 deg. C	0.14 R-ratio	Pulse
NR/BR	1.32E-06	7.70E-05	6.08E-07	4.09E-05
NR/SBR	3.15E-05	1.69E-04	7.49E-07	3.36E-04
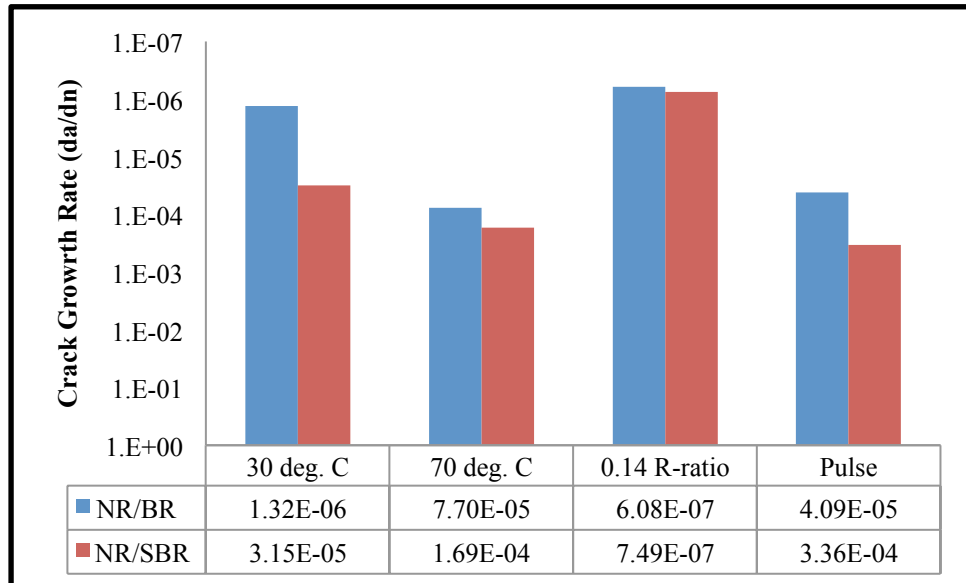
Figure 5.30 Crack growth rate at 1.5 N/mm tearing energy

5.5 SUMMARY

In this chapter, FCG characteristics of pure NR, BR, SBR, NR/BR and NR/SBR blend compounds are discussed. The contribution of different rubbers in the blend has been studied. The influence of temperature, R-ratio and waveform on FCG behaviour has been presented. Out of these parameters, waveform type has the highest influence. FCG results revealed that, a threshold tearing energy exists for each material above which crack growth rate increases significantly. The reversal of FCG ranking was also observed above the threshold value. Hence, this must be considered as an important criterion for tread compound selection. The FCG rate in Pulse mode is much higher in comparison with the Sine mode. This is due to the higher strain rate associated with Pulse mode testing. Pulse mode should be used for FCG evaluation as it closely simulates the tyre loading pattern during rolling condition. Overall NR/BR blends exhibited superior FCG resistance over NR/SBR blend compounds.

CHAPTER 6

WEAR CHARACTERISTICS OF RUBBER BLENDS

This chapter describes the influence of material composition and test variables on wear characteristics of NR/BR and NR/SBR blend compounds based on the wear measurement results obtained from LAT 100 equipment. The detailed test methodology has been described in section 3.2.10 of Chapter 3.

6.1 WEAR CHARACTERISTICS OF NR/BR BLENDS

In this section, wear results of NR/BR blends measured under variable speed and slip angle condition on different abrading surfaces is discussed. The influence of speed and slip angle on wear is discussed in detail.

6.1.1 Speed

The influence of speed on wear characteristics of NR/BR blend compounds measured on Corundum 60 and 180 surfaces is shown in Figures 6.1 to 6.6. These plots represent the wear variation with speed at constant slip angle of 5.5^0, 9^0 and 16^0 in double logarithmic scale. It can be observed that the wear increases linearly with the speed for all the slip angles except at 5.5^0 for both the abrading surfaces. At 5.5^0 slip angle, in both surfaces, wear increases linearly up to certain speed and then shows a decreasing trend. The increase in wear with speed is attributed to the increase in energy dissipation at the contact patch leading to increase in surface temperature as considerable amount of the input energy is converted into heat (Grosch, 2005). Due to temperature increase, strength of the material also changes. Therefore wear is a combined effect of speed and temperature. According to Veith (1992), rate of tyre wear (R_w) is a function of the fourth power of speed and can be expressed as,

$$R_w = KWV^4/R^2G^2 \tag{6.1}$$

where, K is a constant, W is vehicle weight, V is the speed, R is curve radius and G is acceleration constant. This literature also discussed the temperature dependence on rate of wear which is given as,

$$R_w = R_w(50)[1+\alpha(T-T_0)]$$ (6.2)

where, R_w is rate of wear at any temperature T, $R_w(50)$ is the rate of wear at reference temperature of 50^0 C, T_0 is reference temperature, α is temperature coefficient of wear (0.04 - NR, 0.02 - SBR). The variation of rubber surface temperature with speed at constant slip angle of 16^0, measured using IR Thermography is presented in Figures 6.7 and 6.8 for Corundum 60 and 180 respectively. A considerable amount of temperature increase ($\sim 35^0$ C) is observed in both the surfaces while moving from 2.5 kmph to 25 kmph speed. This is in agreement with the results reported by Heinz and Grosch (2007).

The work of Grosch et al. (2001) compared wear of carbon black filled NR and SBR compounds with speed. It was observed that the speed dependence of NR compound is higher and can be explained from equation 6.2, where α value for NR is higher when compared to SBR. The results of the present experiments also revealed that the wear characteristics of the studied compounds (A1-A4) also vary widely which could be attributed to the differences in cut growth resistance property and temperature coefficient of wear. The wear is highest in all the slip angles for pure NR compound (A1) and it decreases with increasing BR content (A2-A4), which corroborates the findings of Gent and Pulford (1983). As per them, thermal degradation also plays a role in wear process and it is known that BR has got very high decomposition temperature (> 500^0 C) in comparison with NR ($\sim 260^0$ C). It was suggested that there are three major chemical contributions which influence wear process: thermal degradation because of frictional heating, temperature aided oxidation and free radical generation during fracture which also takes part in the oxidation process. BR has the highest resistance against all these degradation process and this is the major reason for achieving superior wear resistance despite having its lower strength property in comparison with the NR.
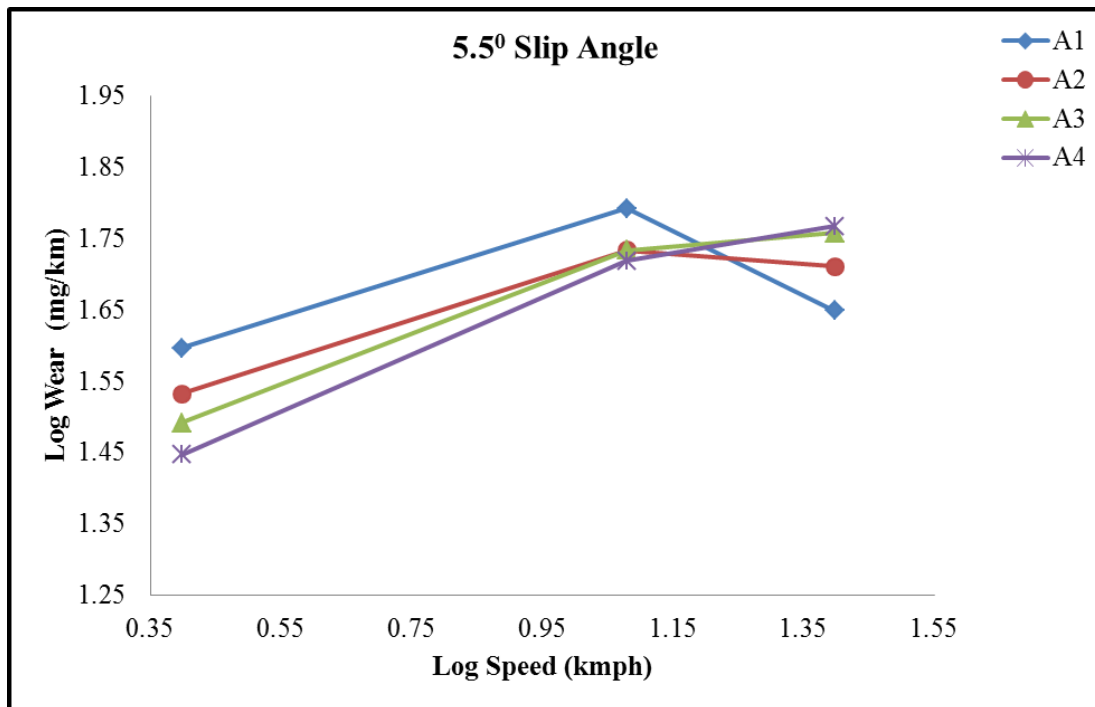
Figure 6.1 Variation of wear with speed at 5.5^0 slip angle on Corundum 60
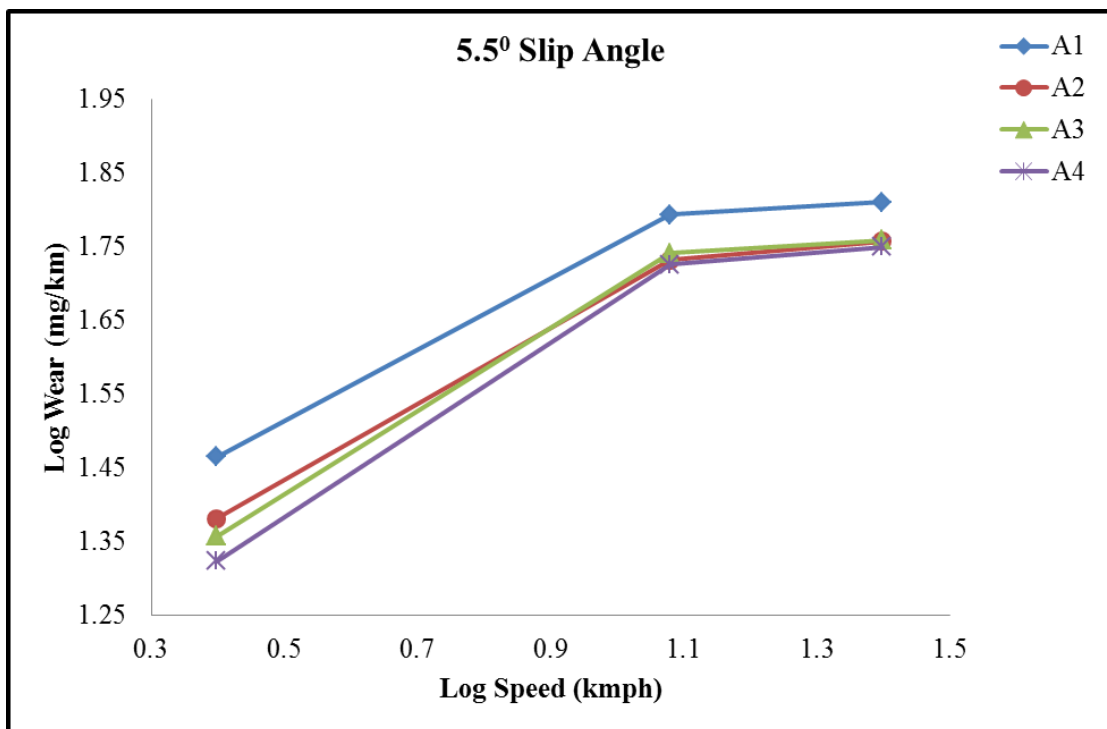
Figure 6.2 Variation of wear with slip angle at 5.5^0 slip angle on Corundum 180
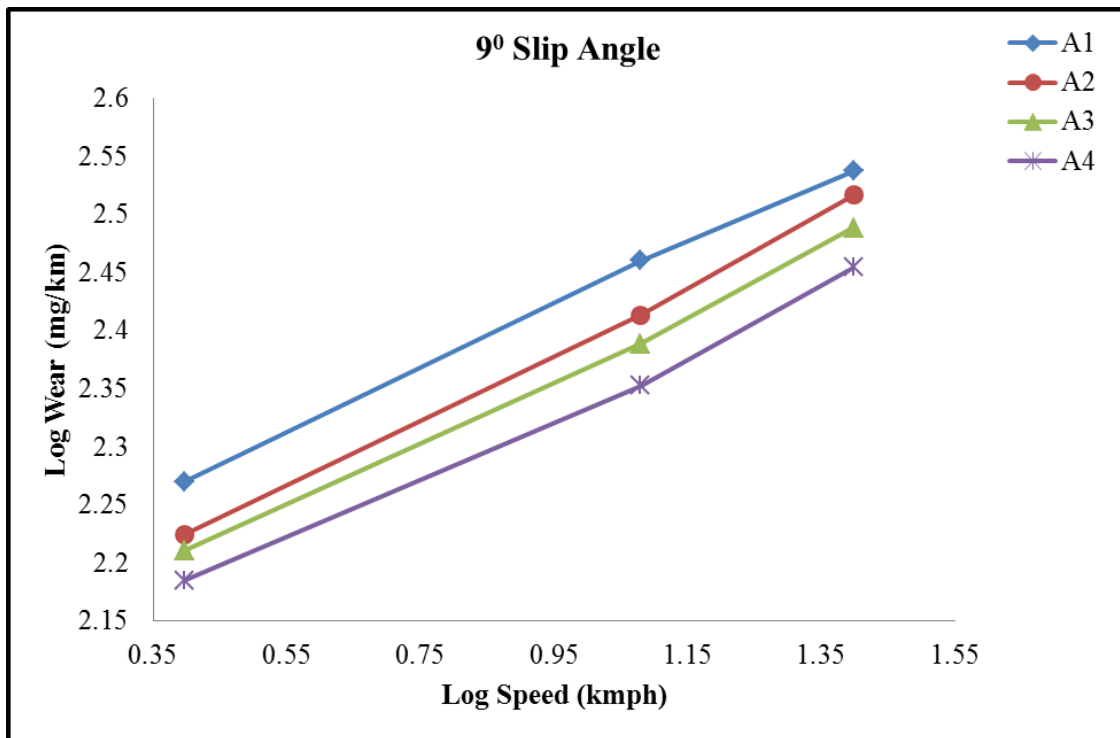
Figure 6.3 Variation of wear with speed at 9^0 slip angle on Corundum 60
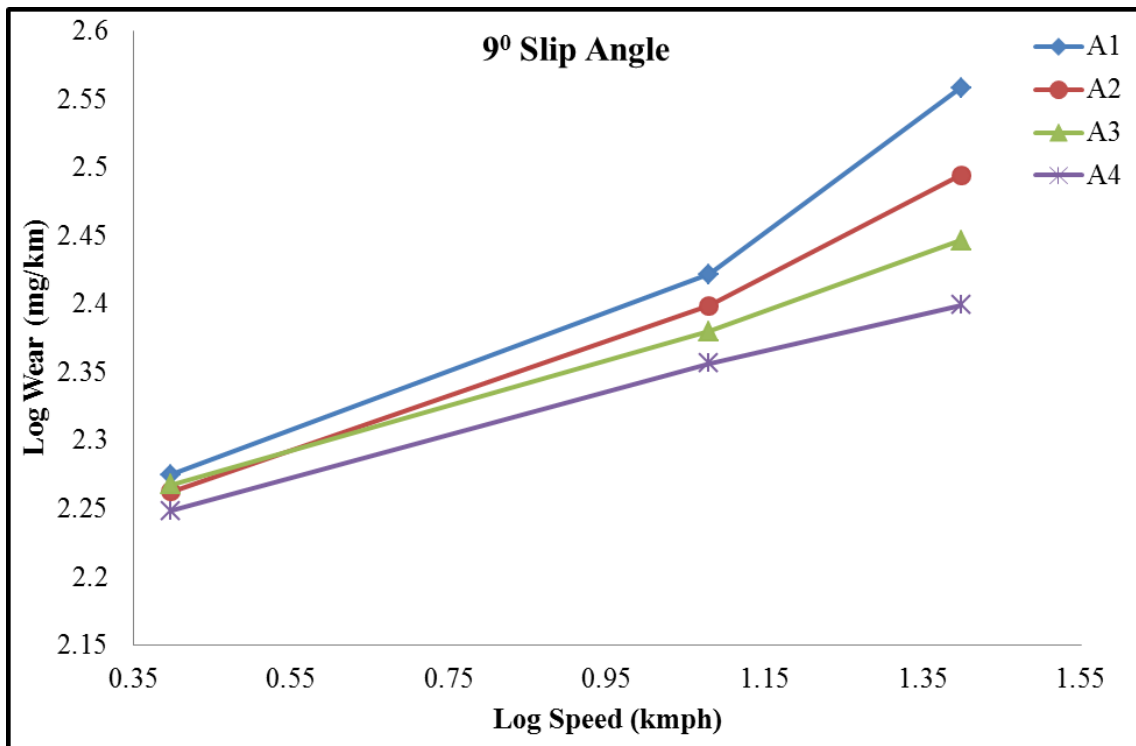
Figure 6.4 Variation of wear with slip angle at 9^0 slip angle on Corundum 180
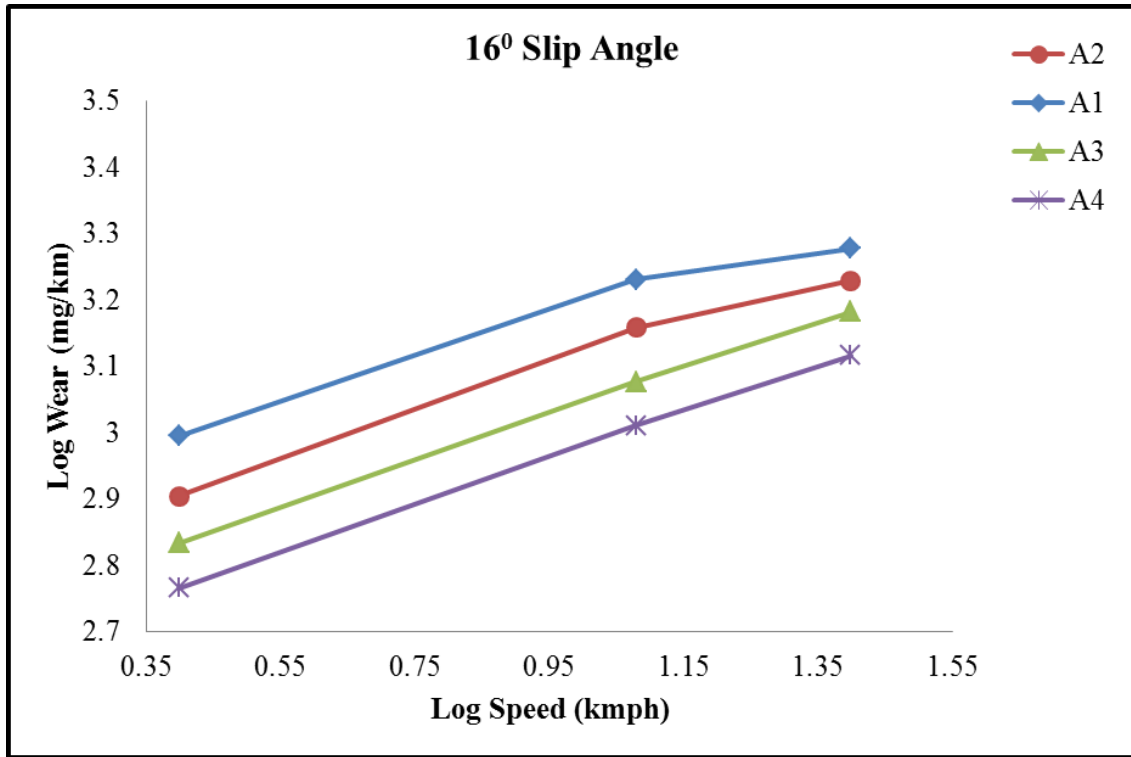
Figure 6.5 Variation of wear with speed at 16^0 slip angle on Corundum 60
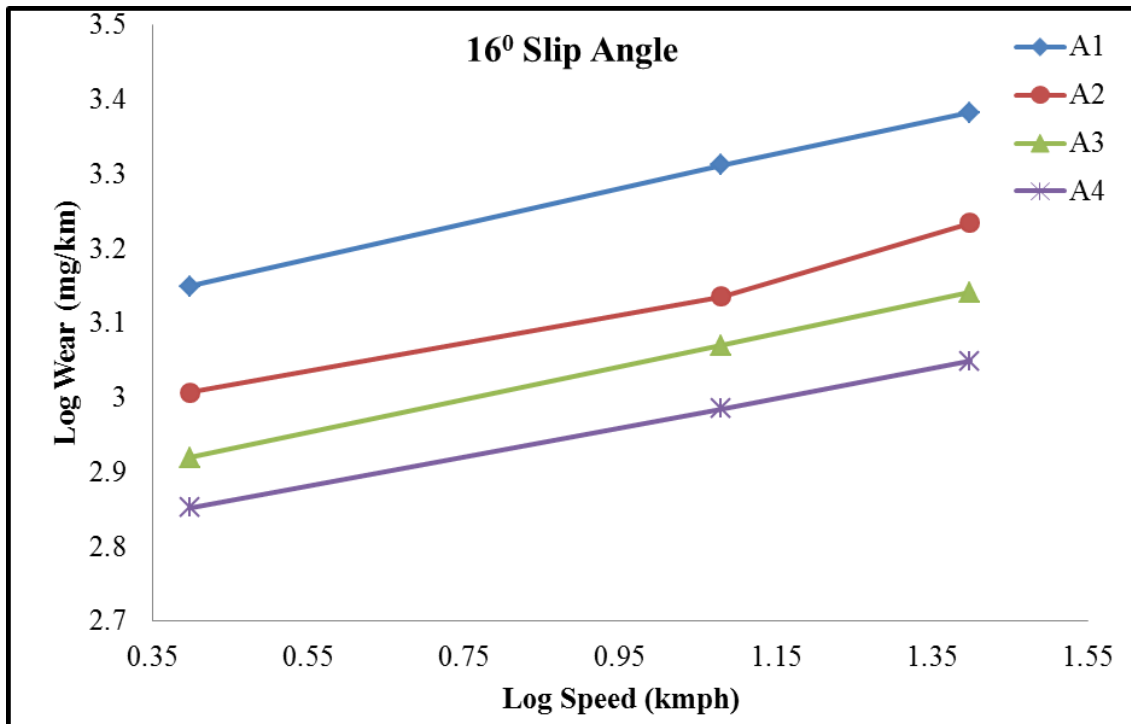
Figure 6.6 Variation of wear with slip angle at 16^0 slip angle on Corundum 180

92
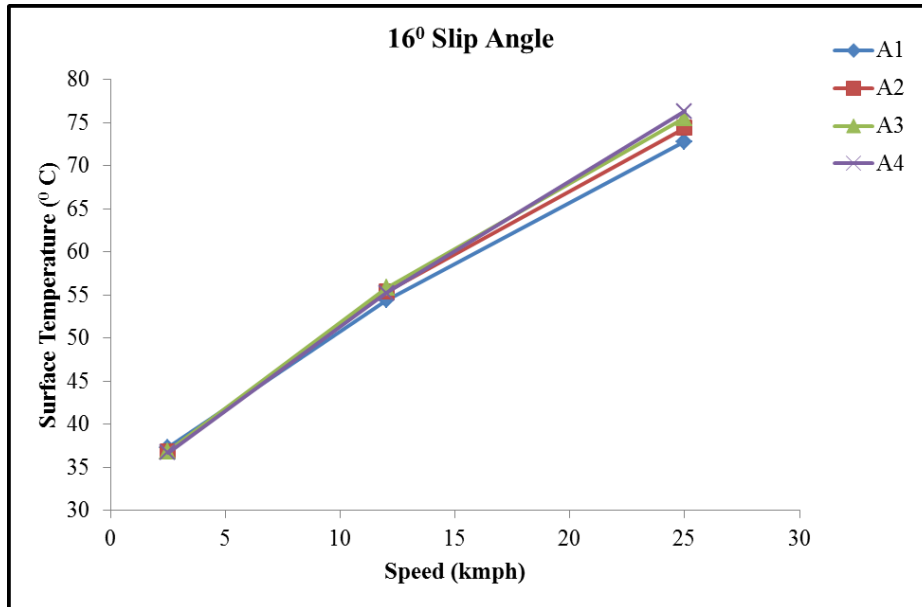
Figure 6.7 Variation of surface temperature with speed for Corundum 60
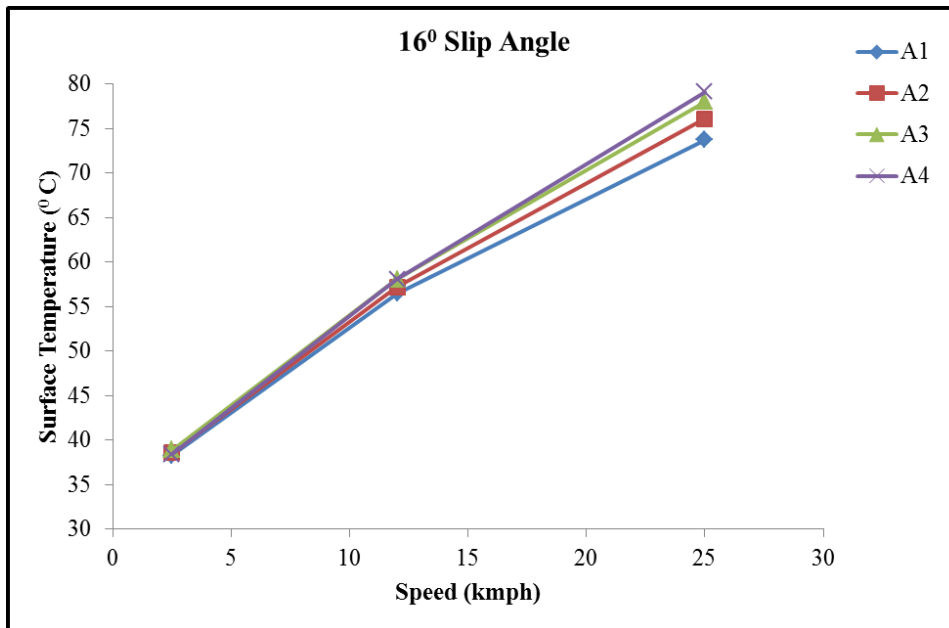
Figure 6.8 Variation of surface temperature with speed for Corundum 180

6.1.2 Slip Angle

The influence of slip angle variation on wear characteristics are shown in Figures 6.9 to 6.14 for both Corundum 60 and 180 surfaces at three different speeds (2.5 kmph, 12 kmph and 25 kmph). It has been observed that the wear increases linearly with

slip angle similar to the speed variation and can be attributed to the energy dissipation at the contact patch. The energy dissipation of a rotating rubber disk with slip angle can be expressed as (Grosch, 2005),

$$W = S. \, Sin\theta \qquad (6.3)$$

where, S is the side force and θ is the slip angle.

It can be seen that at lower slip angles, difference in wear amongst the studied materials is less when compared to higher slip angles. Similar observation is also reported in Grosch (2005) where, 80-20 NR/BR blend shows higher wear at larger slip angles but it becomes lower at small slip angles in comparison with the oil extended SBR compound. The same reason of temperature rise cited for speed dependence also holds true for the slip angle variation. At higher slip angles, there will be significant surface temperature rise at the contact patch of the rubber wheel. The temperature variation with slip angle at constant speed of 25 kmph is shown in Figures 15 and 16 for Corundum 60 and 180 surfaces respectively. The surface temperature of rubber wheel increases significantly from 5.5^0 to 16^0 slip angle in both the Corundum surfaces. It has also observed that the incremental temperature rise is higher due to the slip angle increase in comparison with the speed and is more prominent for Corundum 60 surface.
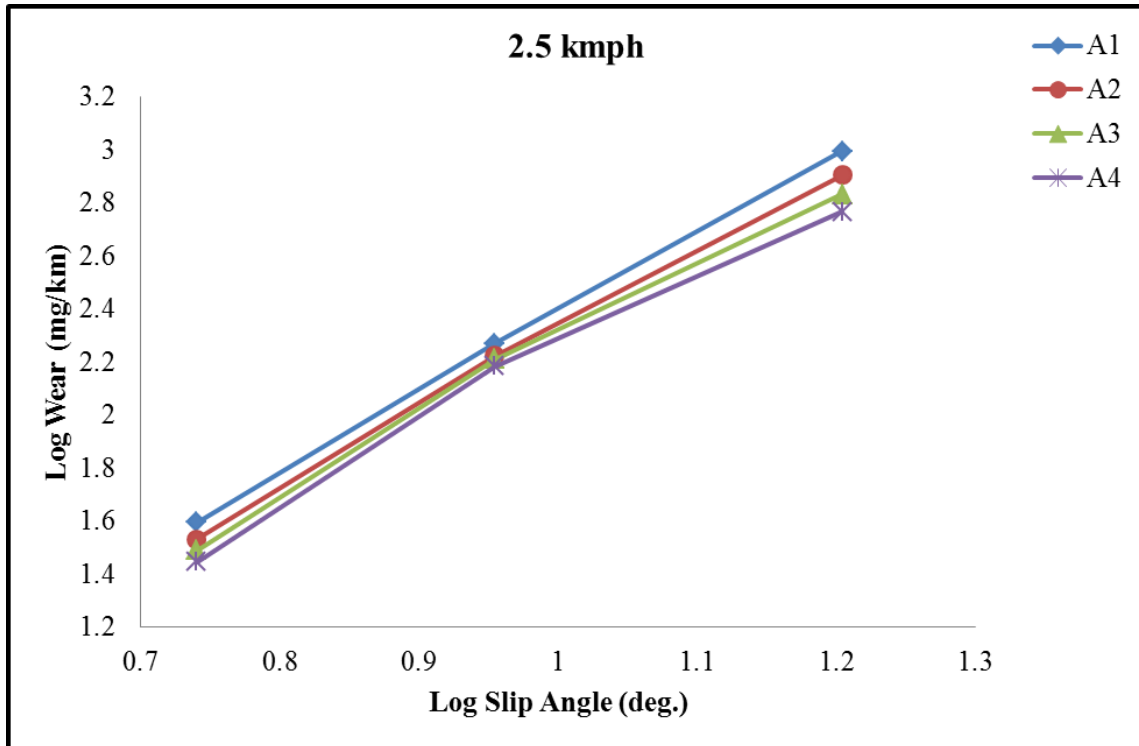
Figure 6.9 Variation of wear with slip angle at 2.5 kmph speed on Corundum 60
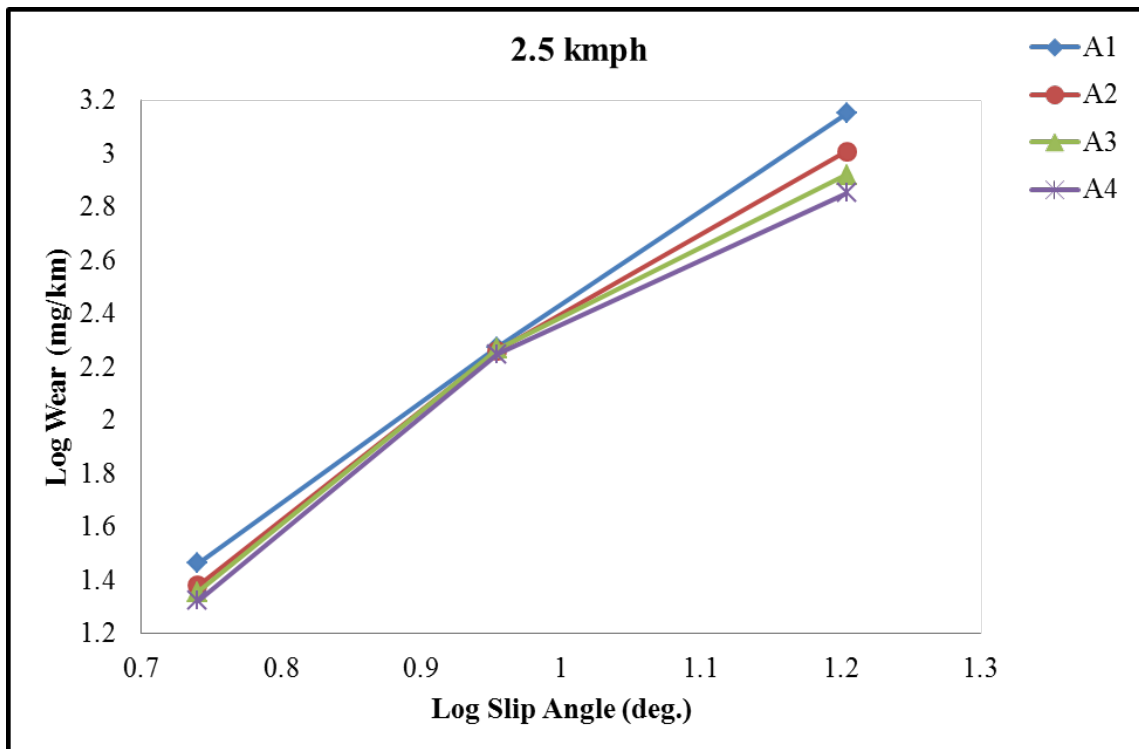
Figure 6.10 Variation of wear with slip angle at 2.5 kmph speed on Corundum 180
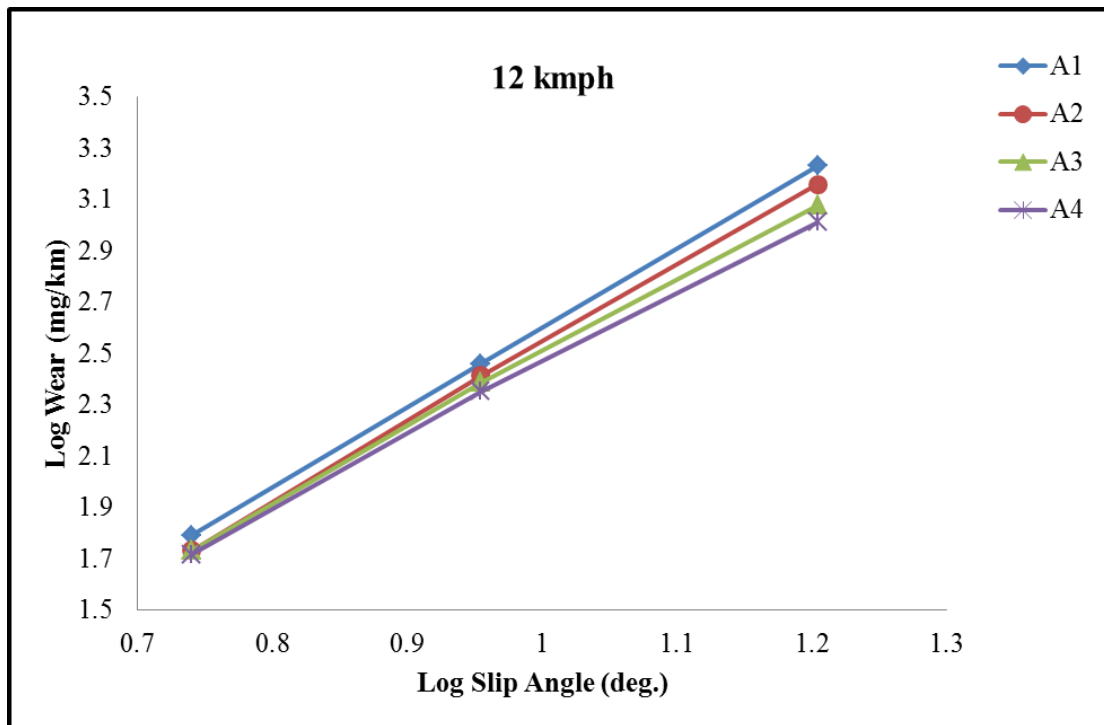
Figure 6.11 Variation of wear with slip angle at 12 kmph speed on Corundum 60
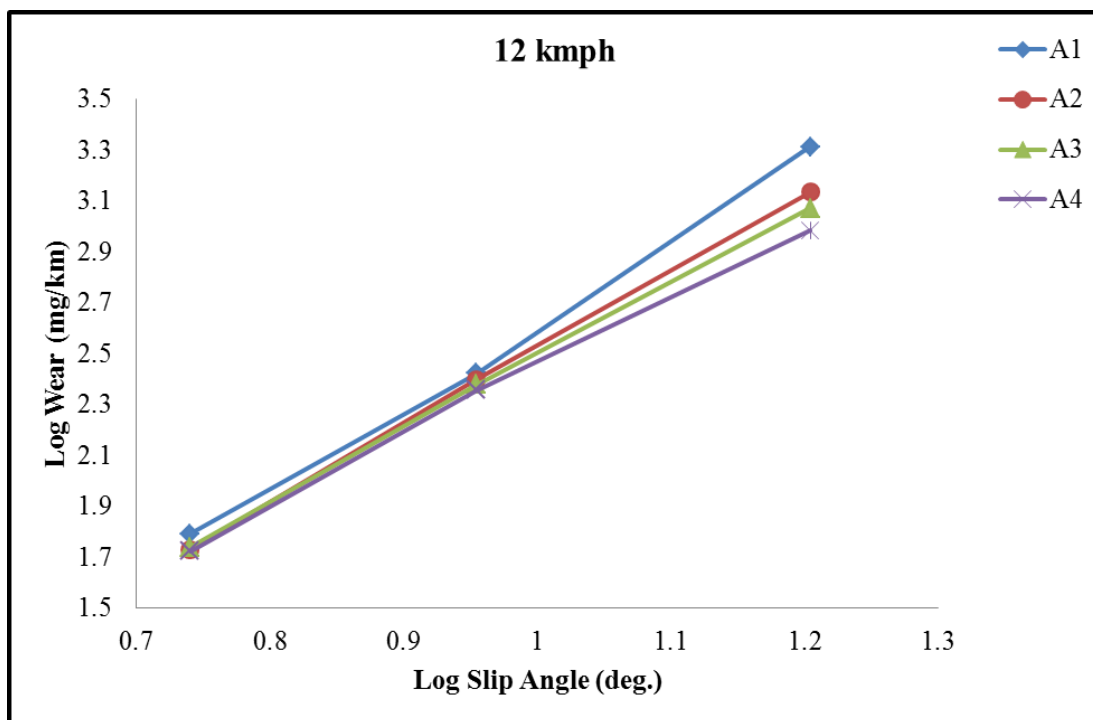
Figure 6.12 Variation of wear with slip angle at 12 kmph speed on Corundum 180
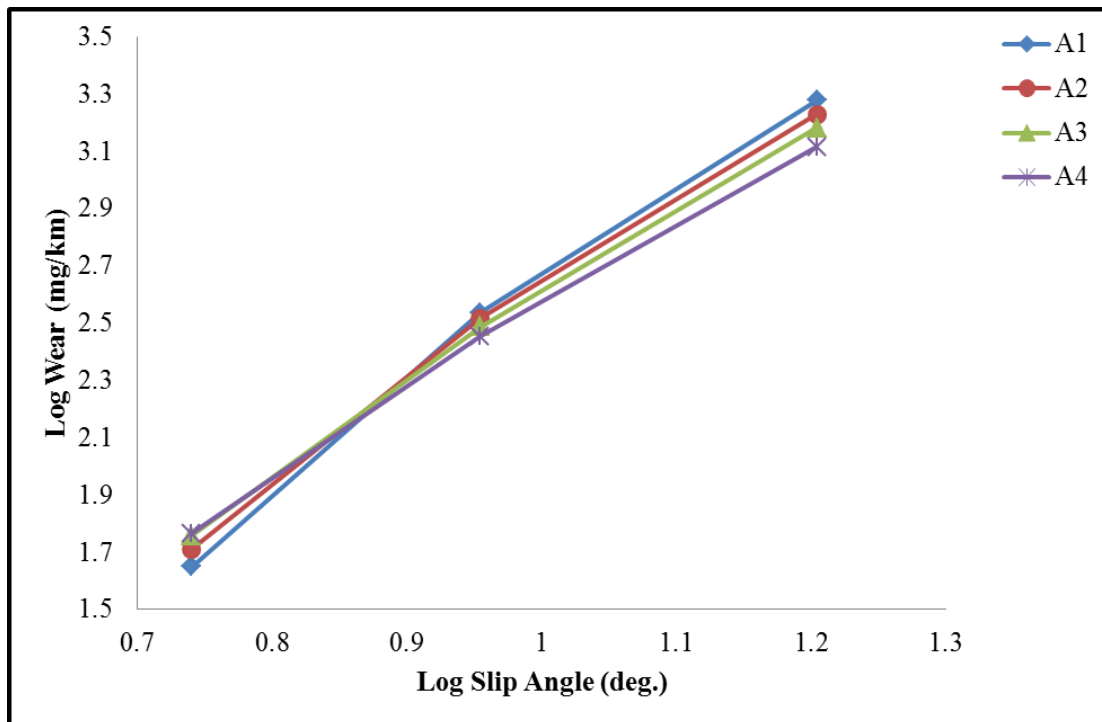
Figure 6.13 Variation of wear with slip angle at 25 kmph speed on Corundum 60
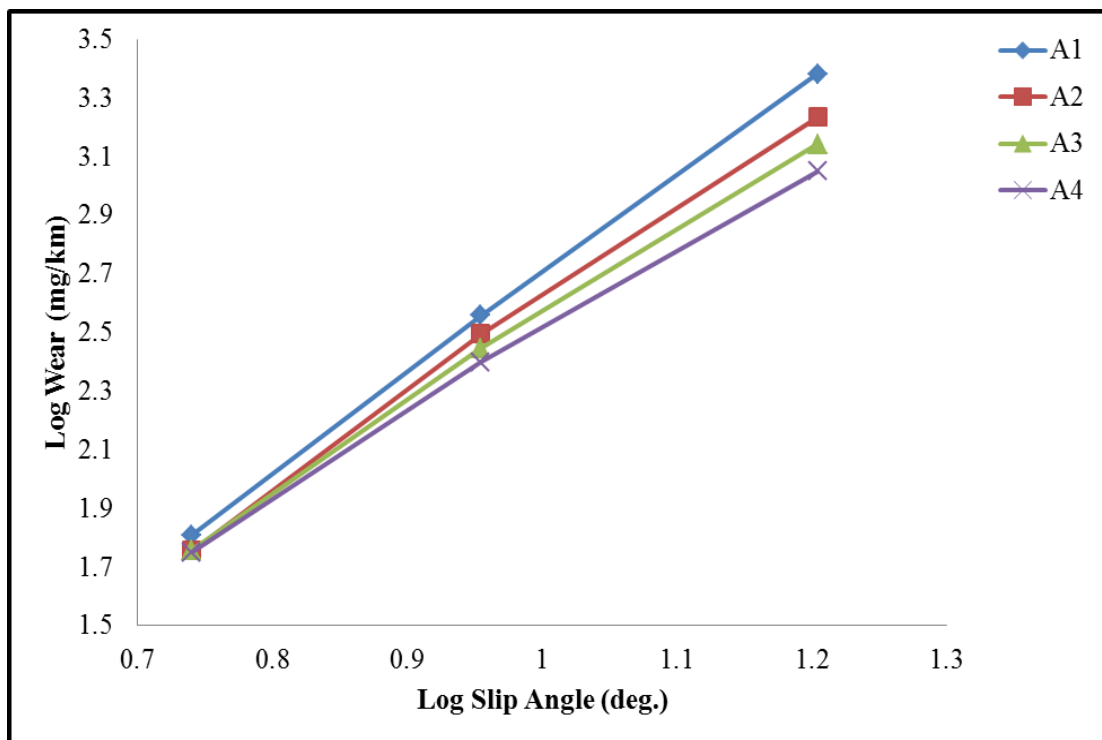
Figure 6.14 Variation of wear with slip angle at 25 kmph speed on Corundum 180
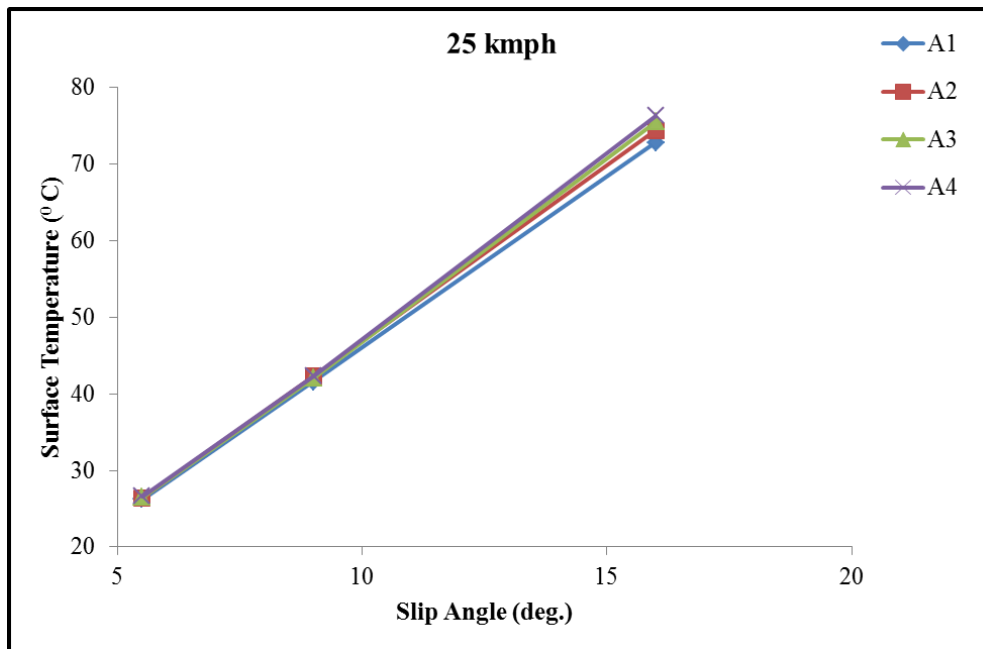
Figure 6.15 Variation of surface temperature with slip angle on Corundum 60
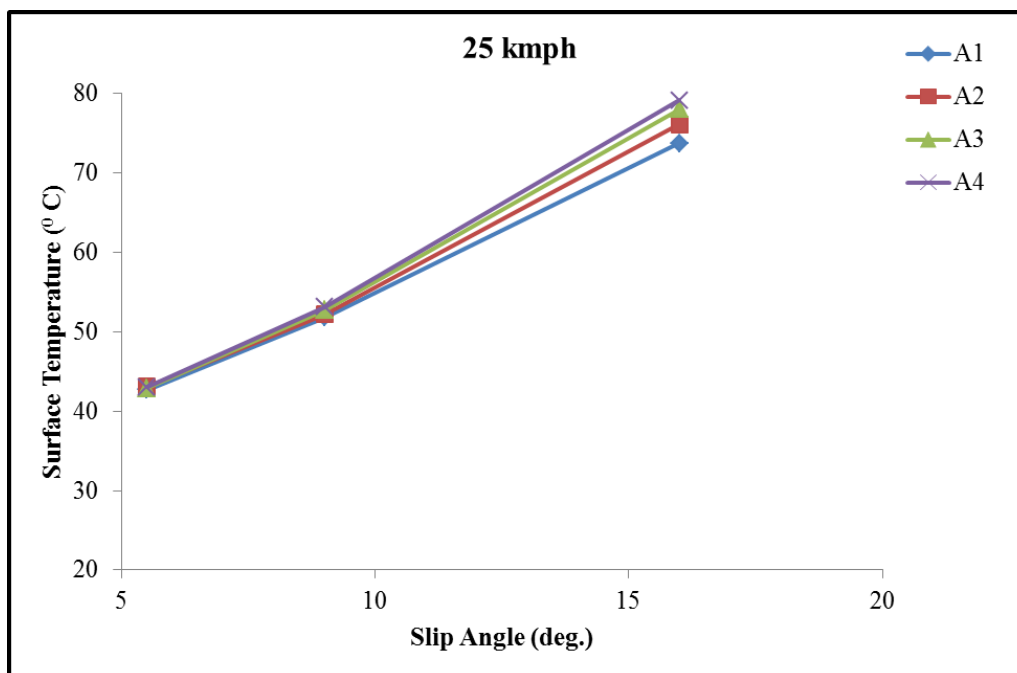
Figure 6.16 Variation of surface temperature with slip angle on Corundum 180

The wear with respect to speed and slip angle variation clearly indicates that the energy dissipation is responsible for the material loss. The variation of wear with energy dissipation is shown in Figures 6.17 and 6.18 for Corundum 60 and 180

surfaces respectively. As described by Grosch (2005), the energy and speed dependence of wear can be represented by the following equation,

$$[\log (A)] = a + b_1 [\log (W) + b_2 [\log (v)] + b_3 [\log (W)] \cdot [\log (v)] \qquad (6.4)$$

where, a, b_1, b_2 and b_3 are coefficients. A is the abrasion or wear per km, W represents energy dissipation per km and V is the speed.

The physical meaning of the above coefficients is very important form the view point of gaining an insight concerning the influence of material composition and surface condition on the wear characteristics. The coefficient, 'a' represents the abrasion loss at an energy dissipation of 1 kJ/km and a speed of 1 kmph. 'b_1' is the power index of the abrasion-energy relation at constant speed and temperature. 'b_2' is related to abrasion-speed relation at constant energy and temperature. 'b_3' is due to the temperature originated from speed and energy effect. These coefficients are calculated from the measured data and presented in Table 6.1 and 6.2 for Corundum 60 and 180 respectively. It can be observed that the values of coefficient 'a' are positive for both the surfaces and for all the compounds under study. The higher 'a' values for Corundum 60 surface indicates that at equal energy level, the contribution towards wear is more because of sharp asperities compared to 180. These results revealed that the coefficient 'b_1' is the major contributor to the wear process for both the surfaces and this finding is in accordance with the Grosch (2005). It was also suggested that when the values are positive and greater than 1 then it implies that the cut growth dominates the wear process. Further, it can also be observed that 'b_1' values are higher for Corundum 180 surface when compared to Corundum 60 for all the compounds. The higher 'b_1' values are expected for Corundum 180, as it is a blunter surface compared to 60 and therefore fatigue failure dominates. For Corundum 60 surface, negative 'b_2' value is only exhibited by A1 compound and the rest of the compounds have positive value. As reported in the literature (Grosch, 2005) viscoelastic effect on abrasion resistance can be attributed to the negative 'b_2' coefficient for the A1 compound which is made of 100 parts of NR. However, in the case of Corundum 180 surface, positive and higher 'b_2' values are reported for all the compounds and this may be due to the difference in grit size between these two surfaces. The next important observation is that the values of 'b_3' are positive for

Corundum 60 whereas negative values are reported for Corundum 180 surface. The positive 'b_3' value is expected because of the temperature rise from speed and energy effect and hence contributes towards more material loss. However reasons for exhibiting negative 'b_3' values for Corundum 180 surface is not clearly understood. This may require further investigation and is important as it contributes towards better wear resistance.

These coefficients are very useful for the estimation of wear over a wide range of energy and speed level and can be used for the ranking of various tread compounds. Further, relative rating of the experimental compounds with respect to a standard control compound is also advantageous from a practical usage point of view as reversal in ranking is very common depending upon the severity of the test. Relative rating is defined as the ratio of wear of control compound (W_C) to wear of experimental (W_E) compound and usually expressed in terms of percentage.

For the present study, A1 compound is taken as the control compound and the relative wear rating for other compounds are provided in Tables 6.3 to 6.8 for both the Corundum surfaces. The mildest (low energy and high speed) and severest conditions (high energy and high speed) are represented by the top left corner and bottom right corner of the tables respectively. Values greater than 100 indicate superior wear resistance over control compound. The result of Corundum 60 revealed that all the experimental compounds (A2-A4) are better in most of the severity zones except in small portions of top right corner of the tables (Table 6.3 to 6.5). In the case of Corundum 180 surface, experimental compounds are inferior only in top portion of the tables (Table 6.6 to 6.8) and shown superior wear characteristics in most of the other regions. In summation, for both the Corundum surfaces, experimental compounds exhibited better wear resistance potential in the higher severity zone in comparison with the control compound. In the higher severity zone, temperature rise will be more and hence NR/BR blends have shown superiority over pure NR compound. Further, according to Liang *et al.* (2010), in BR material, due to smaller tongue on the asperity compared to NR, former material generates low values of strain energy release rate. Hence, wear rate is also low in BR material. This is in accordance with the findings of the present work. The better wear resistance of BR compound compared to NR and SBR was also reported by Kim *et al.* (1999).
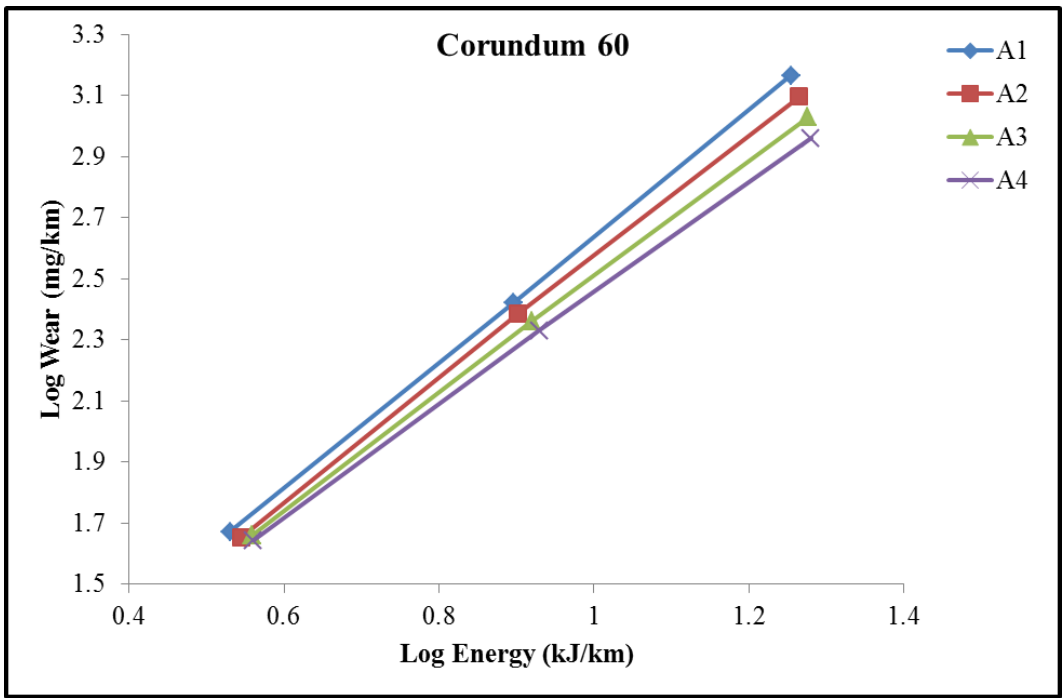
Figure 6.17 Variation of wear with energy on Corundum 60
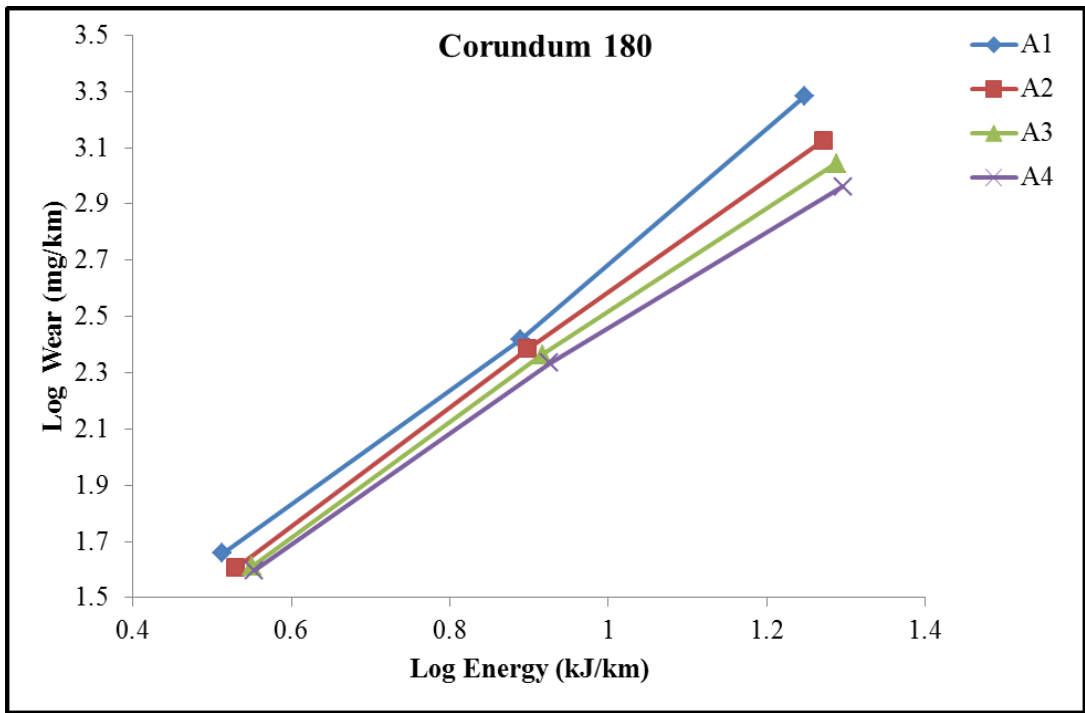
Figure 6.18 Variation of wear with energy on Corundum 180

Table 6.1 Coefficients of NR/BR blends on Corundum 60

Compound	a	b1	b2	b3
A1	0.6942	1.7192	-0.1309	0.3657
A2	0.5127	1.7992	0.0552	0.2153
A3	0.4712	1.7736	0.1318	0.1405
A4	0.4451	1.7518	0.1829	0.0827

Table 6.2 Coefficients of NR/BR blends on Corundum 180

Compound	a	b1	b2	b3
A1	0.0446	2.4039	0.4774	-0.2039
A2	0.1231	2.2267	0.4254	-0.1866
A3	0.1637	2.1293	0.4091	-0.1935
A4	0.1682	2.0852	0.4529	-0.2610

Table 6.3 Relative rating of A2 compound on Corundum 60

log energy, W	log speed, v (kmph)								
	0	0.2	0.4	0.6	0.8	1	1.2	1.4	1.6
0	151.9	139.4	128	117.5	107.8	**99**	**90.8**	**83.4**	**76.5**
0.2	146.4	136.3	126.8	118	109.9	102.2	**95.2**	**88.6**	**82.4**
0.4	141.1	133.2	125.7	118.6	111.9	105.6	**99.7**	**94**	**88.7**
0.6	136	130.1	124.5	119.2	114	109.1	104.4	**99.9**	**95.6**
0.8	131.1	127.2	123.4	119.7	116.1	112.7	109.3	106.1	102.9
1	126.4	124.3	122.3	120.3	118.3	116.4	114.5	112.6	110.8
1.2	121.8	121.5	121.2	120.9	120.5	120.2	119.9	119.6	119.3
1.4	117.4	118.7	120.1	121.4	122.8	124.2	125.6	127	128.4
1.6	113.2	116	119	122	125.1	128.3	131.5	134.9	138.3

Table 6.4 Relative rating of A3 compound on Corundum 60

log energy, W	log v (kmph)								
	0	0.2	0.4	0.6	0.8	1	1.2	1.4	1.6
0	167.1	148.1	131.2	116.3	103	**91.3**	**80.9**	**71.7**	**63.5**
0.2	163	147.5	133.4	120.7	109.2	**98.8**	**89.3**	**80.8**	**73.1**
0.4	159	146.8	135.6	125.2	115.7	106.8	**98.7**	**91.1**	**84.2**
0.6	155	146.2	137.8	130	122.6	115.6	109	102.8	**96.9**
0.8	151.2	145.6	140.1	134.9	129.9	125	120.4	115.9	111.5
1	147.5	144.9	142.4	140	137.6	135.3	132.9	130.7	128.4
1.2	143.8	144.3	144.8	145.3	145.8	146.3	146.8	147.3	147.8
1.4	140.3	143.7	147.2	150.8	154.5	158.3	162.2	166.1	170.2
1.6	136.8	143.1	149.6	156.5	163.7	171.2	179.1	187.3	195.9

Table 6.5 Relative rating of A4 compound on Corundum 60

log energy, W	log v (kmph)								
	0	0.2	0.4	0.6	0.8	1	1.2	1.4	1.6
0	177.5	153.6	132.9	115.1	99.6	**86.2**	**74.6**	**64.6**	**55.9**
0.2	174.8	155.3	138	122.6	108.9	**96.7**	**85.9**	**76.3**	**67.8**
0.4	172.2	157	143.2	130.6	119	108.5	**99**	**90.2**	**82.3**
0.6	169.7	158.8	148.6	139.1	130.2	121.8	114	106.7	**99.8**
0.8	167.2	160.6	154.2	148.2	142.3	136.7	131.3	126.1	121.2
1	164.7	162.4	160.1	157.8	155.6	153.4	151.2	149.1	147
1.2	162.2	164.2	166.1	168.1	170.1	172.2	174.2	176.3	178.4
1.4	159.8	166	172.4	179.1	186	193.2	200.7	208.4	216.5
1.6	157.4	167.8	178.9	190.8	203.4	216.8	231.2	246.4	262.7

Table 6.6 Relative rating of A2 compound on Corundum 180

log energy, W	log speed, v (kmph)								
	0	0.2	0.4	0.6	0.8	1	1.2	1.4	1.6
0	**83.5**	**85.5**	**87.6**	**89.7**	**91.9**	**94.1**	**96.4**	**98.7**	101.1
0.2	**90.6**	**92.6**	**94.7**	**96.8**	**99**	101.3	103.6	105.9	108.3
0.4	**98.3**	100.3	102.4	104.6	106.8	109	111.3	113.6	116
0.6	106.6	108.7	110.8	112.9	115.1	117.3	119.6	121.9	124.3
0.8	115.7	117.7	119.8	121.9	124.1	126.3	128.5	130.8	133.1
1	125.5	127.5	129.6	131.7	133.8	136	138.1	140.4	142.6
1.2	136.2	138.1	140.1	142.2	144.2	146.3	148.5	150.6	152.8
1.4	147.7	149.6	151.6	153.5	155.5	157.5	159.6	161.6	163.7
1.6	160.3	162.1	163.9	165.8	167.7	169.6	171.5	173.4	175.4

Table 6.7 Relative rating of A3 compound on Corundum 180

log energy, W	log speed, v (kmph)								
	0	0.2	0.4	0.6	0.8	1	1.2	1.4	1.6
0	**76**	**78.4**	**80.9**	**83.5**	**86.2**	**89**	**91.8**	**94.7**	**97.8**
0.2	**86.3**	**88.9**	**91.7**	**94.5**	**97.5**	100.5	103.6	106.8	110.1
0.4	**97.9**	100.8	103.8	107	110.2	113.5	116.9	120.4	124
0.6	111.1	114.3	117.6	121	124.5	128.1	131.9	135.7	139.6
0.8	126.1	129.6	133.2	136.9	140.8	144.7	148.8	153	157.2
1	143	146.9	150.9	155	159.1	163.5	167.9	172.4	177.1
1.2	162.3	166.6	170.9	175.3	179.9	184.6	189.4	194.3	199.4
1.4	184.2	188.8	193.6	198.4	203.4	208.5	213.7	219.1	224.5
1.6	209	214.1	219.2	224.5	229.9	235.4	241.1	246.9	252.9

Table 6.8 Relative rating of A4 compound on Corundum 180

log energy, W	log speed, v (kmph)								
	0	0.2	0.4	0.6	0.8	1	1.2	1.4	1.6
0	**75.2**	**76.1**	**76.9**	**77.8**	**78.7**	**79.6**	**80.5**	**81.4**	**82.4**
0.2	**87.1**	**88.6**	**90.1**	**91.6**	**93.1**	**94.6**	**96.2**	**97.8**	**99.5**
0.4	100.9	103.1	105.4	107.7	110.1	112.5	115	117.5	120.1
0.6	116.8	120	123.3	126.7	130.2	133.8	137.5	141.2	145.1
0.8	135.3	139.8	144.3	149.1	154	159.1	164.3	169.7	175.3
1	156.7	162.7	168.9	175.4	182.1	189.1	196.4	203.9	211.7
1.2	181.5	189.4	197.7	206.4	215.4	224.8	234.7	245	255.7
1.4	210.2	220.5	231.4	242.8	254.8	267.3	280.5	294.3	308.8
1.6	243.4	256.7	270.8	285.6	301.3	317.8	335.3	353.6	373

6.2 WEAR CHARACTERISTICS OF NR/SBR BLENDS

In this section, wear results of NR/SBR blends measured under variable speed and slip angle condition on different abrading surfaces is discussed. The influence of speed and slip angle on wear is discussed in detail.

6.2.1 Speed

The effect of speed on wear characteristics of NR/SBR blend compounds measured on Corundum 60 and 180 surfaces at three different slip angles are shown in Figures 6.19 to 6.24. The increase in wear with rise in speed is also observed here but slight

deviation from the linearity can be seen in comparison with NR/BR compounds especially at 5.5^0 and 9^0 slip angles. One more difference for NR/SBR blend compounds is that the wear variations amongst the compounds are comparatively less than that of NR/BR compounds. This could be attributed to the less speed dependence of SBR as reported in the literature (Grosch, 2005). Between Corundum 60 and 180 surfaces, more variation could be observed in the case of Corundum 180. Surface temperature variation due to speed increase is provided in Figures 6.25 and 6.26 for Corundum 60 and 180 surfaces respectively. Significant temperature increase is observed in all the materials and for both the surfaces. Overall, NR/SBR blend compounds showed similar speed dependence on wear as observed in NR/BR blend compounds. Hence the same reasoning could be cited to explain the results which are discussed in section 6.1.1.
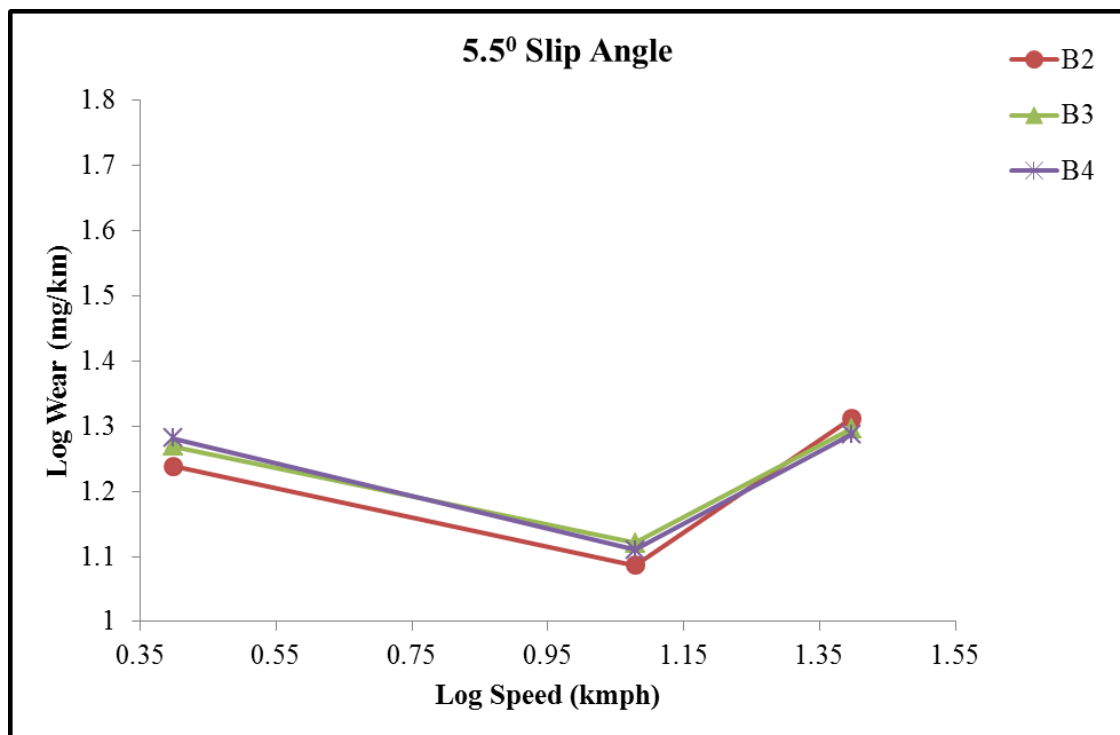
Figure 6.19 Variation of wear with speed at 5.5^0 slip angle on Corrundum 60
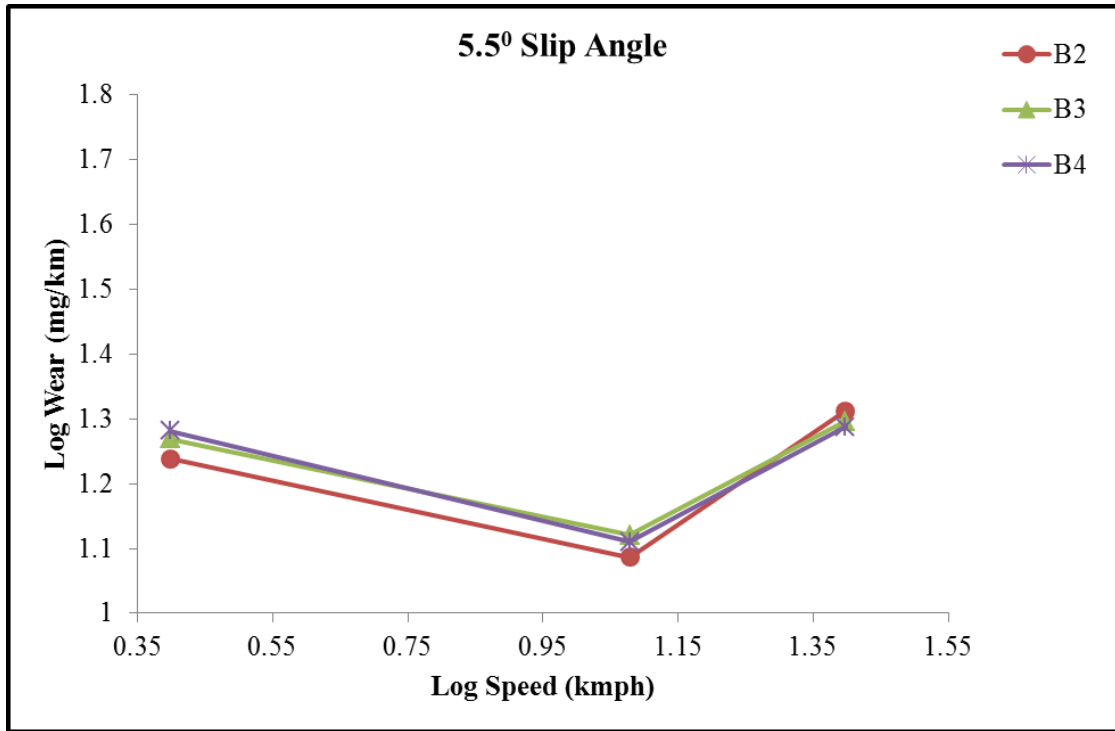
Figure 6.20 Variation of wear with speed at 5.5^0 slip angle on Corrundum 180
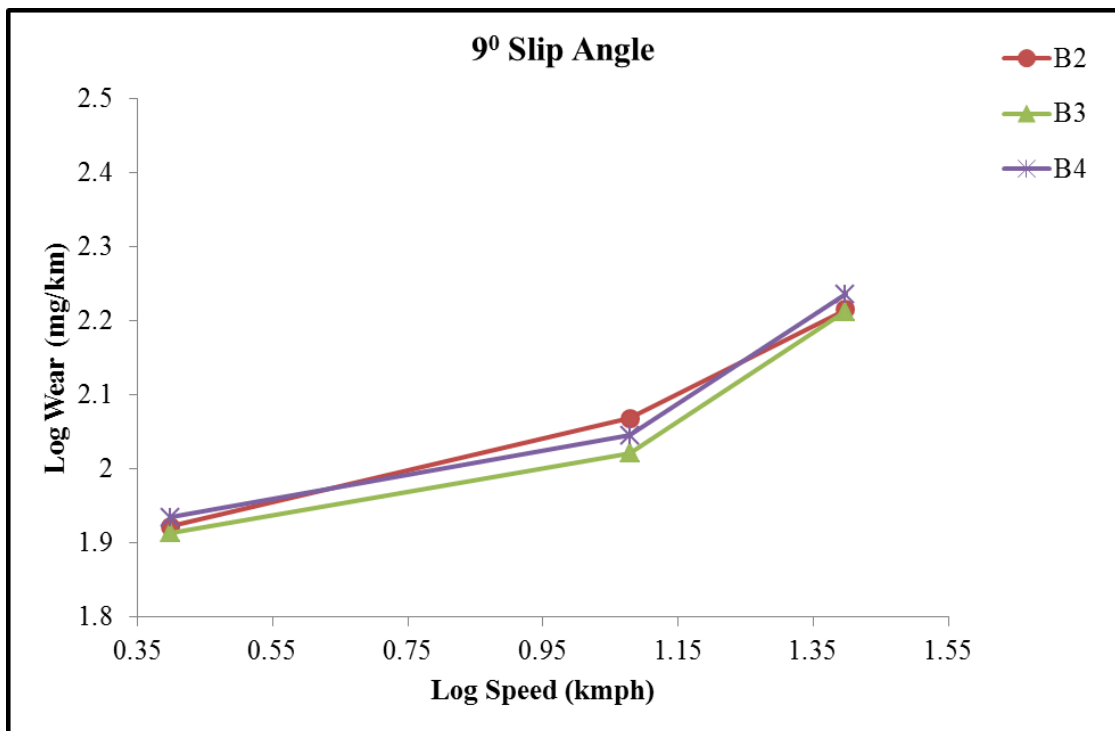
Figure 6.21 Variation of wear with speed at 9^0 slip angle on Corrundum 60
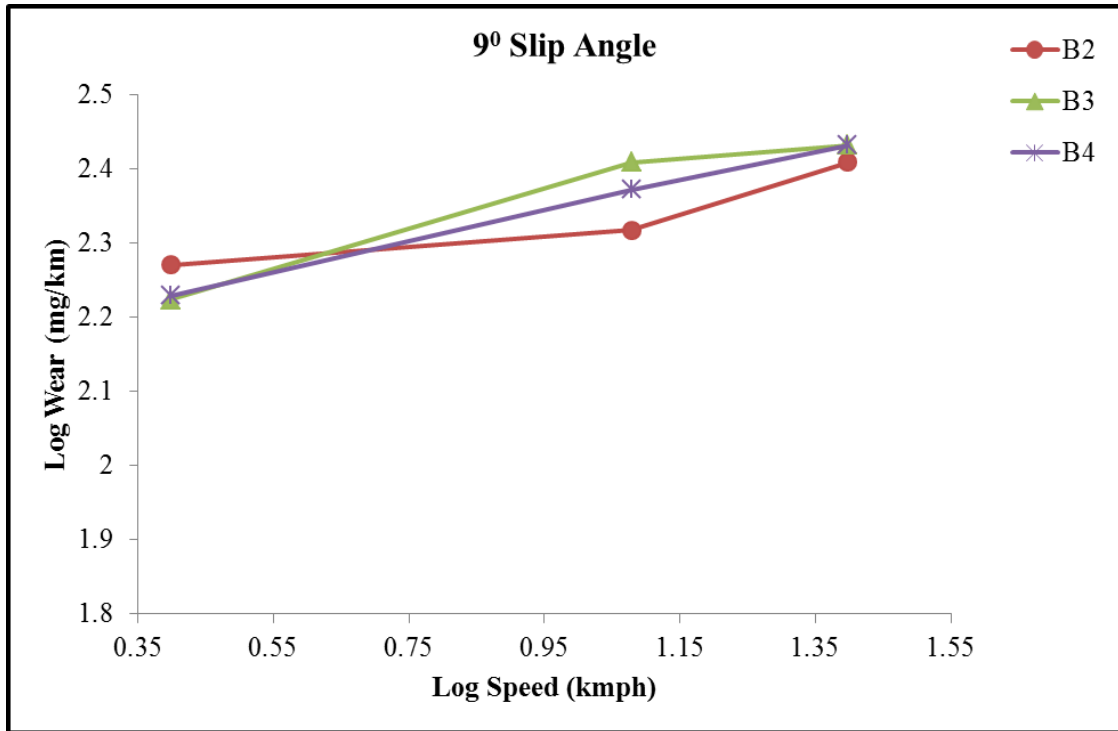
Figure 6.22 Variation of wear with speed at 9^0 slip angle on Corrundum 180
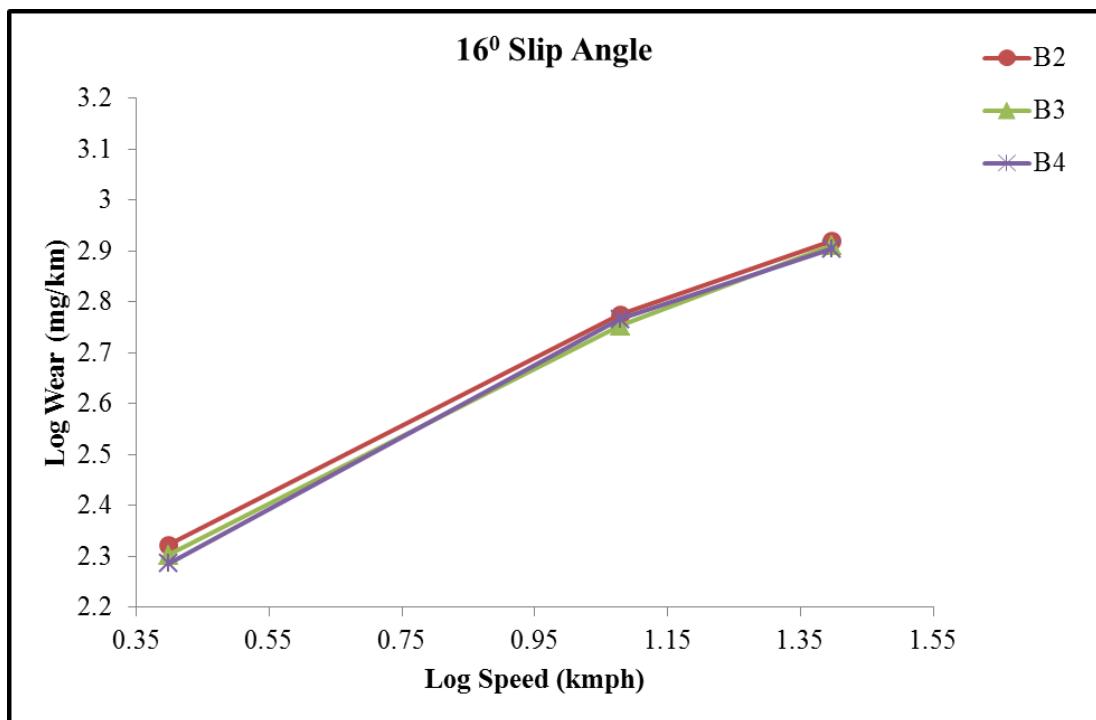
Figure 6.23 Variation of wear with speed at 16^0 slip angle on Corrundum 60

107
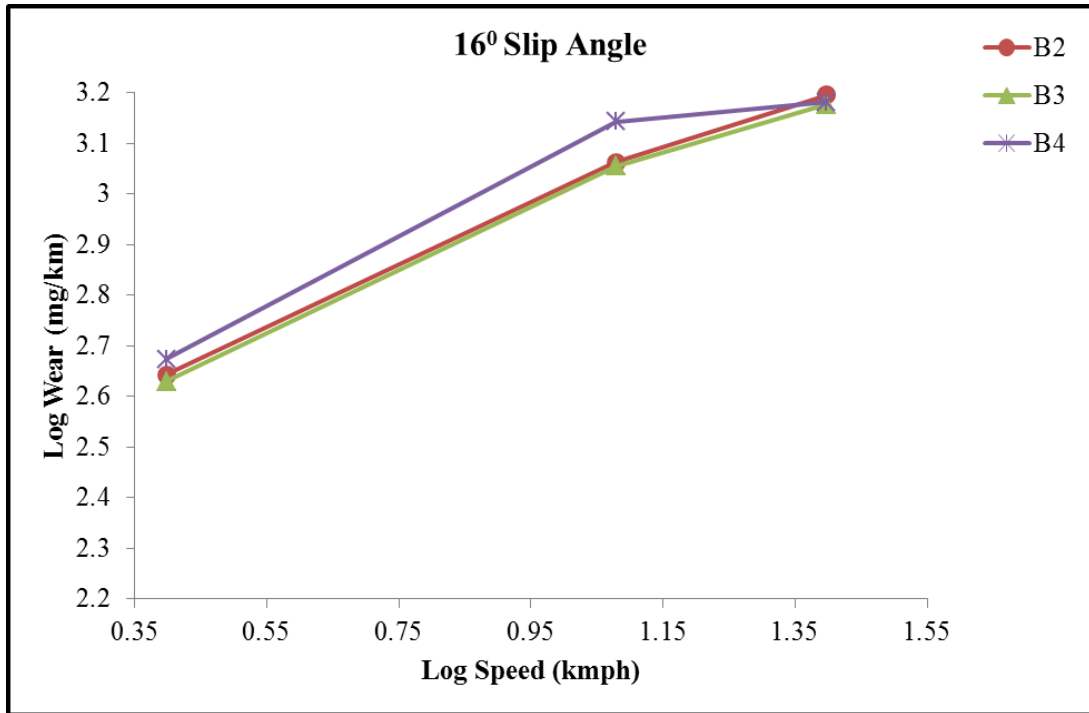
Figure 6.24 Variation of wear with speed at 16^0 slip angle on Corrundum 180
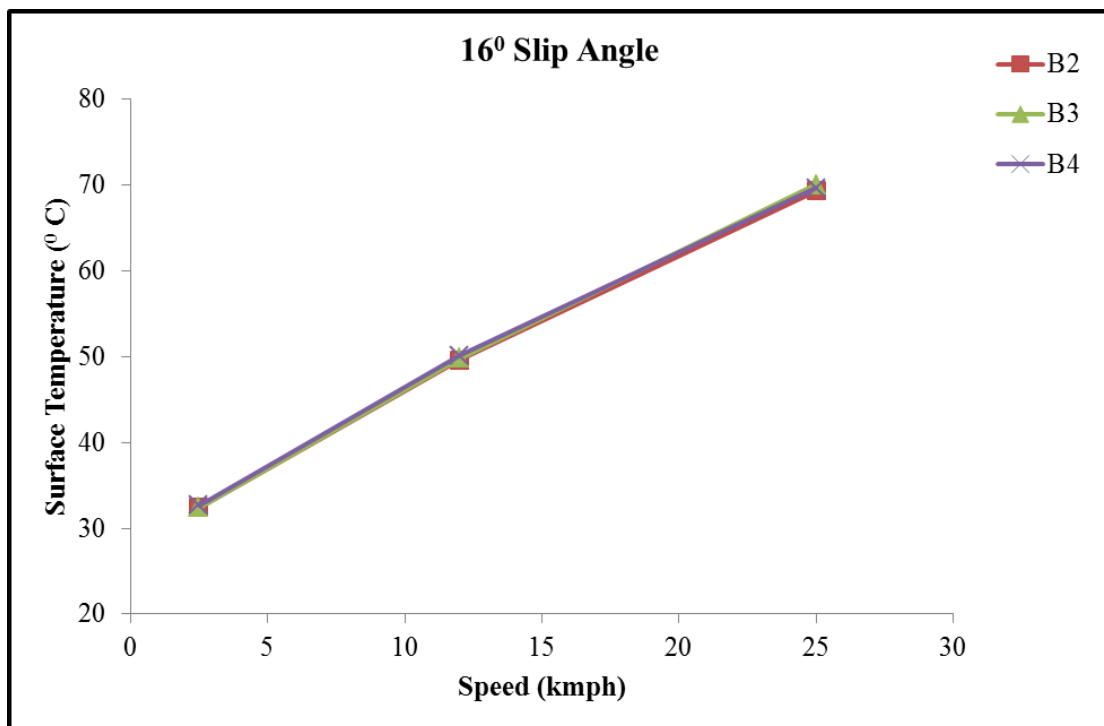
Figure 6.25 Variation of surface temperature with speed on Corundum 60

108
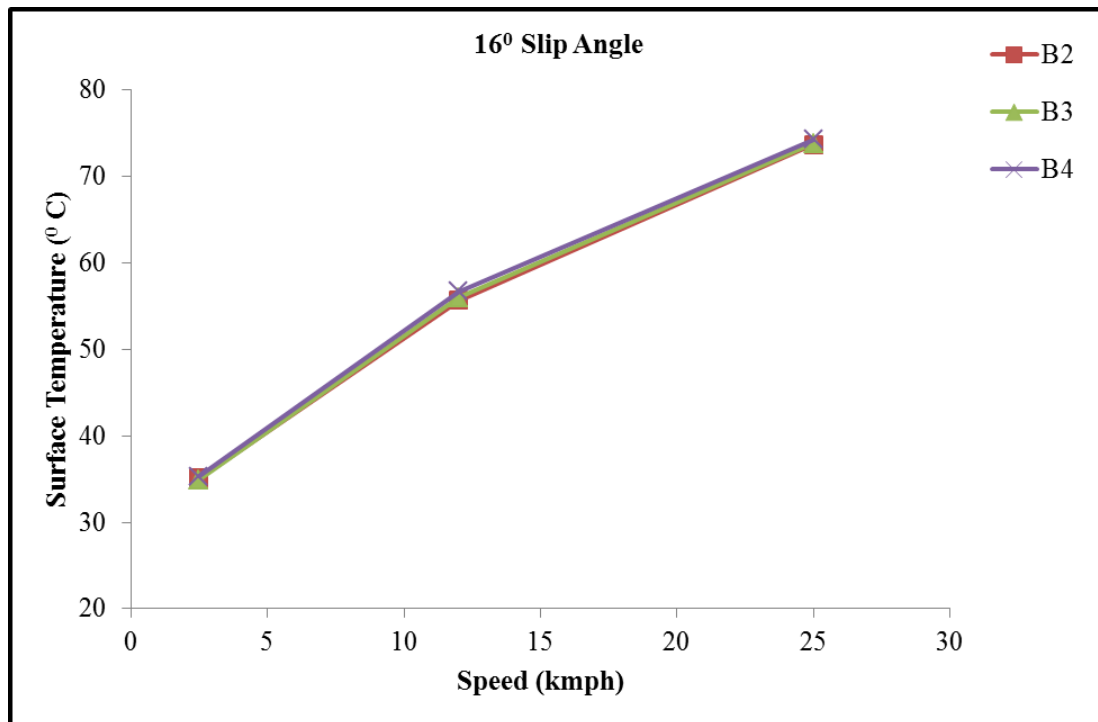
Figure 6.26 Variation of surface temperature with speed on Corundum 180

6.2.2 Slip Angle

The influence of slip angle variation on the wear characteristics are presented in Figures 6.27 to 6.32 for both Corundum 60 and 180 surfaces at three different speeds (2.5 kmph, 12 kmph and 25 kmph). It has been observed that the wear increases linearly with slip angle as observed in the case NR/BR blend compounds. The temperature rise due to slip angle variation is also shown in Figures 6.33 and 6.34 for Corundum 60 and 180 respectively. Both surfaces show considerable temperature rise in the range of 25-30^0 C which is attributing to the increased wear rate.

The coefficients of equation 6.4 are also calculated for these sets of compounds and are reported in Table 6.9 and 6.10. It can be observed that the b1 values are greater than 1 for all the compounds and are the major contributor for wear process. As observed in NR/BR blend, b1 values are higher for Corundum 180 in comparison with the Corundum 60 surface which is again confirming the fatigue dominating wear process.

The relative ratings of these compounds for both Corundum 60 and 180 surfaces are provided in Table 6. 11 to 6.16. The relative ratings of these compounds measured on Corundum 60 differ from 180 surface. In Corundum 60 surface, experimental compounds (B2-B4) showed superior wear resistance in most of the severity zone except top left corner of the tables (Table 6.11 to 6.13) which is low energy and low speed zone. In Corundum 180, it is the top right corner of the table (Table 6.14 to 6.16) where the experimental compounds showed inferior wear resistance characteristics compared to the control compound. Overall, in both the surfaces, NR/SBR blends also showed superior wear resistance characteristics in the highest severity zone i.e. bottom right corner as observed in NR/BR blends.
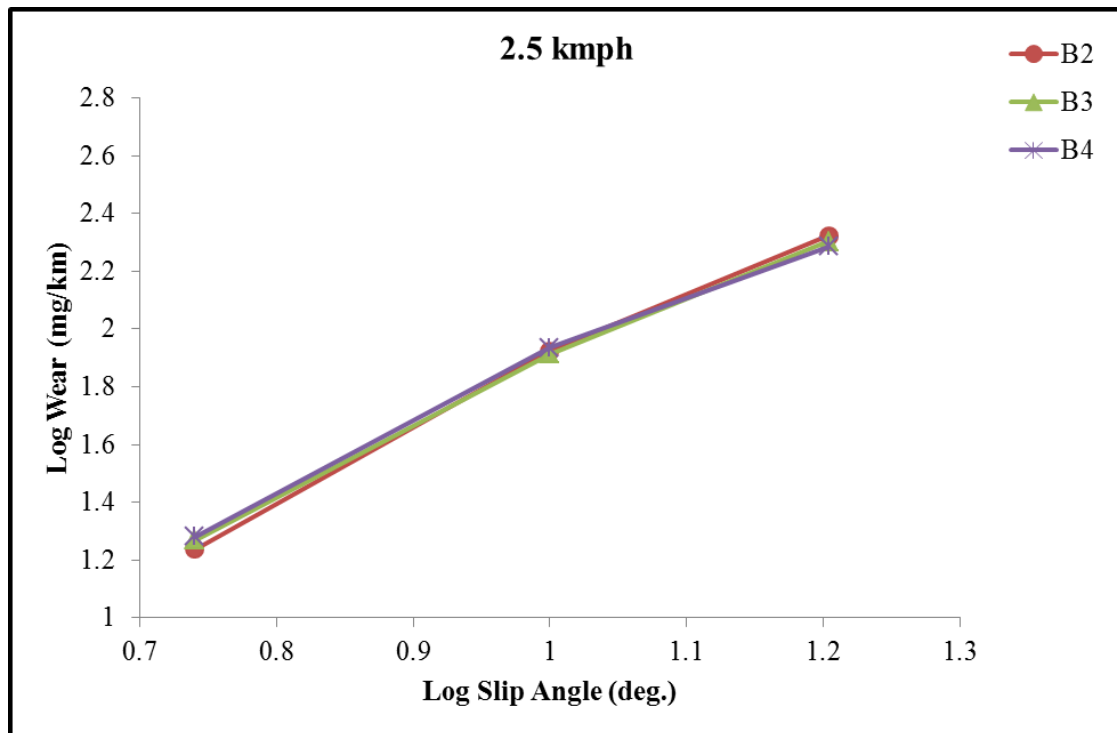
Figure 6.27 Variation of wear with slip angle at 2.5 kmph speed on Corrundum 60
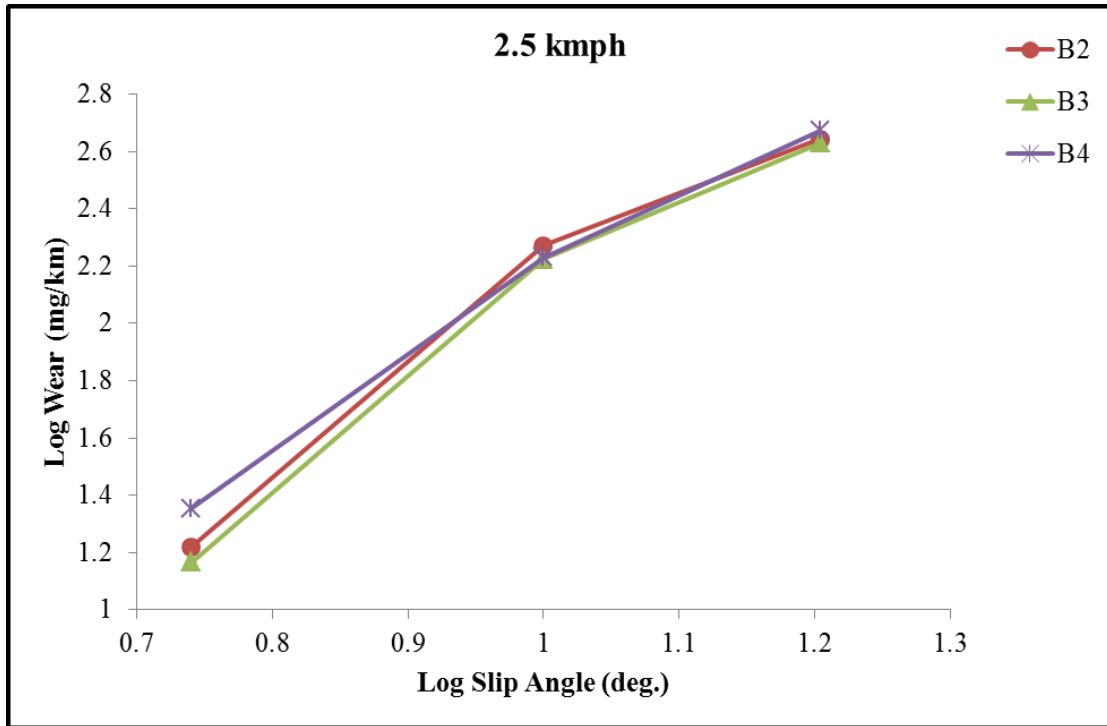
Figure 6.28 Variation of wear with slip angle at 2.5 kmph speed on Corrundum 180
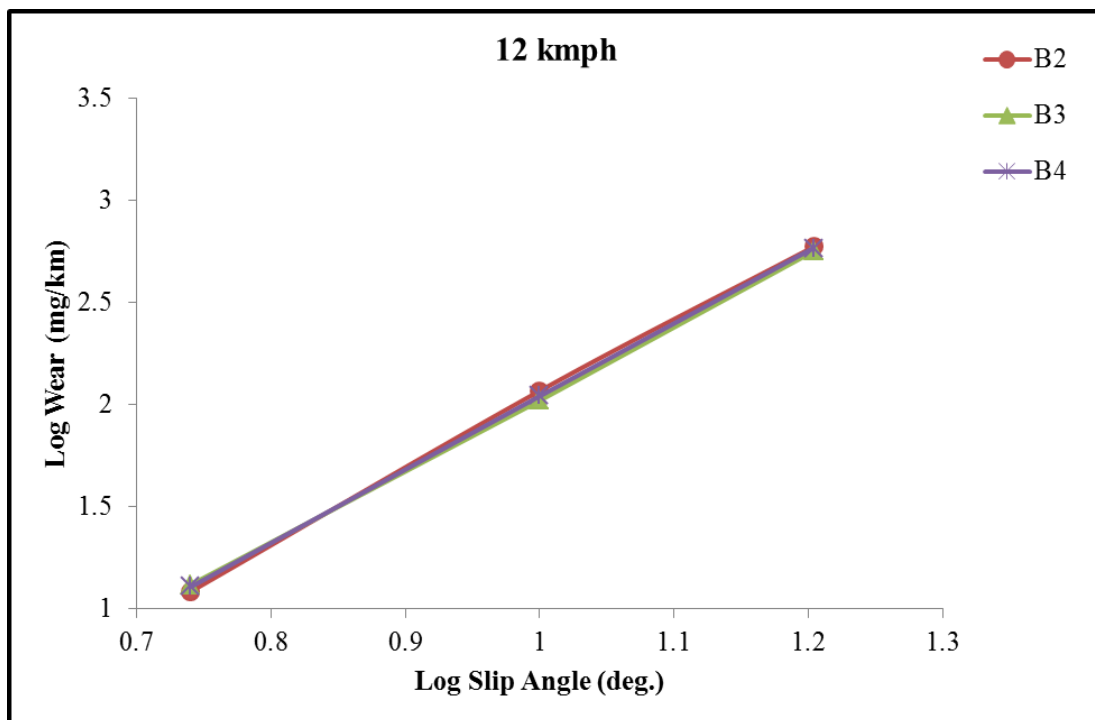
Figure 6.29 Variation of wear with slip angle at 12 kmph speed on Corrundum 60
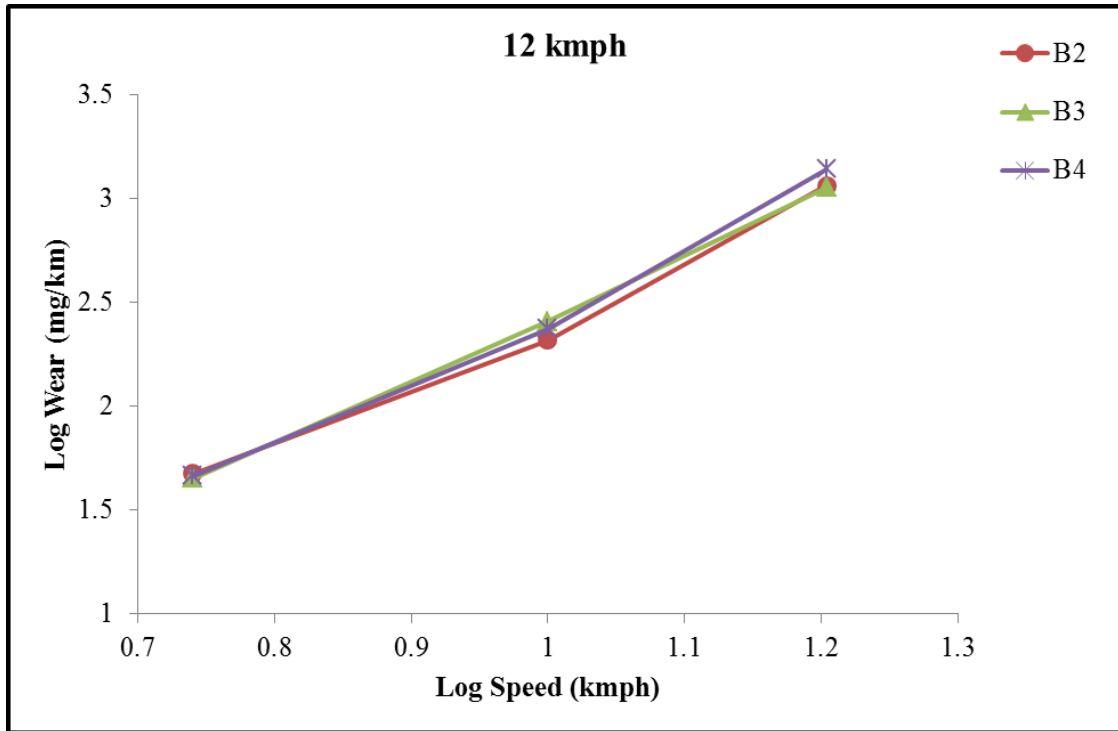
Figure 6.30 Variation of wear with slip angle at 12 kmph speed on Corrundum 180
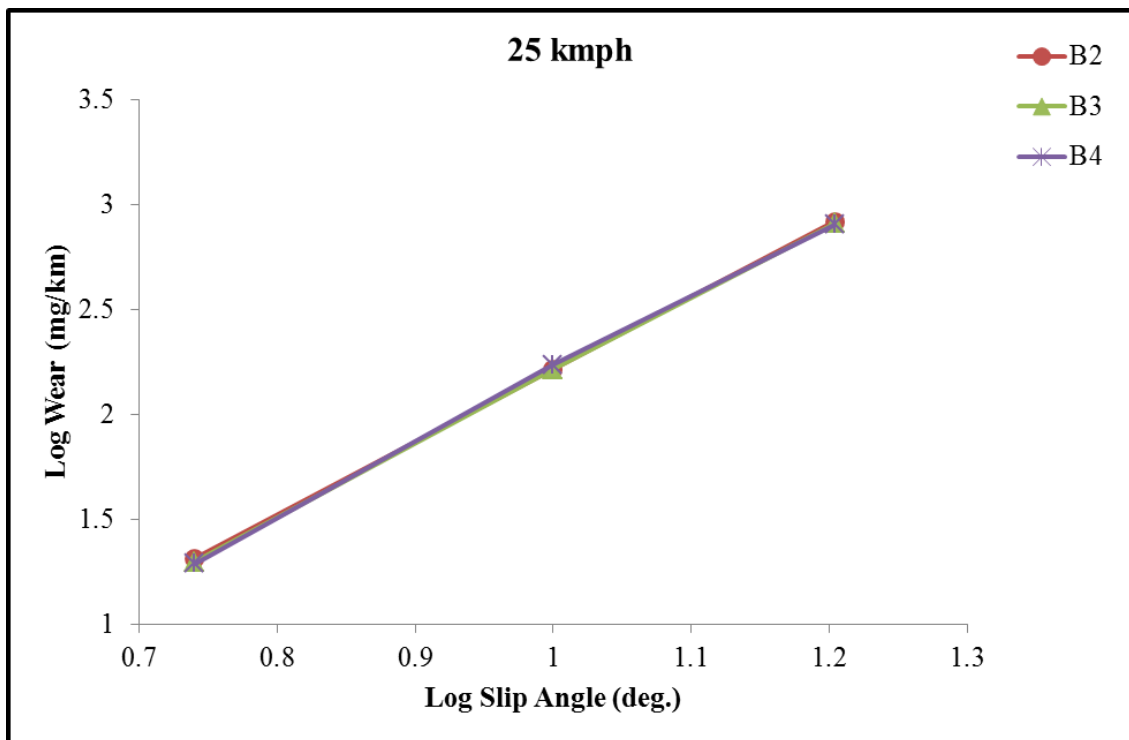
Figure 6.31 Variation of wear with slip angle at 25 kmph speed on Corrundum 60
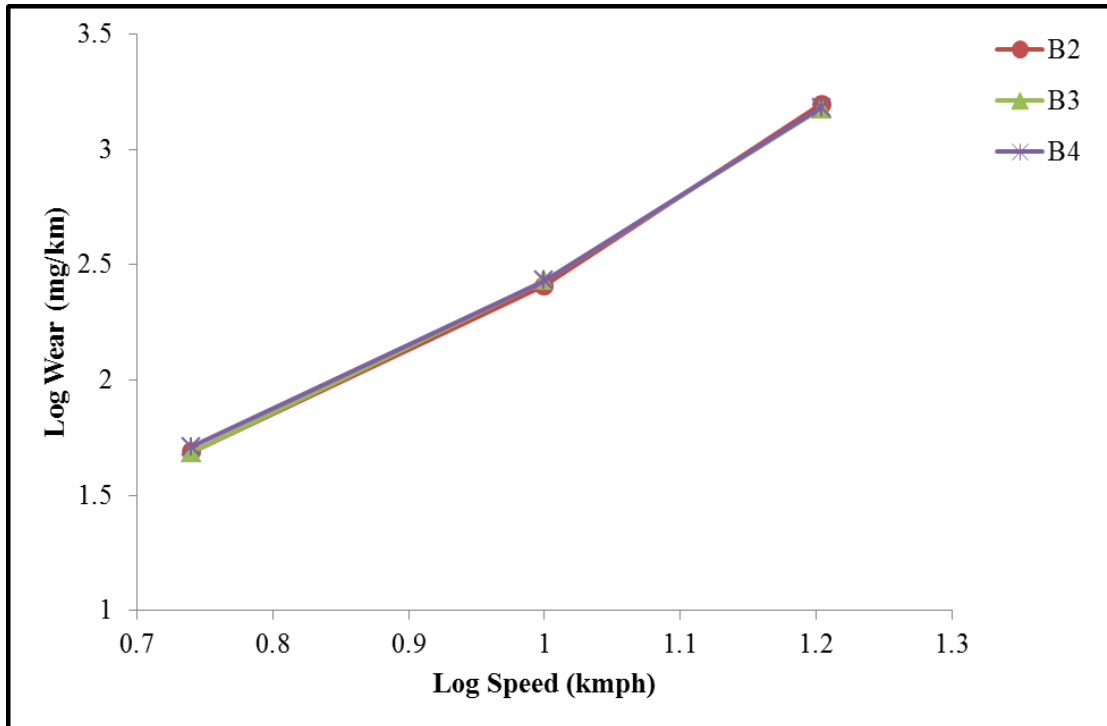
Figure 6.32 Variation of wear with slip angle at 25 kmph speed on Corrundum 180
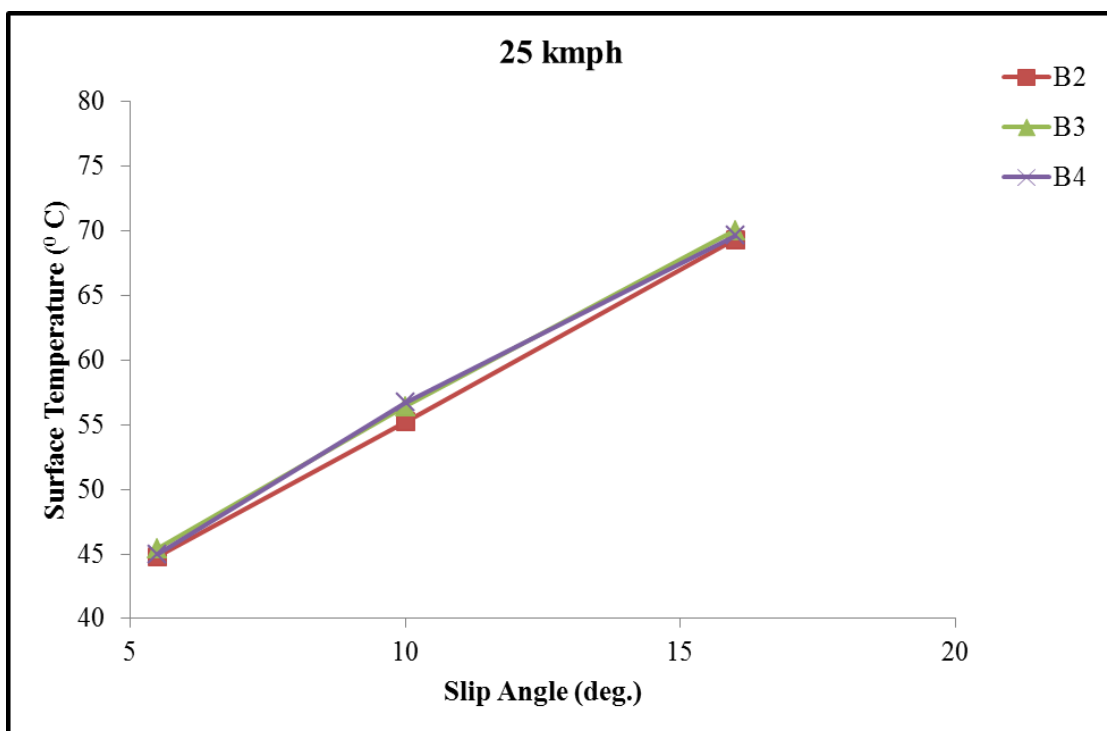
Figure 6.33 Variation of surface temperature with slip angle on Corundum 60
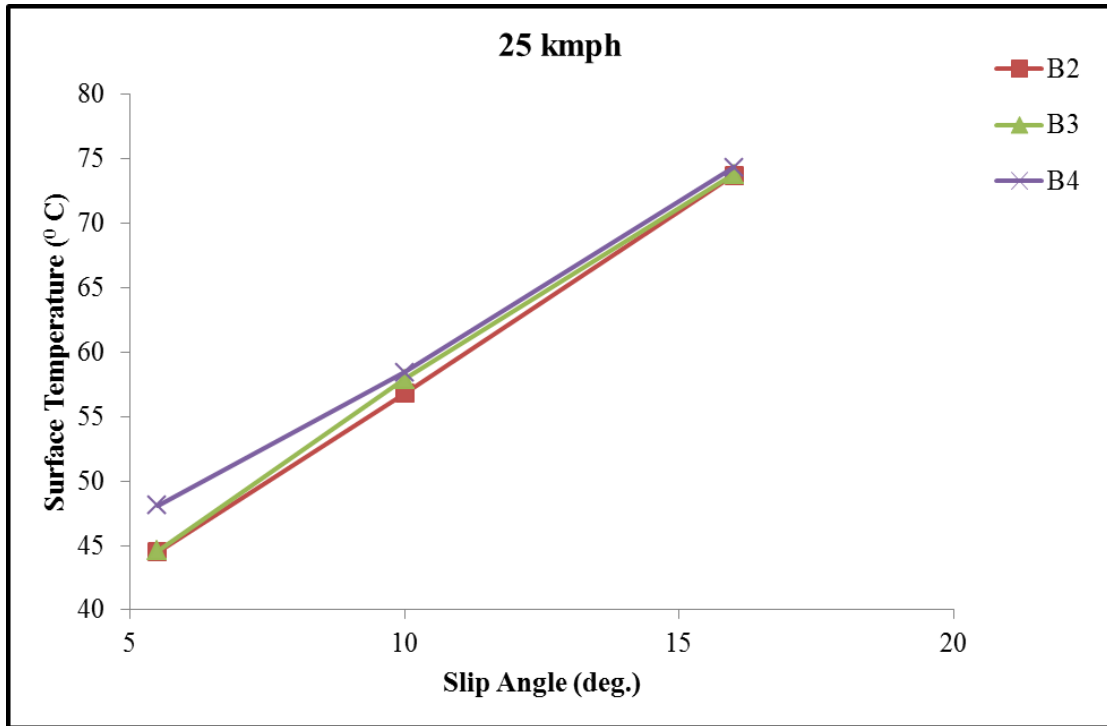
Figure 6.34 Variation of surface temperature with slip angle on Corundum 180

Table 6.9 Coefficients of NR/SBR blends on Corundum 60

Compound	a	b1	b2	b3
B2	0.4598	1.3962	-0.3848	0.7042
B3	0.5295	1.3267	-0.4554	0.7566
B4	0.5579	1.2909	-0.5044	0.8174

Table 6.10 Coefficients of NR/SBR blends on Corundum 180

Compound	a	b1	b2	b3
B2	0.1251	1.9848	0.3325	-0.0095
B3	-0.0352	2.0847	0.4291	-0.0645
B4	0.2405	1.8798	0.2356	0.0827

Table 6.11 Relative rating of B2 compound on Corundum 60

log energy, W	log speed, v (kmph)								
	0	0.2	0.4	0.6	0.8	1	1.2	1.4	1.6
0	**85.9**	**95**	105.1	116.2	128.5	142	157	173.6	192
0.2	**88.2**	**96.1**	104.8	114.2	124.5	135.7	147.8	161.1	175.6
0.4	**90.5**	**97.2**	104.5	112.2	120.6	129.6	139.2	149.5	160.7
0.6	**92.9**	**98.4**	104.2	110.3	116.8	123.7	131	138.8	147
0.8	**95.3**	**99.5**	103.9	108.4	113.2	118.2	123.4	128.8	134.4
1	**97.8**	100.6	103.6	106.6	109.7	112.9	116.1	119.5	123
1.2	100.4	101.8	103.3	104.8	106.3	107.8	109.3	110.9	112.5
1.4	103	103	103	103	102.9	102.9	102.9	102.9	102.9
1.6	105.7	104.2	102.7	101.2	**99.7**	**98.3**	**96.9**	**95.5**	**94.1**

Table 6.12 Relative rating of B3 compound on Corundum 60

log energy, W	log speed, v (kmph)								
	0	0.2	0.4	0.6	0.8	1	1.2	1.4	1.6
0	**73.2**	**83.6**	**95.5**	109.1	124.6	142.3	162.6	185.7	212.1
0.2	**77.6**	**86.9**	**97.4**	109.1	122.3	137	153.5	172	192.7
0.4	**82.2**	**90.3**	**99.3**	109.1	120	131.9	145	159.3	175.1
0.6	**87.1**	**93.9**	101.2	109.2	117.7	126.9	136.9	147.6	159.2
0.8	**92.3**	**97.6**	103.2	109.2	115.5	122.2	129.3	136.7	144.6
1	**97.8**	101.5	105.3	109.2	113.4	117.6	122.1	126.7	131.4
1.2	103.6	105.5	107.3	109.3	111.2	113.2	115.3	117.3	119.4
1.4	109.8	109.6	109.5	109.3	109.2	109	108.8	108.7	108.5
1.6	116.3	113.9	111.6	109.3	107.1	104.9	102.8	100.7	**98.6**

Table 6.13 Relative rating of B4 compound on Corundum 60

log energy, W	log speed, v (kmph)								
	0	0.2	0.4	0.6	0.8	1	1.2	1.4	1.6
0	**68.6**	**80.1**	**93.6**	109.3	127.7	149.3	174.4	203.7	238
0.2	**73.9**	**84.2**	**95.9**	109.3	124.6	142	161.9	184.5	210.3
0.4	**79.6**	**88.5**	**98.3**	109.3	121.6	135.2	150.3	167.1	185.7
0.6	**85.7**	**93**	100.8	109.3	118.6	128.6	139.5	151.3	164.1
0.8	**92.3**	**97.7**	103.3	109.3	115.7	122.4	129.5	137	144.9
1	**99.5**	102.6	105.9	109.3	112.8	116.5	120.2	124	128
1.2	107.1	107.9	108.6	109.3	110.1	110.8	111.6	112.3	113.1
1.4	115.4	113.3	111.3	109.3	107.4	105.5	103.6	101.7	**99.9**
1.6	124.3	119.1	114.1	109.3	104.7	100.4	**96.1**	**92.1**	**88.3**

Table 6.14 Relative rating of B2 compound on Corundum 180

log energy, W	log speed, v (kmph)								
	0	0.2	0.4	0.6	0.8	1	1.2	1.4	1.6
0	148.3	132.3	118.1	105.4	**94**	**83.9**	**74.9**	**66.8**	**59.6**
0.2	146.1	133.6	122.2	111.7	102.2	**93.4**	**85.4**	**78.1**	**71.5**
0.4	143.9	134.8	126.4	118.4	111	104	**97.5**	**91.4**	**85.6**
0.6	141.7	136.1	130.7	125.5	120.6	115.8	111.2	106.8	102.6
0.8	139.6	137.4	135.2	133.1	131	128.9	126.9	124.9	122.9
1	137.5	138.7	139.9	141.1	142.3	143.5	144.8	146	147.3
1.2	135.4	140	144.7	149.5	154.6	159.8	165.1	170.7	176.5
1.4	133.4	141.3	149.6	158.5	167.9	177.9	188.4	199.6	211.4
1.6	131.4	142.6	154.8	168	182.4	198	215	233.4	253.3

Table 6.15 Relative rating of B3 compound on Corundum 180

log energy, W	log speed, v (kmph)								
	0	0.2	0.4	0.6	0.8	1	1.2	1.4	1.6
0	214.5	183.1	156.3	133.4	113.9	**97.2**	**83**	**70.8**	**60.4**
0.2	201.8	177.4	156	137.1	120.5	106	**93.2**	**81.9**	**72**
0.4	189.8	171.9	155.6	140.9	127.6	115.6	104.7	**94.8**	**85.8**
0.6	178.6	166.5	155.3	144.9	135.1	126	117.6	109.6	102.3
0.8	168	161.4	155	148.9	143.1	137.4	132	126.8	121.9
1	158	156.3	154.7	153.1	151.5	149.9	148.3	146.7	145.2
1.2	148.6	151.5	154.4	157.3	160.4	163.4	166.6	169.8	173
1.4	139.8	146.8	154.1	161.7	169.8	178.2	187.1	196.4	206.2
1.6	131.5	142.2	153.8	166.2	179.8	194.4	210.1	227.2	245.7

Table 6.16 Relative rating of B4 compound on Corundum 180

log energy, W	log speed, v (kmph)								
	0	0.2	0.4	0.6	0.8	1	1.2	1.4	1.6
0	113.7	106.1	**99**	**92.4**	**86.2**	**80.4**	**75.1**	**70**	**65.4**
0.2	117.5	111.4	105.7	100.2	**95**	**90.1**	**85.4**	**81**	**76.8**
0.4	121.5	117.1	112.8	108.7	104.7	100.9	**97.2**	**93.6**	**90.2**
0.6	125.6	123	120.4	117.9	115.4	113	110.6	108.3	106
0.8	129.8	129.2	128.5	127.8	127.2	126.5	125.9	125.2	124.6
1	134.2	135.7	137.2	138.7	140.2	141.7	143.2	144.8	146.4
1.2	138.8	142.5	146.4	150.4	154.5	158.7	163	167.4	172
1.4	143.4	149.7	156.3	163.1	170.2	177.7	185.5	193.6	202
1.6	148.3	157.3	166.8	176.9	187.6	199	211	223.8	237.4

6.3 CORRELATION BETWEEN WEAR AND FCG PROPERTY

From the previous discussions it is evident that the cut growth process is the major contributor towards wear. Therefore, it is desirable to find a correlation of wear with the FCG characteristics of NR/BR and NR/SBR blend compounds. It can be hypothesized that the micro cracks developed at the surface propagates during rolling of the wear sample and due to the interaction with the surface asperities. The crack growth rates (da/dn) of these compounds at 1 N/mm tearing energy are reported in Table 6.17. The correlations between crack growth rate and wear for NR/BR and NR/SBR blend compounds on both the surfaces are shown in Figure 6.35 and 6.36 respectively. It has been observed that, for both the blends, higher correlation (R^2= 0.943 for NR/BR and 0.886 for NR/SBR) is observed with Corundum 180 surface when compared to 60 surface (R^2= 0.883 for NR/BR and 0.318 for NR/SBR). This finding is in agreement with Muhr and Roberts (1992), where it was indicated that the wear in blunt tracks are due to fatigue crack growth mechanism. Lower R^2 value for NR/SBR blend compounds as shown in Figure 6.36, even though the fitted curve appears to be passing through all the points, due to the scaling of the graph.

Table 6.17 FCG rate of NR, NR/BR and NR/SBR blends at 1 N/mm tearing energy

Compound	Crack growth rate (mm/cycle)
A1	8.43E-06
A2	5.93E-06
A3	2.90E-06
A4	2.84E-06
B2	8.56E-06
B3	3.28E-06
B4	1.51E-06
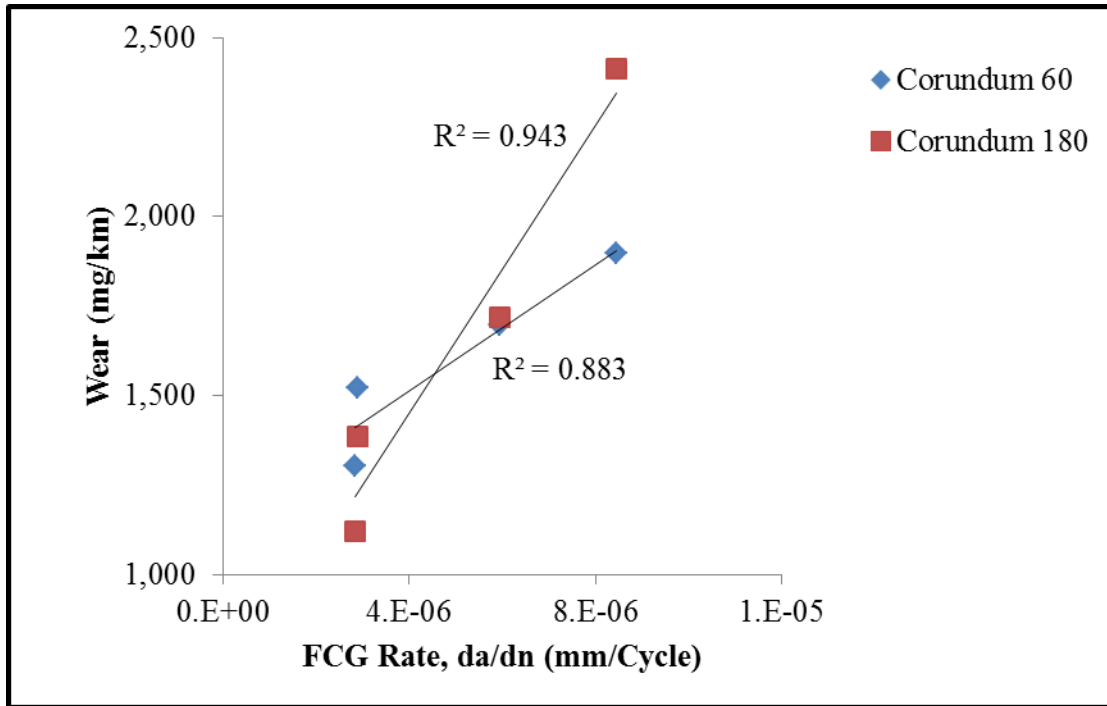
Figure 6.35 Correlation between wear with FCG rate for NR/BR blends
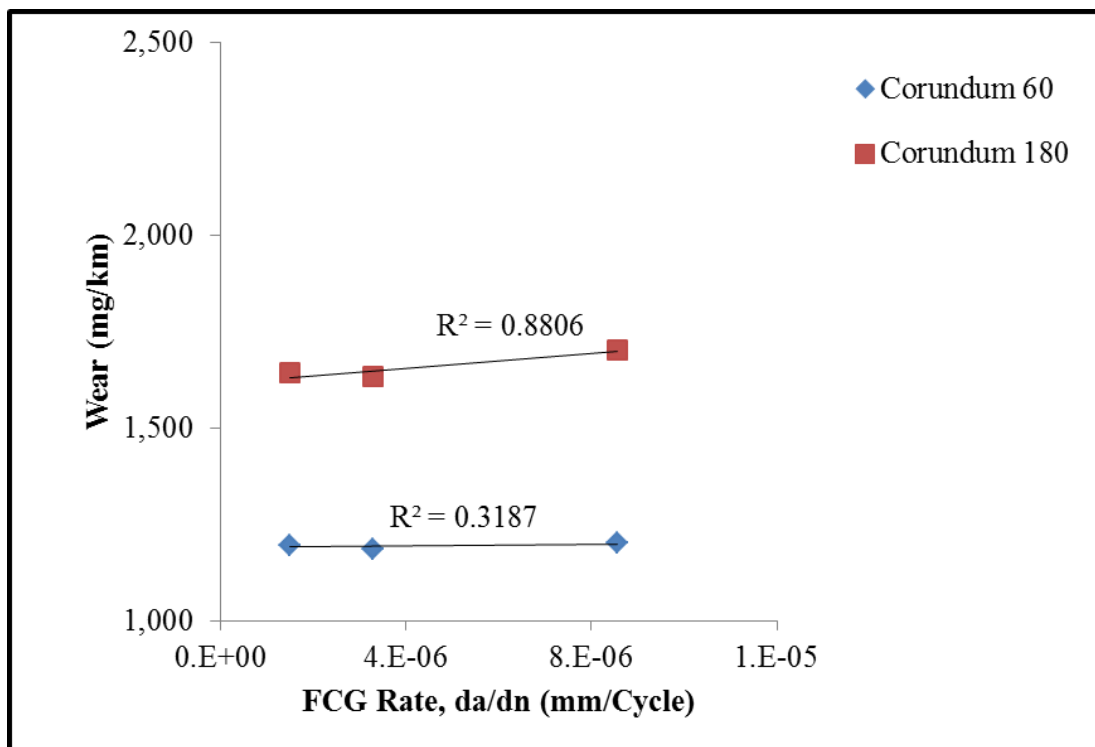
Figure 6.36 Correlation between wear with FCG rate for NR/SBR blends

118

6.4 SUMMARY

In this chapter, wear characteristics of NR/BR and NR/SBR blends is discussed. The influence of speed, slip angle and surface on the wear behaviour is presented. All these parameters significantly influence the wear characteristics. In both the blends, wear resistance increases with increase in BR and SBR content in the respective blends. A considerable amount of temperature rise on sample surface due to speed and slip angle is reported for both the blends. The results of wear coefficients revealed that the crack growth is the major contributor in the wear process. It was also observed that this phenomenon is more prominent for blunter surface (Corundum 180) which indicated fatigue dominant wear mechanism. A good correlation is found between the wear and the FCG properties as discussed in Chapter 5, especially with Corundum 180 results and this surface should be recommended for laboratory wear measurement.

CHAPTER 7

FINITE ELEMENT ANALYSIS OF FATIGUE LOADING OF PURE SHEAR SAMPLE UNDER SINE AND PULSE MODES

This chapter describes the Finite Element Analysis (FEA) of pure shear sample and simulation of cyclic loading using Sine and Pulse modes as used in FCG testing.

7.1 FINITE ELEMENT MODELLING

The image of a pure shear sample (discussed in section 3.2.9 of Chapter 3) used for FCG testing is provided in Figure 7.1. It is a double sided notched sample having initial crack length of 21 mm on both sides.

Figure 7.1 Pure shear specimen used for FCG testing

For the purpose of FE modelling, half of the sample geometry is modelled because of the symmetry. 3D FE mesh is generated in Abaqus FE software (Abaqus, 2013) and the mesh model is shown in Figure 7.2. The FE model consists of 1983 C3D8R element (continuum, three dimensional, eight noded with reduced integration formulation). C3D8R elements are chosen to carry out the transient analysis as followed by Rao *et al.* (2003). Self-contact has been defined at the crack interfaces with a coefficient of friction value 0.5.

Yeoh hyperelastic material model, generally used for tyre rubber materials (Rao *et al.*, 2003) is used to define the time independent (elastic) material property of the rubber sample. The boundary conditions are defined in the following manner. Zero displacement is assigned to all the nodes at the bottom portion of the sample as these

nodes are not supposed to move in any direction. The displacements of the nodes on the top and left side of the sample are constrained in the X and Z directions, allowing specifying displacements only in the Y direction. There was no boundary condition applied on the nodes of the right side of the sample. The analysis is carried out under displacement control mode and the required displacement is specified on top nodes in the positive Y direction. Sine and Pulse loading inputs are shown in Figure 7.3.
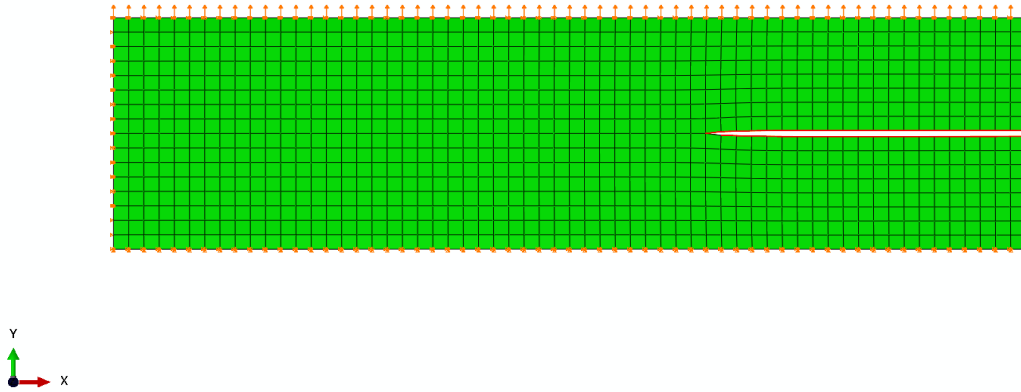
Figure 7.2 FE mesh of pure shear sample
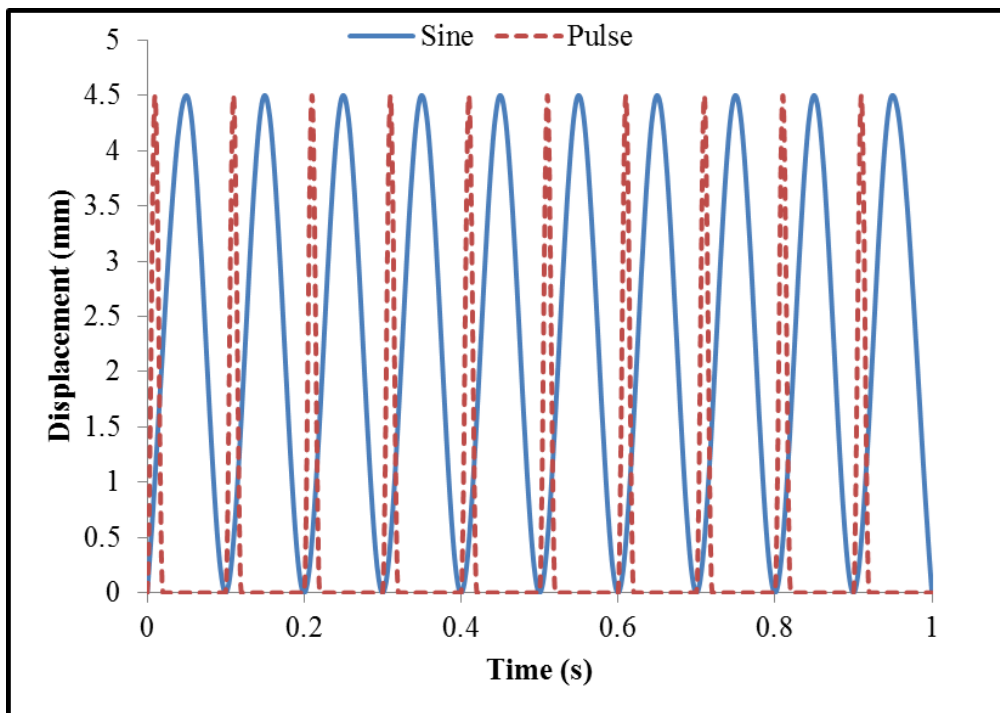
Figure 7.3 Sine and Pulse inputs

In the subsequent sections results of the FE analysis considering pure hyperelasticity, hyperelasticity with linear viscoelasticity and non-linear viscoelasticity behaviours are discussed in detail.

7.1.1 Pure Hyperelasticity

The analyses were carried out for both Sine and Pulse loading at 30% strain for the A1 material. In the material definition, Yeoh hyperelastic coefficients of the A1 material were used as reported in Table 4.7. For both the Sine and Pulse loadings, analyses were performed for 9 sec time duration to capture the long term behaviour of the material. Figures 7.4 and 7.5 show Strain Energy Density (SENER) and Maximum Principal Stress for Sine and Pulse modes respectively. As expected, there is no difference in the results, as observed from these contours. The Stored Energy (ALLSE) values for the whole model are also the same in both the modes as shown in Figure 7.6. From these results it can be inferred that the hyperelastic material definition alone cannot capture the differences between the Sine and Pulse modes. Since these modes differ in loading time, inclusion of the viscoelastic property definition must be taken into consideration to represent the time dependent response of the material. Analysis scheme and results using the viscoelastic properties are discussed in subsequent sections.
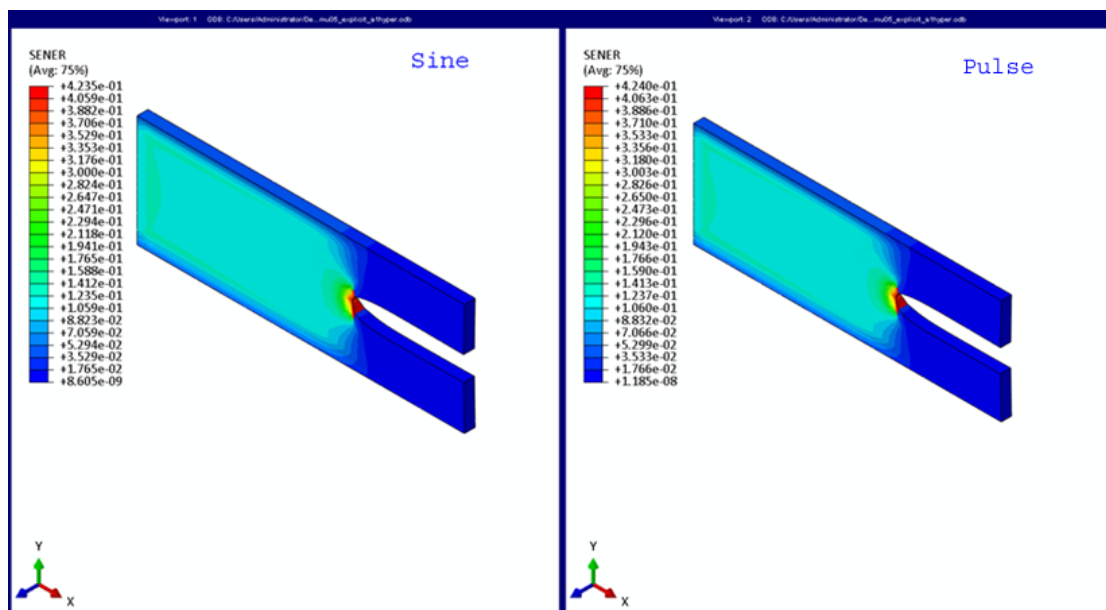
Figure 7.4 SENER contour plots with pure hyperelastic analysis
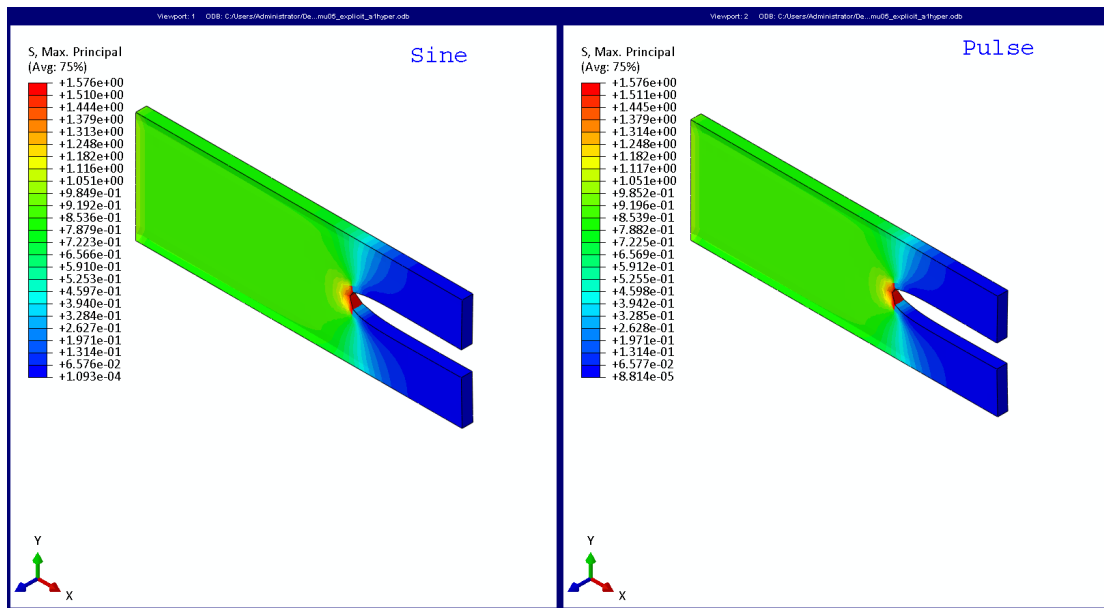
Figure 7.5 Max. Principal Stress contour plots with pure hyperelastic analysis
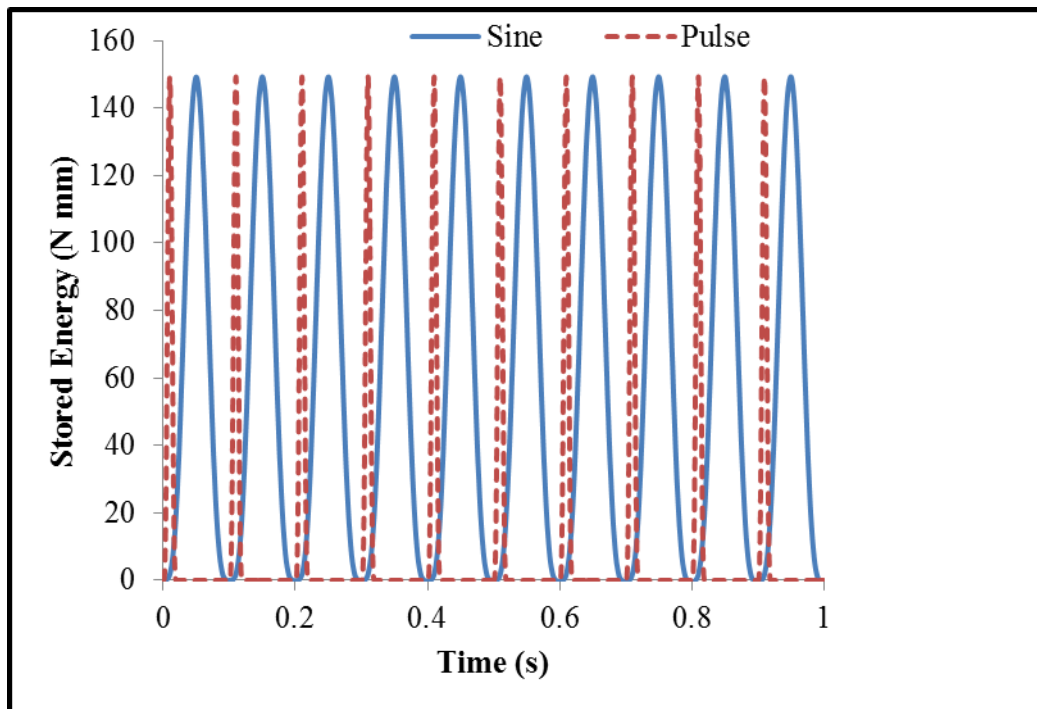
Figure 7.6 ALLSE of the whole model with pure hyperelastic analysis

7.1.2 Linear Viscoelasticity

Analyses were carried out for both the Sine and Pulse loading using Prony series constants of the A1 material as reported in Table 4.11. Figures 7.7 and 7.8 show SENER and maximum principal stress at the crack tip for both the loadings. There is no difference in the SENER values between the Sine and Pulse modes. However, Pulse mode reported slightly higher maximum principal stress at the crack tip when compared to the Sine mode. Figure 7.9 shows the comparison of ALLSE for the whole model of these two modes. It can be observed that the peak values in all cycles are almost same for both the modes. Further, Abaqus/Explicit does not report Dissipated Energy (ALLCD) and Dissipated Energy Density (CENER) for the models which use linear viscoelasticity i.e. Prony series definition, limiting realistic interpretation of the results. Hence, the necessity of better viscoelastic model to address this limitation is to be studied. Non-linear viscoelastic (PRF model) model discussed in the next section addresses this limitation.

Figure 7.7 SENER contour plots with linear viscoelasticity
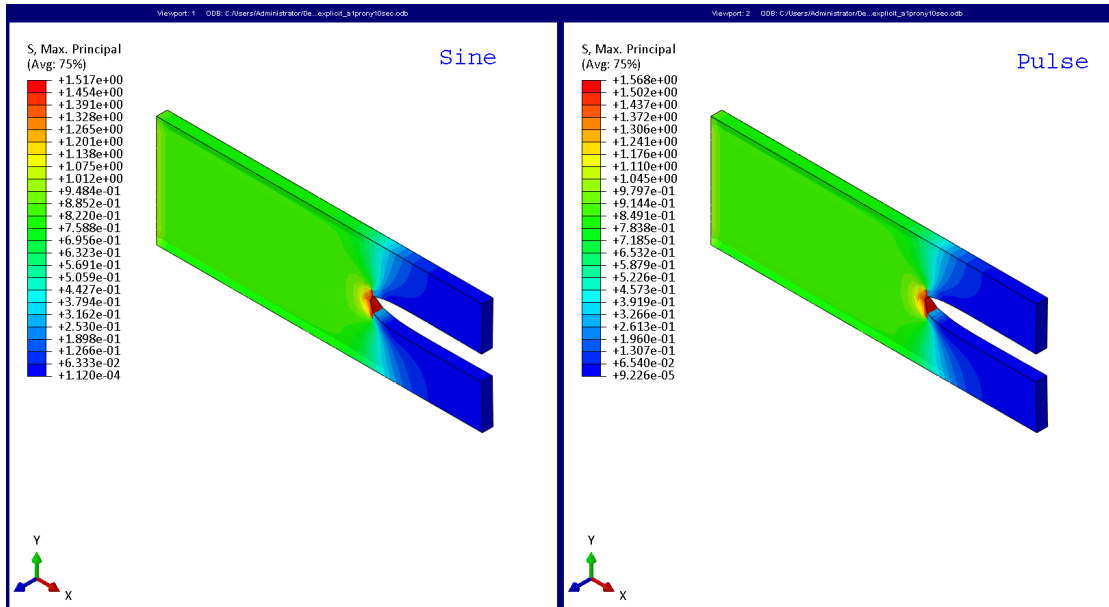
Figure 7.8 Max. Principal Stress contour plots with linear viscoelasticity
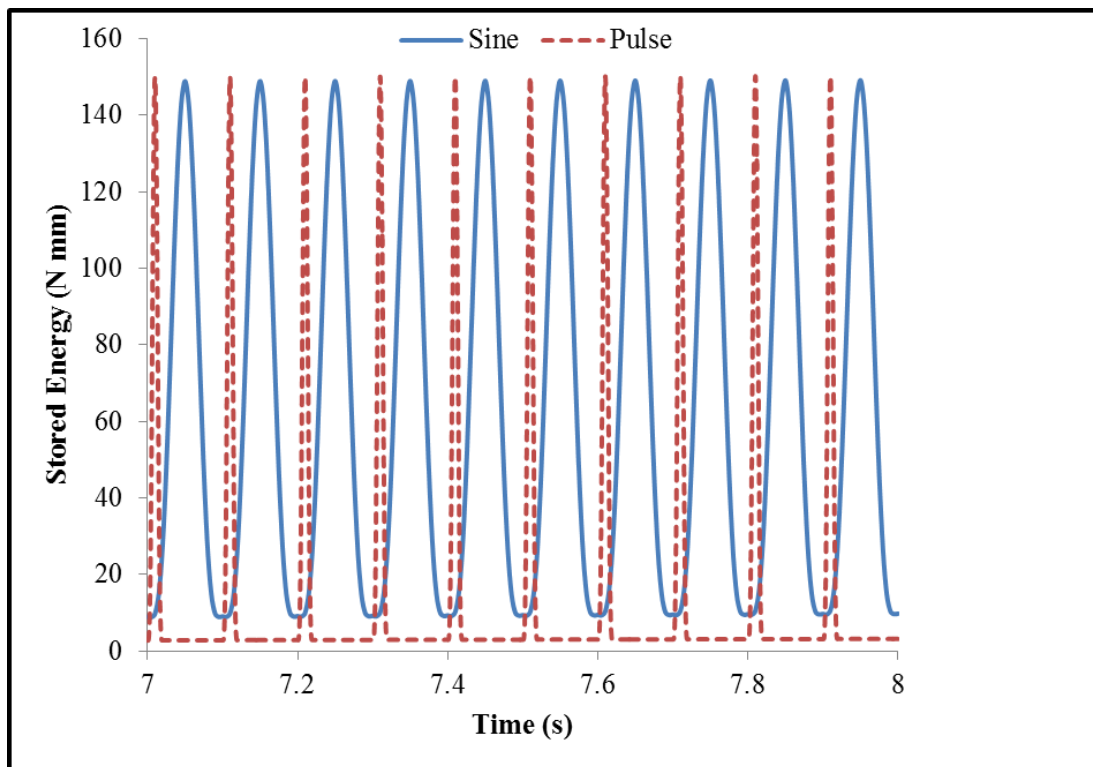
Figure 7.9 ALLSE of the whole model with linear viscoelasticity

7.1.3 Non-linear Viscoelasticity

Analyses using non-linear viscoelastic model (PRF model) were performed for both the Sine and Pulse loadings. The material properties of the A1compound as reported in Table 4.12 were used for these set of analysis. The SENER and Max. Principal Stress contour plots are shown in Figures 7.10 and 7.11 respectively. It can be observed that for both these parameters, the Pulse mode reported higher values compared to the Sine mode. This is due to the higher strain rate associated with the Pulse mode. Figure 7.12 shows the comparative SENER at the crack tip for both the modes. It has been observed that the peak value is higher with Pulse mode in every cycle of loading. It is also interesting to note that the differences in the peak SENER values between the Sine and Pulse modes keep increasing with the progression of the fatigue cycles.

The ALLSE and ALLCD energy outputs for the whole model are reported in Figures 7.13 and 7.14 respectively. It has been observed that the ALLSE is higher for the Pulse mode whereas in the case of ALLCD, the Sine mode reported higher values. Figure 7.15 shows the Viscous Energy Dissipation per unit volume (CENER) of these cases. It can be seen that the CENER at the crack tip is higher in the Sine mode when compared to the Pulse mode. Higher viscoelastic dissipation is advantageous from the fracture resistance point of view and also in accordance with the literature (Persson *et al.*, 2005; D'Amico *et al.*, 2013). The higher the energy dissipation, lesser will be the energy available for the crack growth. As the Pulse mode has higher stored energy and therefore higher crack propagation can be expected than the Sine mode, which is in agreement with the experimental findings as presented in Chapter 5. Further, it can also be argued that the higher energy dissipation may also lead to temperature rise at the crack tip. It appears that the temperature effect is not as important as the energy availability, as shown by these experimental results. This needs further investigation.

126
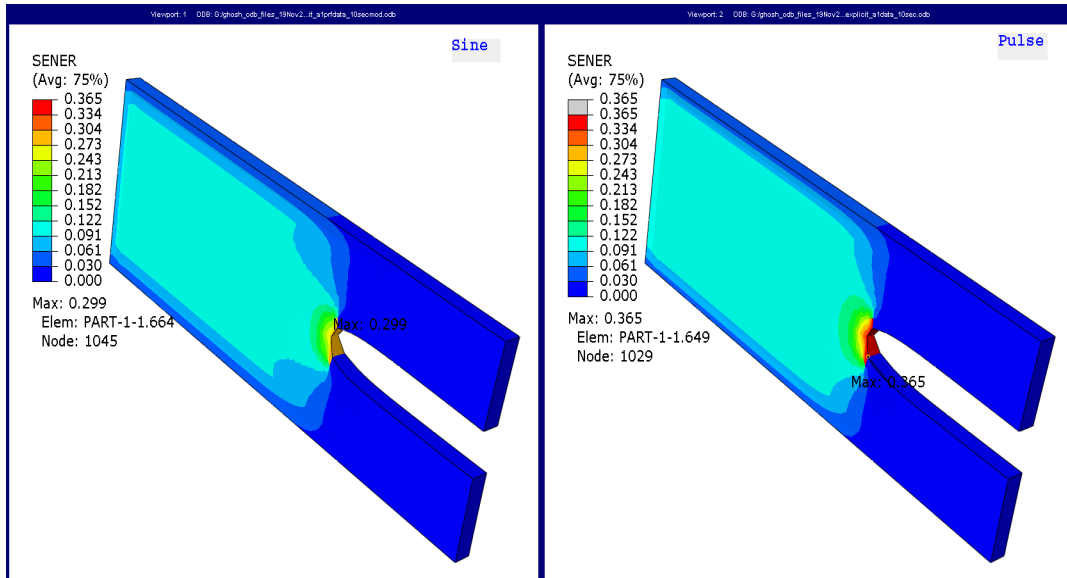
Figure 7.10 SENER contour plots with non-linear viscoelasticity
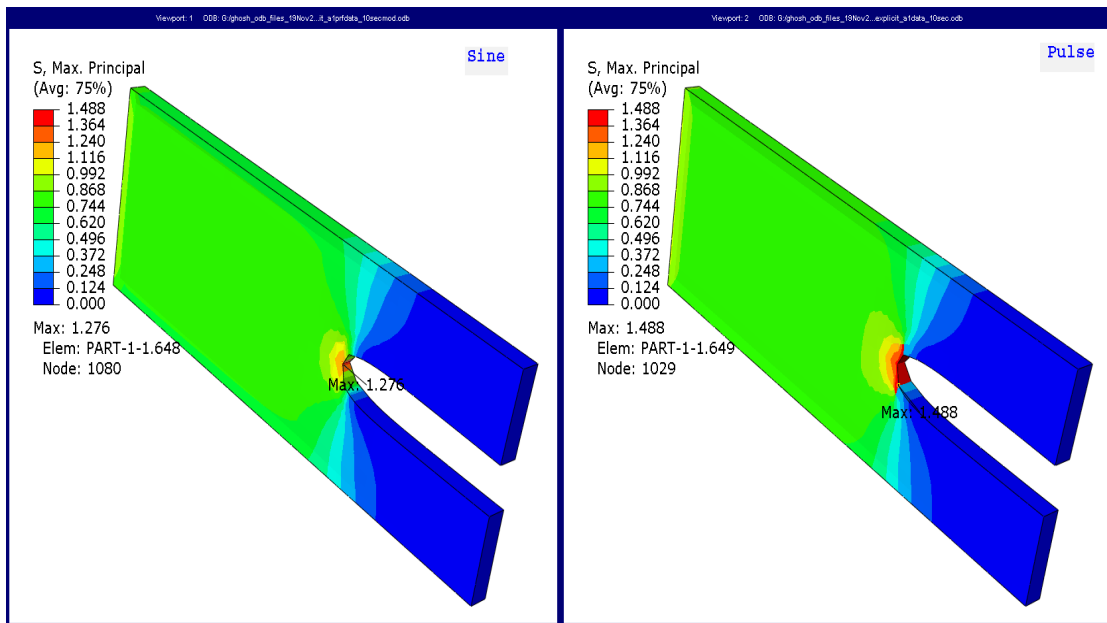
Figure 7.11 Max. Principal Stress contour plots with non-linear viscoelasticity
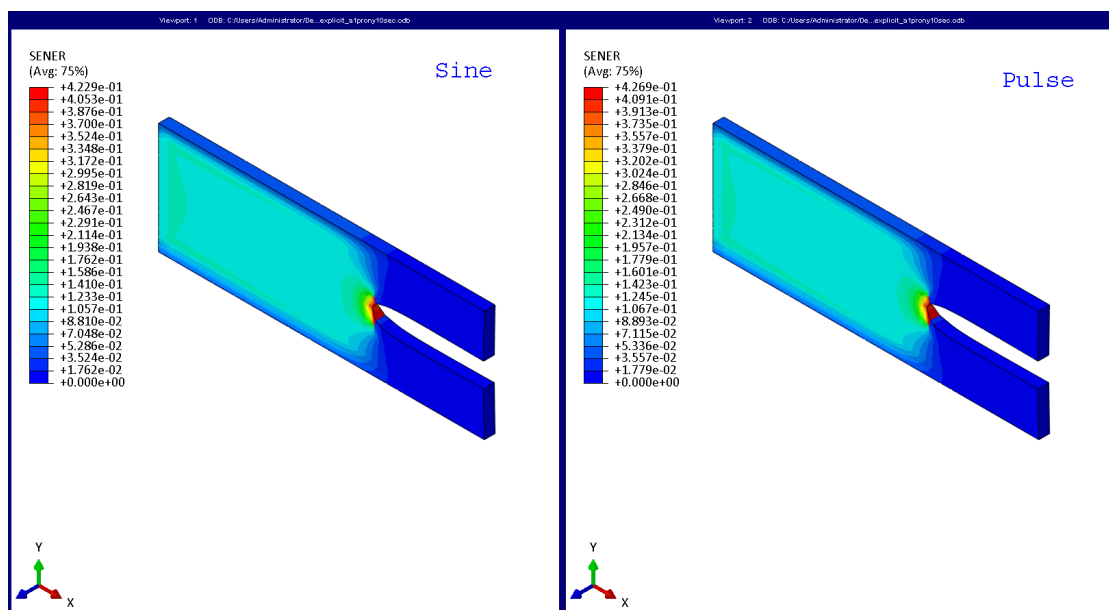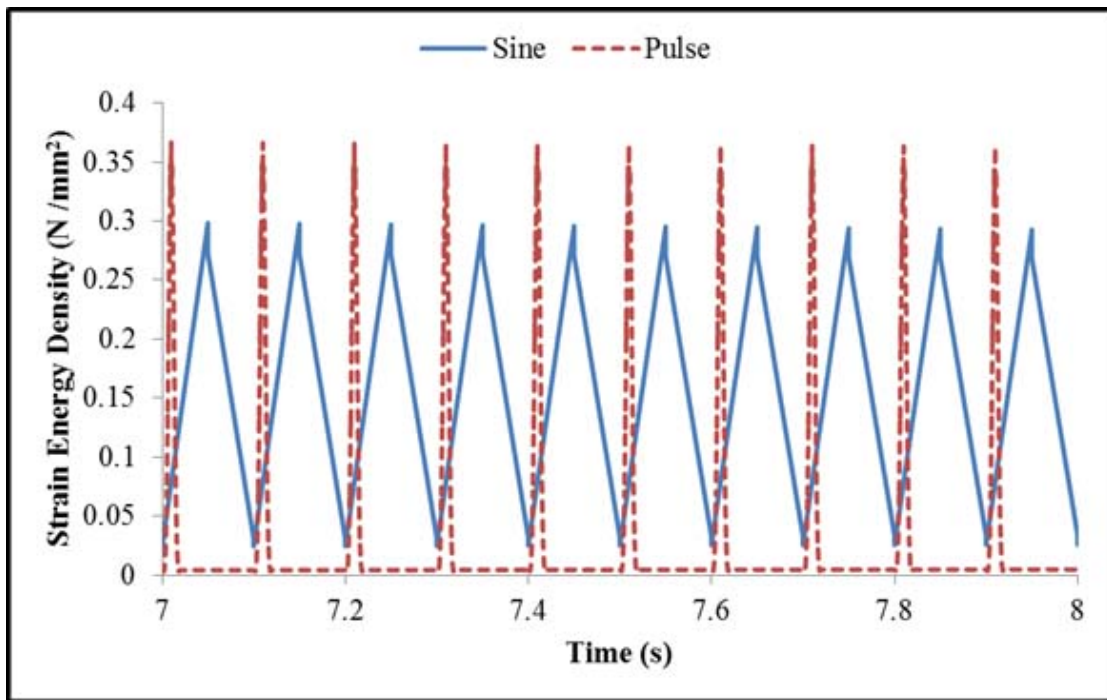
Figure 7.12 SENER at crack tip with non-linear viscoelasticity
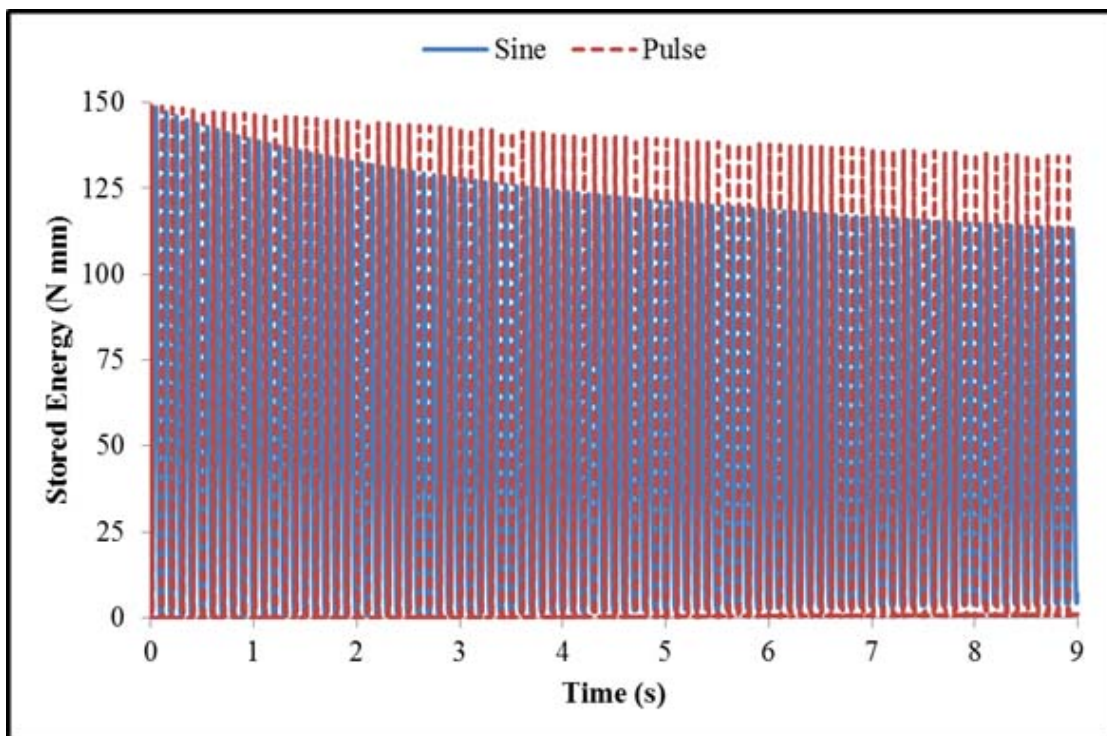
Figure 7.13 ALLSE of the whole model with non-linear viscoelasticity
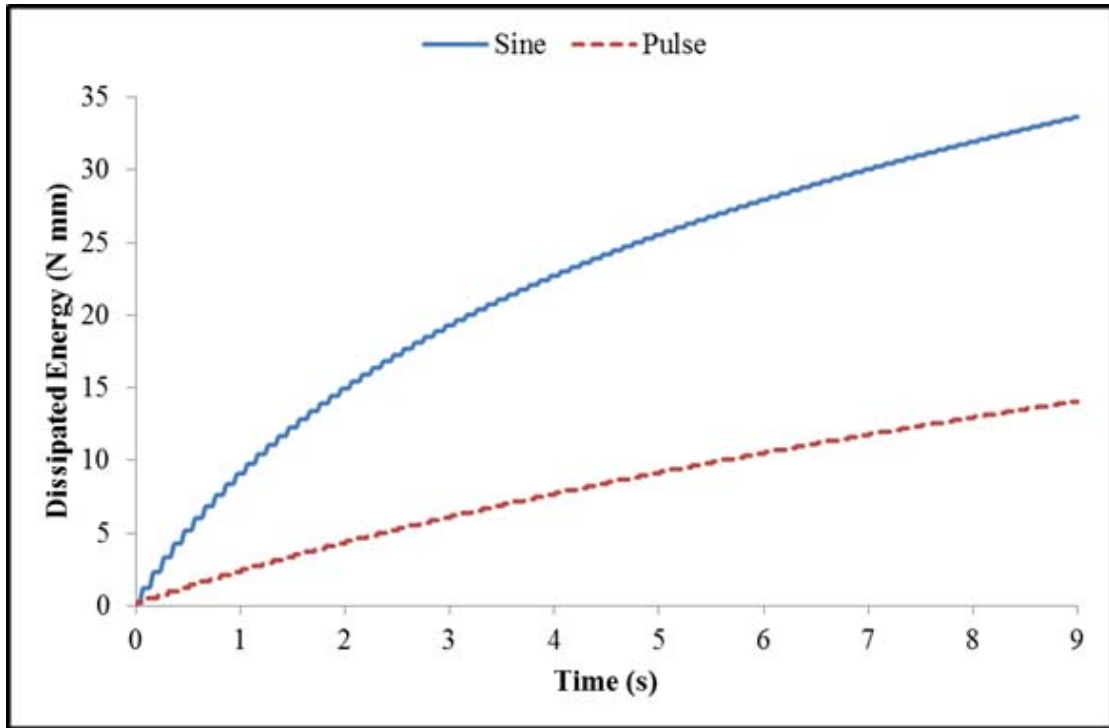
Figure 7.14 ALLCD of the whole model with non-linear viscoelasticity
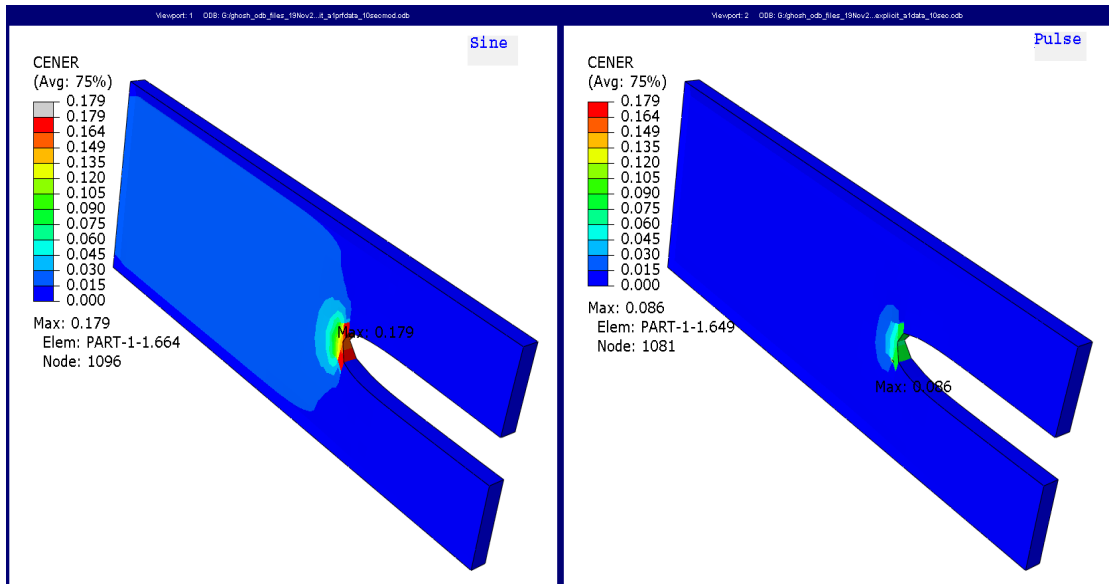
Figure 7.15 CENER contour plots with non-linear viscoelasticity

129

In order to verify the hypothesis, the dwell time and the Pulse widths were varied. Experimental results with a variation of dwell time and Pulse width have been reported in Chapter 5 and the details are given in Figure 3.7. As can be seen from Figure 5.13, the rate of crack growth is the highest for Pulse I, followed by Pulse IV and Pulse II. The lowest crack growth rate is seen for the Sine loading. Details of simulation conditions are summarised in Table 7.1.

Table 7.1 Simulation conditions for various Pulse modes and Sine mode

Mode	Pulse Width (ms)	Dwell Time (ms)
PI	20	80
PII	20	980
PIV	20	180
Sine	100	0

Figures 7.16 and 7.17 show the ALLSE and ALLCD results of the Sine and the Pulse modes. It has been observed that the peak value of ALLSE is higher in the Pulse modes (PI, PII and PIV) when compared to the Sine mode. This order of variation also follows the crack growth rate as observed in experimental results, thus confirming the hypothesis that the energy availability at the crack tip is a key criterion for growth.

The ALLCD results reveal that dwell time plays important role. The amount of dissipated energy follows the order of Sine > PI > PIV > PII. Out of these four conditions, Sine has no dwell time followed by PI, PIV and PII. It may be inferred from this result that lower the dwell time higher is the dissipated energy.
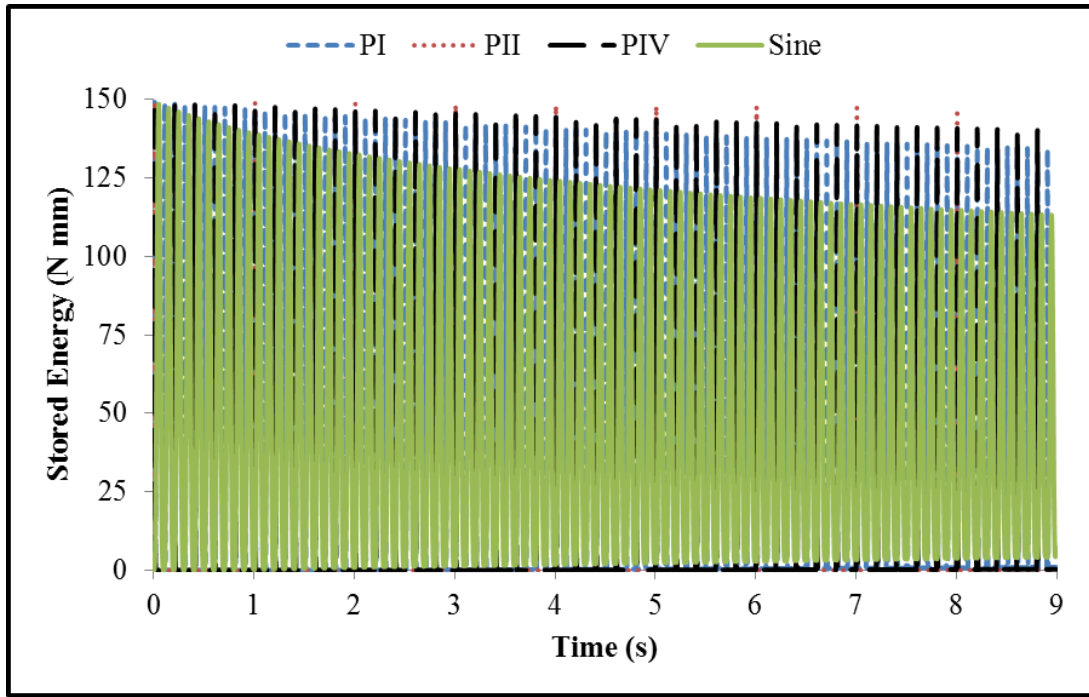
Figure 7.16 Stored energy (ALLSE) in the whole model for various Pulse modes and Sine mode
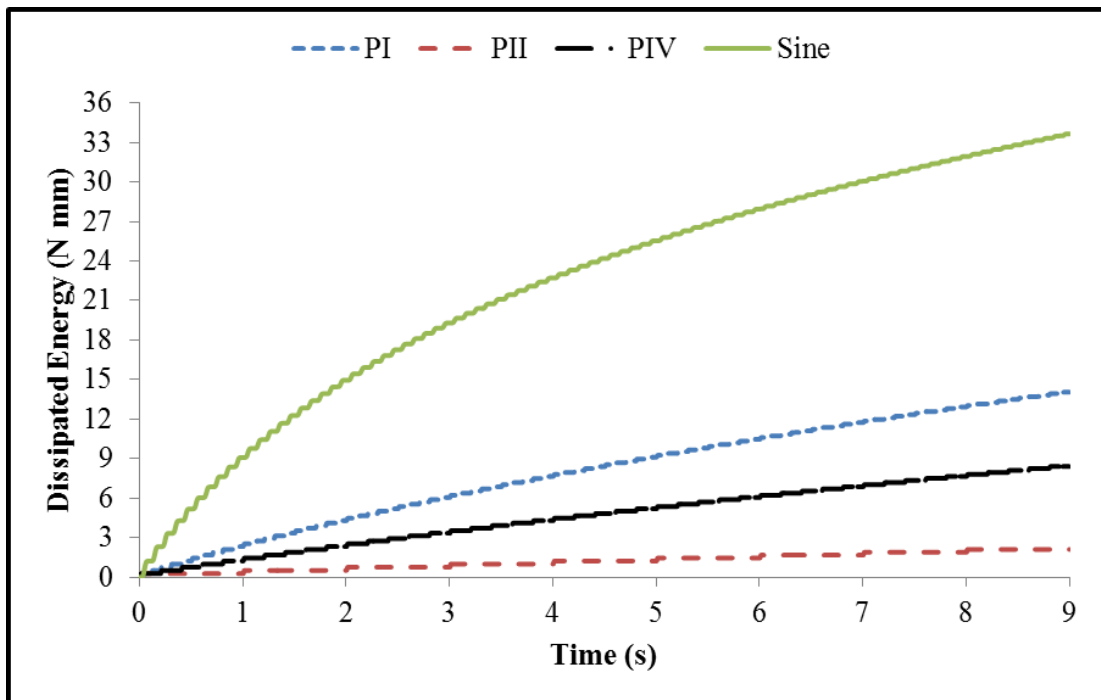
Figure 7.17 Dissipated energy (ALLCD) in the whole model for various Pulse modes and Sine mode

7.2 SUMMARY

In this chapter, FEA analysis of FCG loading under Sine and Pulse modes is discussed. Analyses were carried out using hyperelastic and viscoelastic material property definitions. Pure hyperelastic and hyperelastic with linear viscoelastic models are not adequate to capture the phenomena associated with the Sine and the Pulse loadings. PRF model is able to describe the mechanics of the influence of these loading modes more appropriately. It gives a clear insight into the role of the stored and dissipated energies on the crack growth phenomena.

CHAPTER 8

CONCLUSIONS

8.1 CONTRIBUTIONS

In this thesis, detailed investigation on wear and fracture behaviour of tyre tread rubber compounds is presented. Tread compounds based on various rubber blends are developed and fundamental properties are characterized. Fatigue Crack Growth (FCG) behaviour of these compounds is measured over a wide range of tearing energy and critical strain limits are identified. The influence of various factors on FCG characteristics is studied and associated mechanisms are explained in detail. The most significant influencing parameter is identified and further investigation is also made using Finite Element (FE) simulation to gain better insights of the phenomena. Wear measurements are carried out under variable speed, slip angle and on various surfaces to cover wide range of severity and for better replication of the actual service conditions. Correlation between the wear and the FCG behaviour is discussed. The salient points of overall contributions from the present work are given below.

- Truck bus radial tyre tread compounds comprising of NR, BR, SBR, NR/BR and NR/SBR blends are developed. A series of properties viz., rheometric, mechanical, hyperelastic, viscoelastic etc. are characterized.

- FCG behaviour is measured using pure shear specimen geometry using Tear & Fatigue Analyser. Measurements are carried out under variable strain, temperature, R–ratio, waveform etc. in order to understand the influence of these parameters on FCG characteristics.

- FE simulation is carried out using pure hyperelasticity, hyperelasticity with linear and non-linear viscoelasticity to understand inherent mechanism of FCG in different waveforms.

- Wear measurement is done under various operating conditions using LAT 100 equipment. The dominant wear mechanism is identified. Relative ranking of the compounds are presented. A correlation is established between the wear and the FCG behaviour.

8.2 CONCLUSIONS

The following conclusions can be drawn based on the present research.

1. FCG measurements revealed that, there exists a threshold tearing energy for each material above which crack growth rate increases significantly. The reversal of FCG ranking is also observed above the threshold value. Hence this must be considered as important criteria for tyre tread compound selection.

2. All the test variables, temperature, R-ratio and waveform, significantly influence the FCG characteristics of rubber compounds. Out of these test variables, waveform type has the highest influence.

3. The FCG rate in Pulse mode is much higher in comparison with the Sine mode. This is due to a higher strain rate associated with the Pulse mode testing. Pulse mode should be used for the FCG evaluation as it closely simulates the tyre loading pattern during rolling conditions.

4. NR/BR blends exhibited superior FCG resistance over NR/SBR blend compounds.

5. It is clear from the wear measurements that the wear is due to the cut growth process and has a good correlation with Corundum 180 surface. Corundum 180 surface is a better representation of fatigue wear and should be used for laboratory wear characterization purpose.

6. FEA simulation results show that in Pulse mode loading, crack tip experiences higher SENER and less CENER in comparison with the Sine mode. This explains higher FCG rate in the Pulse mode as observed from the experimental results.

8.3 SCOPE FOR FUTURE WORK

FCG studies of tyre tread rubber compounds can be extended for investigating the influence of aging (realistic operating conditions). This study is very important as the rubber compounds undergo significant changes during service. Further, rubber fatigue model can be developed for durability prediction with the help of FE tools. Relation between the ultimate strength of the material and the number of fatigue cycles for various tyre rubber compounds can be studied.

APPENDIX - A

HYPERELASTIC MATERIAL MODELLING FOR RUBBER MATERIALS

Hyperelastic material is defined by strain energy density function (Holzapfel, 2000), W which is a scalar function of one of the strain or deformation tensors, whose derivative with respect to a strain component determines the corresponding stress component. This can be expressed by,

$$S_{ij} = \delta W/\delta E_{ij} \equiv 2 \; \delta W/\delta C_{ij} \tag{A.1}$$

where, S_{ij} = components of the second Piola-Kirchhoff stress tensor

W = strain energy function per unit undeformed volume

E_{ij} = components of the Lagrangian strain tensor

C_{ij} = components of the right Cauchy- Green deformation tensor

The Lagrangian strain can be expressed as follows:

$$E_{ij} = \tfrac{1}{2} \; (C_{ij} - \delta_{ij}) \tag{A.2}$$

where, $\delta_{ij} =$ 1 $i = j$

0     $i \neq j$

1

The deformation tensor C_{ij} is comprised of the products of the deformation gradients $f_{ij.}$

$C_{ij} = f_{ki}.f_{kj}$ = component of the Cauchy-Green deformation tensor

A.1 RIVLIN'S FORMULATION

Rivlin treated rubber as an incompressible material and isotropic in the unstrained state (Treloar, 1975). He proposed that the elastic properties can be represented in terms of a strain energy function W,

$$W = f \, (I_1, \, I_2, \, I_3) \tag{A.3}$$

136

where I_1, I_2, and I_3 are the three principal strain invariants of Green deformation tensor.

$$I_1 = \lambda_1^2 + \lambda_2^2 + \lambda_3^2$$

$$I_2 = \lambda_1^2 \lambda_2^2 + \lambda_2^2 \lambda_3^2 + \lambda_3^2 \lambda_1^2$$

$$I_3 = \lambda_1^2 \lambda_2^2 \lambda_3^2$$

λ_1, λ_2, and λ_3 are the extension ratios.

Rivlin has pointed out that Equation (A.3) can be approximated by the power series

$$W = \sum_{ijk=0}^{n} C_{ijk}(I_1 - 3)^i (I_2 - 3)^j (I_3 - 1)^k \qquad \text{(A.4)}$$

For incompressible materials, $I_3 = 1$, Equation (A.4) is reduced to

$$W = \sum_{ij=0}^{n} C_{ij}(I_1 - 3)^i (I_2 - 3)^j \qquad \text{(A.5)}$$

This is the generalized polynomial form of Rivlin strain energy density function.

A.1.1 Neo-Hookean Model

Taking only the first term of Equation (A.5), yields Neo-Hookean model and expressed as,

$$W = C_{10}(I_1 - 3) \qquad \text{(A.6)}$$

A.1.2 Mooney-Rivlin Model

Taking the first two terms of Equation (A.5) yields Mooney-Rivlin model and expressed as,

$$W = C_{10}(I_1 - 3) + C_{01}(I_2 - 3) \qquad \text{(A.7)}$$

A.1.3 Yeoh Model

Yeoh has considered only the I_1 term of Equation (A.5), and proposed the following model,

$$W = C_{10}(I_1 - 3) + C_{20}(I_1 - 3)^2 + C_{30}(I_1 - 3)^3 \qquad \text{(A.8)}$$

REFERENCES

1. **Abaqus 6.13** Analysis User's Guide (2013), Dassault Systems Simulia Corp.

2. **Abraham, F., T. Alshuth and S. Jerrams** (2004) The effect of minimum stress and stress amplitude on the fatigue life of non strain crystallising elastomers. *Materials & Design*, 26, 239-245.

3. **Andreini, G., P. Straffi , S. Cotugno, G. Gallone and G. Polacco** (2010) Comparison of sine versus pulse waveform effects on fatigue crack growth behaviour of NR, SBR and BR compounds. *Rubber Chemistry and Technology,* 83, 391-403.

4. **Andreini, G., P. Straffi , S. Cotugno, G. Gallone and G. Polacco** (2013) Crack growth behaviour of styrene-butadiene rubber, natural rubber and polybutadiene rubber compounds: Comparison of pure-shear versus strip tensile test. *Rubber Chemistry and Technology*, 86, 132-145.

5. **Bartenev, G. M. and N. M. Lyalina** (1972) Stress relaxation mechanisms in rubbers reinforced with carbon blacks, *Rubber Chemistry and Technology,* 45, 82-93.

6. **Bhowmick, A. K. and S. K. De** (1980) Effect of curing temperature and curing system on structure-property relations of rubber blends. *Rubber Chemistry and Technology*, 53, 960-974.

7. **Boyce, M. C. and E. M. Arruda** (2000) Constitutive models of rubber elasticity: A review. *Rubber Chemistry and Technology*, 73, 504-523.

8. **Bruning, K., K. Schneider, S. V. Roth and G. Heinrich** (2013) Strain-induced crustallization around a crack tip in natural rubber under dynamic load. *Polymer*, 54, 6200-6205.

9. **Callan, J. E, W. M. Hess and C. E. Scott** (1971) Elastomer blends, compatibility and relative response to fillers, *Rubber Chemistry and Technology,* 44, 814-837.

10. **Charlton, D. J, J. Yang and K. K. Teh** (1994) A review of methods to characterize rubber elastic behaviour for use in finite element analysis. *Rubber Chemistry and Technology,* 67, 481-503.

11. **Cho, K. and D. Lee** (2000) Effect of molecular weight between cross-links on the abrasion behavior of rubber by a blade abrader. *Polymer*, 41, 133-140.

12. **Chow, C. L. and C. H. Cundiff** (1987) On the characterisation of mechanical properties of rubber vulcanizates. *Tire Science and Technology,* 15, 73-96.

13. **Chung, W. W. and Y. W. Chang** (2001) Fatigue crack growth behavior of NR/EPDM blend. *Korea Polymer Journal*, 9, 319-326.

14. **Corish, P. J and B. D. W. Powell** (1974) Elastomer blends, *Rubber Chemistry and Technology*, 47, 481-510.

15. **D'Amico, F., G. Carbone, M. M. Foglia and U. Galietti** (2013) Moving cracks in viscoelastic materials: Temperature and energy-release-rate measurements. *Engineering Fracture Mechanics*, 98, 315-325.

16. **De, D. and A.N. Gent** (1996) Tear strength of carbon-black –filled compounds. *Rubber Chemistry and Technology*, 69, 834-850.

17. **Dizon, E. S., A. E. Hicks and V. E. Chirico** (1974) The effect of carbon black parameters on the fatigue life of filled rubber compounds. *Rubber Chemistry and Technology*, 47, 231-249.

18. **Eisele, U., S. A. Kelbch and H. W. Engels** (1992) The Tear Analyzer – A New Tool for Quantitative Measurements of the Dynamic Crack Growth of Elastomers. *Kautschuk Gummi Kunststoffe*, 45, 1064-1069.

19. **Ellis, B. and G.L. Welding** (1964) Estimation, from swelling, of the structural contribution of chemical reactions to the vulcanization of natural rubber Part II. Estimation of equilibrium degree of swelling. *Rubber Chemistry and Technology*, 37, 571-575.

20. **Ellul, M. D.** Mechanical fatigue pp. 129-168. In A. N. Gent (ed.), Engineering With Rubber, Hanser, 1992.

21. **Fukahori, Y. and H. Yamazaki** (1994) Mechanism of rubber abrasion. Part I: Abrasion pattern formation in natural rubber vulcanizate. *Wear*, 171, 195-202.

22. **Fukahori, Y. and H. Yamazaki** (1994) Mechanism of rubber abrasion Part 2. General rule in abrasion pattern formation in rubber like materials. *Wear*, 178, 109-116.

23. **Fukahori, Y. and H. Yamazaki** (1995) Mechanism of rubber abrasion Part 3. Part 3: how is friction linked to fracture in rubber abrasion. *Wear*, 188, 19-26.

24. **Fukahori, Y., H. Liang and J. J. C. Busfield** (2008) Criteria for crack initiation during rubber abrasion. *Wear*, 265, 37-395.

25. **Gent, A.N. and C.T.R. Pulford** (1983) Mechanisms of rubber abrasion. *Journal of Applied Polymer Science*, 28, 943-960.

26. **Gent, A.N., P.B. Lindley and A. G. Thomas** (1965) Cut growth and fatigue of rubbers. I. The relationship between cut growth and fatigue. *Rubber Chemistry and Technology*, 38, 292-300.

27. **Gerspacher, M., C. P. O'Farrel, H. H. Yang, L. Nikiel** (1999) Filler-filler and filler-polymer interactions in carbon black dispersion. *Rubber World* 1999, 220:27.

28. **Grosch, K. A., H. Moneypenny and I. H. Wallace** (2001) A Correlation between truck tyre road wear performance and a system of laboratory abrasion tests, *IRC 2001*, Birmingham.

29. **Grosch, K.A.** (2004) Correlation between road wear of tires and computer road wear simulation using laboratory abrasion data. *Rubber Chemistry and Technology*, 77, 791-814.

30. **Grosch, K.A**. Rubber abrasion and tire wear pp. 534-593. In **A.N. Gent, J.D. Walter** (eds.), The Pneumatic Tire. NHTSA, Washington, 2005.

31. **Groves, S.** (1998) Crosslink density distribution in NR/BR blends: Effect of cure time and temperature, *Rubber Chemistry and Technology,*71, 958-965.

32. **Hamed, G.R.** (1994) Molecular aspects of the fatigue and fracture of rubber. *Rubber Chemistry and Technology,* 67, 529-536.

33. **Hamed, G.R., H. J. Kim and A. N. Gent** (1996) Cut growth in vulcanizates of natural rubber, cis-plybutadiene and a 50/50 blend during single and repeated extension. *Rubber Chemistry and Technology,* 69, 807-818.

34. **Harbour, R. J., A. Fatemi and W. V. Mars** (2008) Fatigue life analysis and predictions for NR and SBR under variable amplitude and multiaxial loading conditions. *International Journal of Fatigue*, 30, 1231-1247.

35. **Harbour, R. J., A. Fatemi and W. V. Mars** (2007) The effect of dwell Period on fatigue crack growth rates in filled SBR and NR. *Rubber Chemistry and Technology*, 80, 838-853.

36. **Harris, J. A.** (1987) Dynamic testing under nonsinusoidal conditions and the consequences of nonlinearity for service performance. *Rubber Chemistry and Technology*, 60, 870-887.

37. **Heinz, M. and K.A. Grosch** (2007) A laboratory method to comprehensively evaluate abrasion, traction and rolling resistance of tire tread compounds. *Rubber Chemistry and Technology*, 80, 580-607.

38. **Hess, W. M., C. E. Scott and J. E. Callan** (1967) Carbon black distribution in elastomer blends. *Rubber Chemistry & Technology*, 40, 371-384.

39. **Holzapfel, G. A.** *Nonlinear Solid Mechanics – A Continuum Approach for Engineering.* John Wiley, West Sussex, England, 2000.

40. **Hurtado, J. A., I. Lapczyk and S. M. Govindrajan** (2013) Parallel Rheological Framework to model non-linear viscoelasticity, permanent set and Mullins effect in elastomers, *Constitutive Models for Rubber VIII*, Spain, June, 95-100.

41. **Kern, W. J. and S. Futamura** (1988) Effect of tread polymer structure on tyre performance. *Polymer,* 29, 1801-1806.

42. **Kim, S. G. and S. H. Lee** (1994) Effect of crosslink structures on the fatigue crack growth behaviour of NR vulcanizates with various aging conditions. *Rubber Chemistry and Technology,* 67, 649-661.

43. **Kim, S. Y., H. S. Byun, S. Kim, W. Y. Kim, S. C. Han and A. N. Gent** (1999) Abrasion of selected rubber compounds with a DIN abrader. *Korea Polymer Journal,* 7, 116-123.

44. **Kim, J. H. and H.Y. Jeong** (2005) A study on the material properties and fatigue life of natural rubber with different carbon blacks. *International Journal of Fatigue*, 27, 263-272.

45. **Kluppel, M.** (2009) Evaluation of viscoelastic master curves of filled elastomers and applications to fracture mechanics. *Journal of Physics: Condensed Matte*r, 21, 1-10.

46. **Krishnan, V., R. Ramakrishnan and J.A. Donovan** (1995) Correlation between laboratory and road rubber wear tests, *Rubber Chemistry and Technology*, 68, 804-814.

47. **Lake, G. J. and P.B. Lindley** (1965) Cut growth and fatigue of rubbers. II. Experiments on a noncrystallizing rubber. *Rubber Chemistry and Technology*, 38, 301-313.

48. **Lake, G. J. and A. G. Thomas.** Strength pp. 95-128. In A. N. Gent (ed.), Engineering With Rubber, Hanser, 1992.

49. **Lake, G. J.** (1995) Fatigue and fracture of elastomers. *Rubber Chemistry and Technology*, 68, 435-460.

50. **Lee, M. P.** (1993) Analysis of fatigue crack propagation in NR/BR rubber blend. *Rubber Chemistry and Technology*, 66, 304-316.

51. **Legorju-jago, K. and C. Bathias** (2002) Fatigue initiation and propagation in natural and synthetic rubbers. *International Journal of Fatigue,* 24, 85–92.

52. **Liang, H.** (2007) Investigating the mechanism of elastomer abrasion. PhD Thesis, Queen Mary University of London.

53. **Liang, H., Y. Fukahori, A.G. Thomas and J.J.C. Busfield** (2010) The steady state abrasion of rubber: Why are the weakest rubber compounds so good in abrasion. *Wear*, 268, 756-762.

54. **Lindley P. B.** (1973) Relation between hysteresis and dynamic crack growth resistance of natural rubber. *International Journal of Fracture*, 9, 449-462

55. **Mangaraj, D.** (2002) Elastomer blends. *Rubber Chemistry and Technology,* 75, 366-428.

56. **Mansilla, M. A., L. Silva, W. Salgueiro, A. J. Marzoca and A. Somoza** (2012) A study about the structure of vulcanized natural rubber/styrene butadiene rubber blends and the glass transition behaviour. *Journal of Applied Polymer Science,125*, 992-999.

57. **Mars, W. V. and A. Fatemi** (2002) A literature survey on fatigue analysis approaches for rubber. *International Journal of Fatigue*, 24, 949-961.

58. **Mars, W. V. and A. Fatemi** (2003) A Phenomenological model for the effect of R-ratio on fatigue of strain crystallizing rubbers. *Rubber Chemistry and Technology*, 76, 1241-1258.

59. **Mars, W. V. and A. Fatemi** (2004) Factors that affect fatigue life of rubber: A literature survey. *Rubber Chemistry and Technology*, 77, 391-412.

60. **Marsh, P. A., A. Voet, L. D. Price and T. J. Mullens** (1968) Fundamentals of electron microscopy of heterogeneous elastomer blends. II. *Rubber Chemistry & Technology,* 41, 344-355.

61. **Mathew, N. M. and S. K. De** (1983) Scanning electron microscopy studies on flexing and tension fatigue failure of rubber. *International Journal of Fatigue*, 5, 23-28.

62. **Mathew, M. N.** Natural Rubber pp 11-45. In **J. R. White, S. K. De** (eds), Rubber Technologist's Handbook, Rapra Technology Limited, UK, 2001.

63. **Moore, D.F.** (1980) Friction and wear in rubbers and tyres. *Wear*, 61, 273-282.

64. **Muhr, A. H. and A. D. Roberts** (1992) Rubber abrasion and wear. *Wear*,158, 213-228.

65. **Nandi, B., T. Dalrymple. J. Yao and I. Lapczyk** (2014) Importance of capturing non-linear viscoelastic material behavior in tire rolling simulations, Presented at 33rd Tire Society Meeting, Akron, September.

66. **Nie, Y., B. Wang, H. Huang, L. Qu, P. Zhang, G and Weng, J. Wu** (2010) Relationship between the material properties and fatigue crack-growth

characteristics of natural rubber filled with different carbon blacks. *Journal of Applied Polymer Science,* 117, 3441-3447.

67. Non-linear viscoelastic calibration using Isight, Internal report from Simulia India, 2014.

68. **Persson, B. N. J., O. Albohr, G. Heinrich, and H. Ueba** (2005) Crack propagation in rubber like materials. *Journal of Physics Condensed Matter,* 17:R1071-R1142.

69. **Petitet, G., J. L. Loubet, H. Zahouani and D. Mazuyer** (2005) A contribution to the understanding of elementary wear mechanisms of rubber filled compounds, *Rubber Chemistry and Technology*, 78, 312-320.

70. **Qazvini, N., N. Mohammadi, A. Jalali, A. Varasteh** (2002) The fracture behaviour of rubbery vulcanizates: I. single component versus blend systems. *Rubber Chemistry and Technology*, 75, 77-82.

71. **Rao, K. V. N., R. K. Kumar and P. C. Bohara** (2003) Transient finite element analysis of tire dynamic behavor . *Tire Science and Technology*, 31, 104-127.

72. **Reincke, K., W. Grellmann and M. Kluppel** (2009) Investigation of fracture mechanical properties of filler-reinforced styrene-butadiene elastomers. *Kautschuk Gumi Kunstoffe* , 5, 246-251.

73. **Rivlin, R.S. and A.G. Thomas** (1953) Rupture of rubber. I. Characteristic energy for tearing. *Journal of Polymer Science*, 10, 291-318.

74. **Sabbabagh-EL, S. H. and A. A. Yehia** (2007), Detection of crosslink density by different methods for natural rubber blended with SBR and NBR. *Egyptian Journal of Solids,* 30, 157-173.

75. **Saintier, N., G. Cailletaud and R. Piques** (2011) Cyclic loadings and crystallization of natural rubber: An explanation of fatigue crack propagation reinforcement under a positive loading ratio. *Materials Science and Engineering A,* 528, 1078-1086.

76. **Schallamach, A.** (1956) Principal considerations on tyre wear. *Rubber Chemistry and Technology*, 29, 781-788.

77. **Scurati, A. and C. Lin** (2006) The hysteresis temperature and strain dependence in filled rubbers. *Rubber Chemistry and Technology*, 79, 170-197.

78. **Seibert, D. J. and N. Schoche** (2000) Direct comparison of some recent rubber elasticity models. *Rubber Chemistry and Technology*, 73, 366-384.

79. **Sircar, A. K. and T. G. Lamond** (1973) carbon black transfer in blends of cis-polybutadiene with other elastomers. *Rubber Chemistry and Technology,* 46, 178-191.

80. **South, J. T** (2001) Mechanical properties and durability of natural rubber compounds. PhD Thesis, Virginia Polytechnic Institute and State University.

81. **Southern, E and A. G. Thomas** (1979) Studies of rubber abrasion. *Rubber Chemistry & Technology*, 52, 1008-1018.

82. **Stacer, R. G., L. C. Yanyo and F. N. Kelly** (1985) Observations on the tearing of elastomers. *Rubber Chemistry and Technology*, 58, 421-435.

83. **Stadlbauer, F., T. Koch, V. M. Archodoulaki, F. Planitzer, W. Fidi and A. Holzner** (2013) Influence of experimental parameters on fatigue crack growth and heat build-up in rubber. *Materials*, 6, 5502-5516.

84. **Stoček, R., G. Heinrich and M. Gehde** (2009) The influence of the test properties on dynamic crack propagation in filled rubbers by simultaneous tensile and pure shear test mode testing. *Constitutive Models for Rubber VI*, Dresden, September, 345-349.

85. **Stoček, R., G. Heinrich, M. Gehde and A. Rauschenbach** (2012) Investigations about notch length in pure-shear test specimen for exact analysis of crack propagation in elastomers. *Journal of Plastics Technology*, 01, 2-22.

86. **Thomas, A. G**. (1994) The development of fracture mechanics for elastomers. *Rubber Chemistry and Technology*, 67, G51-G60.

87. **Treloar, L. R**. G. *The Physics of Rubber Elasticity*. Oxford University Press, Oxford, 1975.

88. **Veith, A.G.** (1992) A review of important factors affecting tread wear. *Rubber Chemistry and Technology*, 65, 601-658.

89. **Wang, M. J.** (2007) Effect of filler-elastomer interaction on tire tread performance Part I. *Kautschuk Gumi Kunstoffe*, 09, 438-443.

90. **Yang, X.** (2011) Finite element analysis and experimental investigation of tyre characteristics for developing strain-based intelligent tyre system. PhD Thesis, The University of Birmingham.

91. **Yanyo, L. C.** (1989) Effect of crosslink type on the fracture of natural rubber vulcanizates. *International Journal of Fracture*, 39, 103-110.

92. **Yeoh, O. H.** (1990) Characterisation of elastic properties of carbon black filled rubber vulcanizates. Rubber *Chemistry and Technology,* 63, 792-805.

93. **Yeoh, O. H.** (1993) Some forms of the strain energy function for rubber, *Rubber Chemistry and Technology,* 66, 754-771.

94. **Young, D. G.** (1985) Dynamic property and fatigue crack propagation research on tire sidewall and model compounds. *Rubber Chemistry and Technology,* 58, 785-805.

95. **Young, D. G. and J. A. Danik** (1994) Effect of temperature on fatigue and fracture. *Rubber Chemistry and Technology,* 67,137-147.

LIST OF PUBLICATIONS BASED ON THE RESEARCH WORK

I. JOURNALS

1. **P. Ghosh, R. Stocek, M. Gehde, R. Mukhopadhyay and R. Krishnakumar** (2014) Investigation of fatigue crack growth characteristics of NR/BR blend based tyre tread compounds, *International Journal of Fracture*, 188, 9-21.

2. **P. Ghosh, R. Mukhopadhyay and R. Krishna Kumar,** Studies on wear characteristics of NR and NR/BR blend based tyre tread compounds and correlation with fatigue crack growth properties. (Communicated to Wear Journal, dt. 07/11/2014).

II. CONFERENCES

1. **R. Stocek, P. Ghosh, R. Mukhopadhyay, R. Kipscoll, G. Heinrich**, Fracture behavior of rubber-like materials under classical fatigue crack growth vs. chip & cut analysis, *ECCMR 2013 Conference*, San Sebastian, Spain, 25-28th June, 2013.

CURRICULUM VITAE

1.	**NAME**	:	Prasenjit Ghosh

2.	**DATE OF BIRTH**	:	20 November 1973

3.   EDUCATIONAL QUALIFICATIONS

1999 Master of Technology (M.Tech)

Institution	:	Indian Institute of Technology Kharagpur
Specialization	:	Rubber Technology

Doctor of Philosophy (Ph.D.)

Institution	:	Indian Institute of Technology Madras
Registration Date	:	18 July 2008

DOCTORAL COMMITTEE

CHAIRPERSON: **The Head**
Department of Engineering Design

GUIDE: **Dr. R. Krishna Kumar**
Professor
Department of Engineering Design

MEMBERS: **Dr. C. S. Shankar Ram**
Associate Professor
Department of Engineering Design

Dr. M. Ramanathan
Associate Professor
Department of Engineering Design

Dr. K. Ramesh
Professor
Department of Applied Mechanics

Dr. R. Sethuraman
Professor
Department of Mechanical Engineering